Evaluation of the design and life cycle of different piping solutions under climate change uncertainties

CIEM0500

Geert de Klerk

TU Delft

TETRA TECH

rps A TETRA TECH COMPANY

Evaluation of the design and life cycle of different piping solutions under climate change uncertainties

by

Geert de Klerk

to obtain the degree of Master of Science
at the Delft University of Technology,

Student number: 4936310
Thesis committee:
Dr. J.P. Aguilar-Lopez, TU Delft
Ir. Y.R. Jongerius RPS & TU Delft
Dr. Ir. A.C. Dieudonné TU Delft
Ir. M.A. Schoemaker TU Delft

Cover: River dike section in the Netherlands [64]

Preface

This thesis is conducted as the last part of my Master of Science programs of Civil Engineering at the Delft University of Technology. The study was performed at RPS, a Tetra Tech company, and the Delft University of Technology.

I would like to thank my thesis committee for providing me with valuable input and critical views. With all the committee members, I have had multiple insightful discussions. I would to thank Juan Aguilar-Lopez for his expertise on the subject and various interesting and fun modelling sessions, making me an enthusiast for the COMSOL software.
I would like to especially thank my daily supervisor Yoeri Jongerius for his weekly time, input and patience. I am grateful for getting in contact with RPS and being allowed to spend my time working on the thesis there.
I want to additionally thank Maarten Schoemaker, for the interesting discussions and the specific knowledge and help on the life cycle assessment.
Lastly, I would like to thank Anne-Catherine Dieudonné for her expertise and knowledge on the SoSEAL barrier, providing me with essential input.

Geert de Klerk
Delft, September 2025

Abstract

Dikes are a primary defence against flooding from the rivers and sea in the Netherlands, but many no longer meet current safety standards. To ensure the dikes keep meeting the safety standards in the future, climate change will need to be taken into account. Increase in river discharge and upstream water levels through rising temperatures, more frequent extreme precipitation, and increasing meltwater run-off, are climate uncertainties that pose additional challenges for dike reinforcement projects. One critical failure mechanism requiring attention is backward erosion piping (BEP), which has historically been underestimated. Over the past decade research has advanced the knowledge on BEP and led to innovative solutions to mitigate this risk, each based on different working principles and associated with distinct performance characteristics and life cycle costs. However, it is currently unclear how the design, performance, and cost-effectiveness of these solutions compare under climate change uncertainties.

This study evaluates the design performance and life cycle of three piping solutions, both innovative and conventional, under climate change uncertainties. Using a numerical model in COMSOL Multiphysics, the performance of each solution is assessed through fragility curves based on the relevant failure criterion for each solution. Due to the different working principles, the fault trees differ between the solutions. The failure criterion for each solution is based on the critical step they tackle in the fault tree that leads to piping failure. Climate impact uncertainties are represented by considering different future climate scenarios. Using Hydra-NL, water levels for different return periods and future scenarios, including both moderate and high-emission pathways, are calculated. The resulting probabilities of the water levels and the conditional failure probabilities from the fragility curves are used to determine and quantify the timespan of the life cycles. The life cycles are evaluated in terms of cost and their sensitivity to design and climate uncertainties is assessed. This assessment is done with a life cycle cost analysis using the Equivalent Annual Cost (EAC) method.

The results show that while the sheet pile and plastic filter screen exhibit similar performance in preventing hydraulic heave, their sensitivity to rising water levels differs, with the filter screen performing slightly better under extreme conditions. The SoSEAL barrier demonstrates lower sensitivity to high water levels but exhibits higher failure probabilities at lower water levels due to heterogeneity in the barrier's hydraulic conductivity and contact zone effects. It is emphasised that the plastic filter screen and SoSEAL barrier have inherent uncertainties due to their innovative designs. Reducing these uncertainties in the future can significantly increase the performance and make them competitive alternatives to conventional solutions like the sheet pile.
The life cycle cost analysis indicates that the sheet pile is currently the most cost-effective solution and least sensitive to the uncertainties across the different scenarios, followed by the filter screen and SoSEAL barrier. Cost uncertainties, particularly in annual maintenance & monitoring, were found to influence the performance more than climate uncertainties. Constant yearly costs, resulted in lower values of equivalent annual costs for longer lifespans, while annually increasing costs produce higher values for longer lifespans, stressing the importance of accurate cost forecasting. Furthermore, the results highlight the trade-offs between the technical and functional lifespan, suggesting that increasing annual costs can offset the benefits of extended design life.
In the future, the uncertainties in the design-related expenses for the innovative solutions will decrease. The amount and range of the yearly costs will then decrease with time, increasing the cost-effectiveness of the SoSEAL barrier and plastic filter and decreasing their sensitivity to future uncertainties.

This study concludes that the performance of the different piping solutions is influenced by both design and climate change uncertainties. Varying lifespans and annual costs significantly affect the performance of the solutions across different scenarios and have a even greater impact than the uncertainties of climate change. Life cycle cost variability underscores the need for considering economic uncertainties alongside the uncertainties in technical performance into current decision-making processes. Decreasing these uncertainties in innovative solutions could improve their performance and make them suitable alternatives in the evaluation and comparison of different solutions.

Contents

1

Introduction

1.1. Context and problem definition

Dikes are one of the main primary flood defences protecting the Netherlands from the sea and rivers. Since the early 2000s, however, safety assessments have shown that many dikes no longer meet the required safety standards [26]. Reinforcement projects have therefore since been implemented to ensure protection from the water with future years to come. However, numerous dikes still require necessary reinforcements. To ensure the dikes keep meeting the safety standards in the future, climate change will need to be taken into account. The changing climate can affect the water levels in the rivers significantly. Increase in meltwater run-off and more frequent extreme precipitation events for example cause the river levels to rise [5]. Given the uncertainty in the rate and magnitude of these changes, several climate scenarios have been defined, each with its own probability. With this increase in future water levels and uncertainties, the need for reinforcements becomes even more urgent.

One key failure mechanism dikes and their reinforcements need to tackle is backward erosion piping (BEP). Piping has been underestimated in the past as a failure mechanism and reinforcements are needed to meet the safety standards [9]. Over the past decade research has advanced the knowledge on BEP and led to innovative solutions that differ from each other and from traditional solutions like sheet piles. These different piping measures vary in their working principles, effectiveness and life cycle costs. Such life cycle costs are further affected by economic and political developments. The performance and cost-effectiveness of these (innovative) piping solutions can be significantly influenced by future climate and economic developments, both of which are subjected to uncertainties.

Currently, it is unclear how the piping solutions with different working principles compare in terms of their design performance and associated life cycle cost under these climate change uncertainties. Current design choices often do not take these differences and uncertainties quantitatively into account.

This thesis, therefore, aims to evaluate different piping solutions and their life cycle under climate change uncertainties. In this evaluation the uncertainties in the performance of the piping solutions and their life cycle costs are assessed across different future scenarios.

1.2. Research scope

To achieve the aim of this thesis, the different piping solutions are evaluated along a river dike. Using a numerical model, fragility curves for the piping solutions are created. With these fragility curves, the failure probabilities are investigated over time, taking climate change into account. With these failure probabilities, different life cycles are determined. By performing a life cycle cost analysis over these life cycles, their performance and sensitivity to the different uncertainties is determined and compared.

This thesis focuses on dikes along the upper river region of the Netherlands, where high water levels can persist for extended periods of time. For this reason, the governing hydraulic loads are treated as stationary [48]. A case study approach is used to obtain concrete results under representative conditions, focusing on the Grebbedijk along the upper river Nederrijn. Several sections of this dike are known to be prone to piping, making it a relevant subject for analysis.

This study evaluates three different piping solutions, covering both traditional and innovative designs. Each solution is based on a different working principle to reflect the broad range of current measures. The exact type of solutions and the justification for their selection are detailed later in the thesis, see section 1.4. Their performance is investigated under different climate uncertainties and scenarios. The climate scenarios are defined by the latest IPCC and KNMI reports, as well as by the GRADE research in which the KNMI looked at the implications of climate projections on river discharges.

The numerical modelling is performed using COMSOL Multiphysics, to evaluate the technical performance of the piping solutions. The constructed models represent each solution under the case study conditions and uncertainties. In addition, the life cycle cost assessment, incorporates economic developments such as discount rates and market price volatility.

The scope of this thesis is limited to the hydraulic and geotechnical performance of the selected piping measures, alongside their life cycle evaluation. Additional social and/or ecological considerations are beyond the scope of this study.

1.3. Research questions

The main research question, following the aim of this thesis, is stated:

How does the design and life cycle of different piping solutions compare under climate change uncertainties?

This main research question is addressed through the following sub-questions:

1. What are the effects and uncertainties of climate change on the different piping solutions, and how are these currently considered in the design guidelines?
2. How can the different solutions be modelled to investigate their performance under climate change uncertainties, using COMSOL?
3. What are the effects of the different designs and climate change uncertainties on the failure probabilities due to piping for each solution, according to the COMSOL model?
4. How does the sensitivity of the different solutions to the design and climate change uncertainties compare, based on a life cycle cost analysis?

1.4. Thesis outline

In Chapter 2 the theoretical background on backward erosion piping, piping solutions measures, and the role of climate uncertainties on BEP are discussed. Chapter 3 introduces the Grebbedijk improvement project as the case study. Chapter 4 discusses the three different piping solutions that are selected for this study. Chapter 5 describes the COMSOL modelling approach and failure criteria of the selected piping solutions. Chapter 6 presents the simulation results, including the fragility curves and failure probabilities, leading to different life cycles. Chapter 7 evaluates the solutions through a life cycle cost analysis. Finally, Chapter 8 provides the conclusions and recommendations.

2

Theoretical background

In this chapter, knowledge and background on the backward erosion piping failure mechanism, the different solutions for backward erosion piping, and climate change aspects relevant to backward erosion piping are provided.

2.1. Backward erosion piping failure mechanism within a dike

The failure mechanism of backward erosion piping within a dike is a mechanism of internal erosion. After a certain hydraulic head is reached, upward pressures on the downstream side lift up the top clay layer until it bursts [36]. After which, heave failure occurs and sand particles are transported through the top layer to the exit point. Due to seepage, grains of sand are then transported underneath the dike to the landside of the structure. This results in the formation of hollow channels, called pipes, which are formed directly underneath the aquitard at the top of the aquifer. The development of these pipes will progress in a backward manner to the river (or upstream) side of the dike. Once the pipes reach this side, they start widening until the dike becomes unstable and eventually fails, leading to a breach of the dike [10]. Figure 2.1 shows this failure mechanism in a schematized way. The different processes resulting in the eventual failure, as described above, can be outlined with the following stages:

1. Uplift failure
2. Heave failure
3. Backward erosion initiation & progression
4. Widening of the pipes
5. Failure and breach of the dike

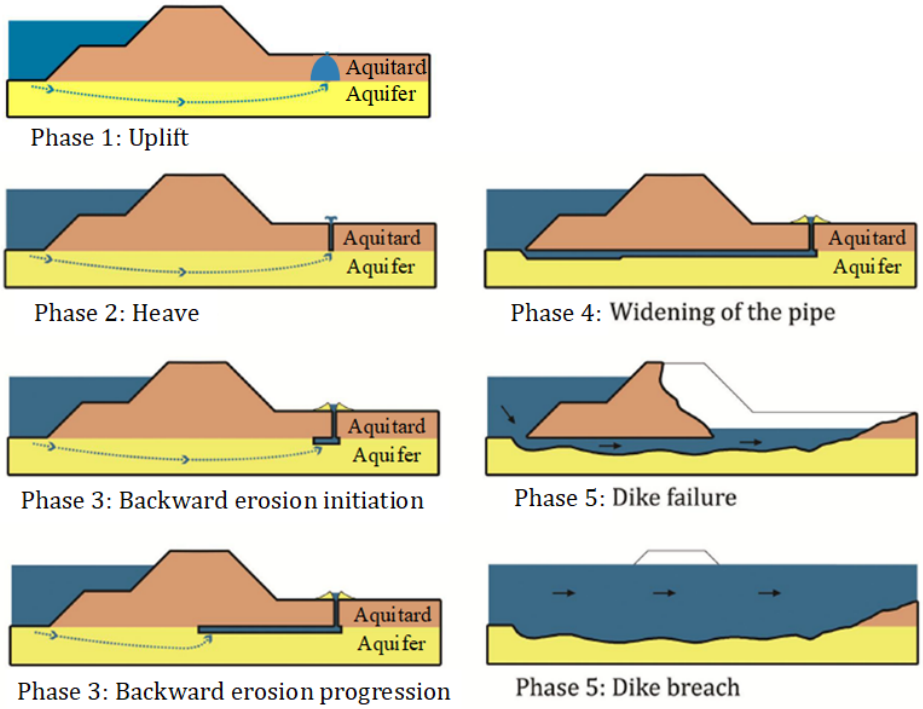

Figure 2.1: Schematization of the different phases of the backward erosion piping failure mechanism

In the continuation of this section the processes regarding these stages are further elaborated and discussed.

2.1.1. Uplift failure

Uplift failure is the bursting of the top clay layer on the downstream side of the dike. The water level difference between the river side and land side of the dike is one of the key driving forces for uplift failure to happen. Increasing the hydraulic head over the dike structure, will increase the upward pressures underneath the clay layer. This causes the clay layer to deform an bend upwards. Once the upward pressure is sufficiently high, meaning the pressure is higher than the weight of the impermeable top layer above, the layer will burst and an open exit is formed [36]. This open exit point can occur already beforehand. The formation of a crack in the top layer, due to shrinkage of the cohesive soil or other environmental changes, can cause an exit point to be there. More common is the occurrence of a ditch for a water channel behind the dike, cutting away a part of the cohesive top soil. This makes the cover layer weaker and prone to uplift failure, since there is less soil to withstand the pressure. The exit point is then formed at the location of the channel. A schematization of these different opening exits can be seen in Figure 2.2.

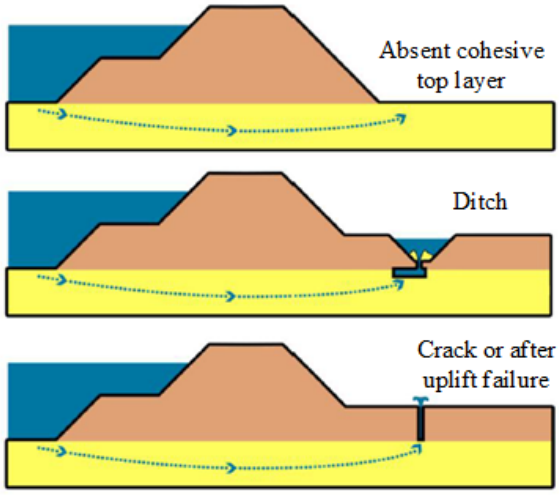

Figure 2.2: Schematization of different opening exits [10]

After an exit is formed in one of the ways, as described and depicted above, the process of heave failure can begin.

2.1.2. Heave failure

Once the layer has burst and an exit point has formed, the heave process initiates. The increase in the hydraulic gradient causes the skeleton of the sand particles at the downstream side near the exit to fluidize. When the vertical outflow gradient at the exit point exceeds the critical gradient, sand particles are transported upwards. The flow velocities overcome the weight of the falling sand particles in the vertical part of the exit and the sand is ejected through the outlet in a ring around it. This ring of sand around the exit is called a 'sand boil' (see Figure 2.3). After the heave mechanism and with a gradient equal to or exceeding the critical gradient, the pipe formation can be initiated and keep on progressing.

Figure 2.3: A sand boil around the exit on the land side of a dike [6]

2.1.3. Backward erosion initiation & progression

Once heave failure has happened and the sand particles keep fluidizing, the initiation of the backward erosion pipes can begin. An additional key aspect for the initiation of the forming of the pipe, is the presence of a so called 'roof'. This roof is the impermeable cohesive layer above the aquifer layer. Due to this roof, a concentration of flow lines will occur near the downstream outlet. This is essential to generate higher flow velocities to transport the sand particles and thus making it possible for the pipe to initiate and grow [10]. Furthermore, the impermeable roof prevents the pipe from collapsing during the backward erosion process.

It is important to note that the pressures can be high enough to cause the fluidization of the skeleton, but not high enough to actually transport the sand outside to the outlet. The pipe formation then comes to a stop and an equilibrium phase is reached. The critical head that is needed for the pipe to start progressing is then not realized. This can be due to a drop in the water pressure, caused by the sand in the vertical section of the soil at the exit. It can also be that the development of the pipe away from the exit causes the local gradient to decrease, due a restriction of inflow in the pipe from the surrounding sand [10].
After the hydraulic head is increased again and the critical head is reached, the pipe development will start again and the formation of the pipe keeps progressing.

Once the critical head is reached and exceeded, the pipe will continue to progress. The pipe will then progress in a backward way from the downstream (or land side) part of the dike to the upstream (or river side) of the dike. When the formation of the pipe has developed to around half of the total seepage length, the pipe will keep on progressing and the equilibrium phase cannot be reached any more. During the backward erosion progression, two categories of erosion can be identified. There is the primary erosion and secondary erosion, see Figure 2.4. The primary erosion takes place at the tip of the pipe. As long as the head achieves the critical head, the sand particles at the tip fluidize. They are then able to be transported to the downstream side through the pipe by the water flow. The secondary erosion has to do with the widening and deepening of the pipe. With increasing inflow of water from the surrounding sand into the pipe, the flow velocities inside the pipe start to increase as well. When this flow reaches a certain critical value, sand particles from the bottom and walls of the pipe will be transported downstream [10].

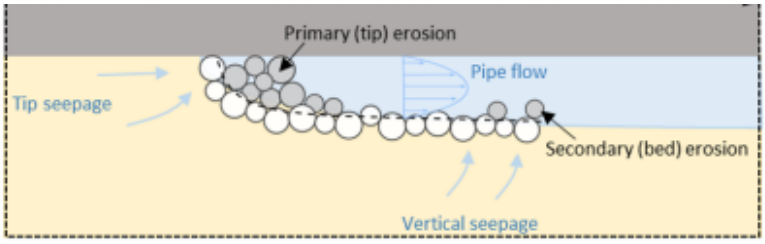

Figure 2.4: Primary and secondary erosion inside the pipe [44]

After reaching the upstream side of the dike, the process of further widening of the pipe will start and progress from the upstream side to the downstream side.

2.1.4. Widening of the pipes

Once the pipe has fully developed from the downstream to the upstream side, there is no tip in the pipe, meaning that there is no sand (only along the bed and walls) to give resistance to the flow of water in the pipe. The flow of water therefore increases at the upstream entry point. This results in surges of water into the pipe, transporting relatively more sand particles downstream. With this process, the pipe starts to widen from the upstream to the downstream side of the dike [10]. Once the pipe has completely widened to the land side of the dike, the flow of water and transportation of sand will increase even further. This leads to a further increase in erosion inside the pipe.

2.1.5. Failure and breach of the dike

The increase in erosion in the pipe, due to the widening process, does not only affect the sand layer. Due to the extensive increase in flow, also the clay layer above the pipe starts to erode. This will eventually lead to the loss of integrity of the dike. The dike will then fail, because of instability [10].
The last part of the backward erosion process, where the clay starts to erode as well, can lead to failure of the dike in a matter of minutes. However, it is also possible for the dike to settle during this process, closing of the pipe. The pipe needs to develop and progress again from the downstream to the upstream side of the dike, to regain a full connection [10]. This way, the flow and erosion can increase again to cause instability of the dike, leading to failure.
The full process of the BEP failure mechanism for a dike has now been realized and the dike has been

breached.

In this study, not all processes are considered and modelled. The main focus lies on the backward progression of the pipe.

2.2. Solutions for backward erosion piping

There are different solutions that can be implemented against backward erosion piping. These solutions tackle one or more aspects that are needed for a dike to fail by the piping mechanism. In this section the different working principles of the solutions are discussed. Additionally, the different piping solutions that are currently being used, designed and/or researched are described. Lastly, a comprehensive overview of the different solutions, categorized by the working principles, is represented.

2.2.1. Working principles

Solutions against piping can tackle one or sometimes more aspects that play a part in backward erosion, preventing a dike of failure. Based on how these piping solutions intervene the process of BEP, they can be categorized in different techniques. Each technique has their own working principles.
In this subsection the different techniques and their working principles will be discussed.

Heave screens

Vertically closed screens, which are inserted in the sand layer that is prone to piping, are called heave screens. They tackle piping by forcing the water flow to change its direction at the location of the screen, see Figure 2.5. The water will have to go underneath or around the screen, which increases the resistance for the pipe to progress. There is now an increase in hydraulic head and upward pressure needed behind the screen, to cause the fluidization of the sand particles. Only when the sand at the downstream side is fluidized over the full length of the heave screen, can the pipe progress again [3].

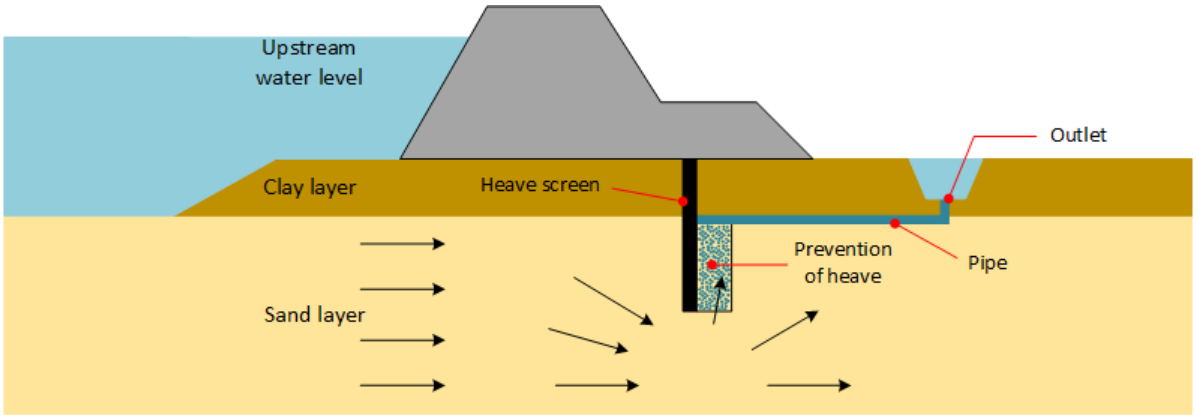

Figure 2.5: A schematization of a heave screen and its working principle

The heave screen does not stop the initial processes of the backward erosion, but tackles the progression of the pipe at the location of the screen. The working principle of the heave screen is to add resistance to the hydraulic heave mechanism on the downstream side of the screen.

Drainage techniques

Drainage techniques can tackle different parts of backward erosion piping. The techniques can be implemented to reduce the risk of bursting of the top layer, heave failure or progression of the pipe. The drainage techniques reduce these risks by extracting water from the aquifer, decreasing the hydraulic head, see Figure 2.6. Decreasing the head underneath the impermeable clay layer, reduces the potential of this top layer to burst. Heave failure can be prevented by draining, to keep the hydraulic gradient below the critical heave gradient. Lastly, by decreasing the head to below the critical head, the progression of pipe formation is stopped [42].

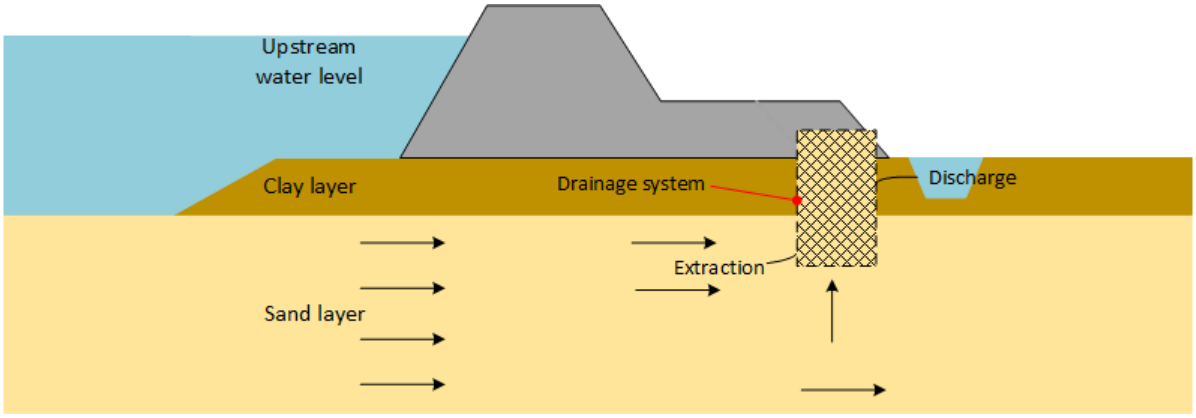

Figure 2.6: A schematization of a drainage system and its working principle

Extracting water from the sand layer to reduce the hydraulic head is the working principle of drainage techniques. However, this process can happen in two different ways. When the head inside the drainage system is lower than the head of the surrounding sand, the water will flow into the system naturally. This is a passive system. If a pump is needed to extract the water from the sand in the aquifer, the drainage technique is an active system.

Filter techniques

Filter techniques prevent further growing of the erosion channel under the dike from the land side to the river side. At the location of the piping solution, a filter is present. This prevents the sand particles from being transported, while allowing the seepage flow to pass toward the downstream side, see Figure 2.7. As a result, a strong seepage flow develops toward the exit point, but the supply of sand is limited. Applying a filter technique does thus not prevent other initial processes from occurring. It does prevent sand transport and consequently the progression of the pipe. [32].

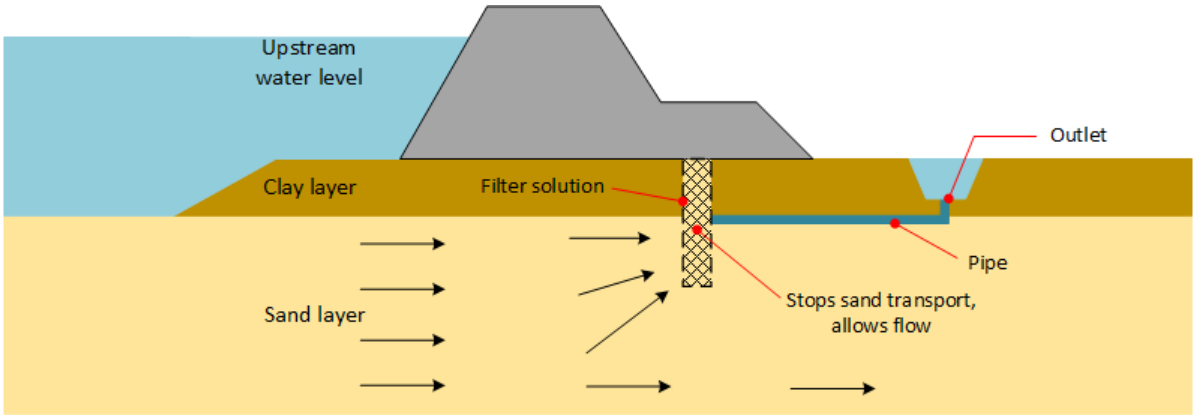

Figure 2.7: A schematization of a filter technique and its working principle

Seepage length extensions

Seepage length extensions are techniques used to horizontally extend the seepage path of the pipe. When applying an impermeable layer, the seepage length is extended by moving the entry point or exit point further away from the dike, see Figure 2.8. The entry point is moved further away, when the extension is implemented in the foreland and the exit point is moved further away when implemented in the hinterland. The seepage length extension increases the resistance of piping by preventing bursting of the layer within the critical seepage length. It is important that the applied extension is sufficiently thick and impermeable, so it can provide enough resistance even when drying of the soil or erosion processes occur.

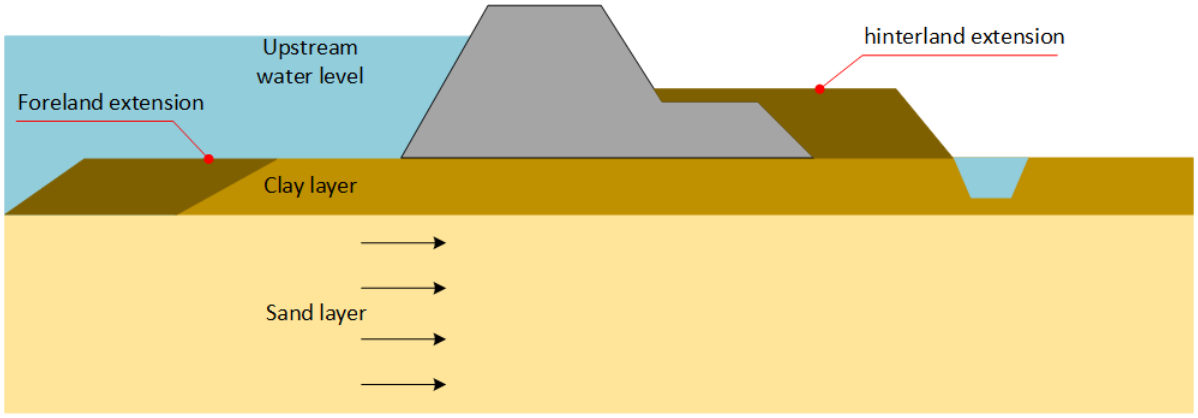

Figure 2.8: A schematization of a seepage length extension by implementing either a foreland or hinterland extension.

2.2.2. Piping solutions

In this subsection different conventional and innovative piping solutions are described. The solutions are classified by the different techniques and working principles as detailed in subsection 2.2.1. At the end of this subsection, a clear overview of all piping solutions is presented.

Heave screens

There are currently different types of heave screens that are conventional and already widely used and implemented. The following heave screen solutions can be classified as conventional [3]:

- **Steel sheet piles**: A vertically closed heave screen made of steel. The steel sheet piles are connected with each other through so called 'locks'. These locks make sure the connection between the sheet piles is watertight.
- **Concrete-Bentonite piles**: A deep trench is excavated in the soil. Guide beams are then applied on either side of the trench. The space between the guided beams is filled with a concrete-bentonite mixture. This creates an impermeable pile in the sand layer. [23]

There are also innovative types of heave screens. These heave screens are relatively new and currently in development, but sometimes also already implemented. The following heave screen solutions can be classified as innovative [3]:

- **Plastic screen**: A vertically closed heave screen made of plastic. Making the sheet pile of plastic reduces emissions. Furthermore, the piles weigh less and a different pile driving method is needed, since the material is less strong.[21]
- **MIP/Soilmix**: Using a milling technique, the soil is mixed, on site, with an additional material. The soil then becomes almost impermeable, forcing the water to flow around the soil mixture.[21]
- **MIP/deep mixing**: A grout suspension is drilled into the soil with a crane. While drilling, the grout suspension is injection into the soil and mixed. It creates a watertight construction that can also be used as a foundation for different structures. [29]

Drainage systems

- **Vertical drain**: A drain is applied from the top of the cover layer to the aquifer. This drain has a well at the top, where water can be collected. If the water pressure in the drainage system is lower than in the surrounding area, water will flow from the aquifer into the drainage system. This is called a passive system. However, when the water pressure in the drain is not low enough, the water is extracted from the aquifer through a pumping system. This is an active system. [42]
- **Horizontal drain**: A horizontal filter tube is applied in the aquifer under the dike body (along the length of the river). Vertical drains are placed at regular intervals, connecting the filter tube with collection wells. The water is then extracted passively or actively with a pumping system. [42]
- **Gravel box**: On of the oldest drainage systems implemented for flood defences and currently applied as a geotextile or granular filter. The gravel box is placed underneath or directly next to

a water channel behind the dike. It is embedded in the aquifer and drains the water directly from the aquifer to the surface water. This means that water is allowed to flow through the filter, but sand particles are not. [42]

There are also secondary effects that need to be considered when implementing a drainage system. By extracting water from the aquifer, the ground water level and quality can change. This could potentially induce settlements or crop damage in the surrounding environment.

Filter techniques

- **VIG (Vertically inserted geotextile)**: The geotextile is vertically inserted into the aquifer. The geotextile consists of perforations that allow water to flow through. However, the perforations are small enough to prevent sand particles from passing through. [32]
- **CSB (Coarse sand barrier)**: The barrier consists of coarser sand with particles larger than the surrounding sand in the aquifer. This increases the resistance to erosion in the filter. Additionally, the coarser sand ensures a higher permeability in the filter than in the background sand. Therefore, the flow through the filter is less strong and the sand particles from the background sand are not able to pass through the filter. The bigger the difference in permeability, the more effective the CSB is. [32]
- **Plastic Filter screen**: This technique is essentially a plastic heave screen with hollow shafts. These shafts have perforations over a limited length of the screen and they are filled with filter sand. Water can pass through the perforations and filter sand, but the background sand is not allowed to pass through. The size of the filter sand particles is specifically calibrated to the background sand. [32]

Seepage length extensions

- **Pipingberm (hinterland)**: A clay cover layer is applied on the downstream side of the dike. It extends the impermeable layer in the hinterland, moving the exit point further away from the dike. When implementing a pipingberm, it is important to consider the stability of the dike body as well. [34]
- **Clay layer (foreland)**: A clay cover layer is applied on the upstream side of the dike. It extends the impermeable top layer in the foreland, moving the entry point further away from the dike. [34]
- **Bentonite mat (foreland)**: An impermeable mat, that is relatively thin and implemented in the foreland. It is installed at a certain (shallow) depth below ground level. [21]
- **SoSEAL barrier**[1]: With this innovative technique, aluminium (Al) and dissolved organic matter (DOM) are injected into the soil at different depths [16]. These two components will interact and bind with the soil. This creates a vertical barrier underneath the dike with a reduced hydraulic conductivity. This reduced hydraulic conductivity increases the resistance for water to flow through and makes it impossible for the background sand particles to pass through.

Seepage length extensions can sometimes be difficult or impossible to implement when the space in the foreland or hinterland is limited.

[1] The SoSEAL barrier does not extend the seepage length horizontally. By reducing the hydraulic conductivity, the flow velocities are reduced, preventing the pipe from progressing [21]. When the hydraulic conductivity is significantly reduced compared to the background sand, the SoSEAL barrier also has the potential to act as a heave screen.

Overview of the piping solutions and their working principles

In Figure 2.9 below, a comprehensive overview of the different techniques and working principles is given. Furthermore, the different solutions for each technique are classified as innovative or conventional.

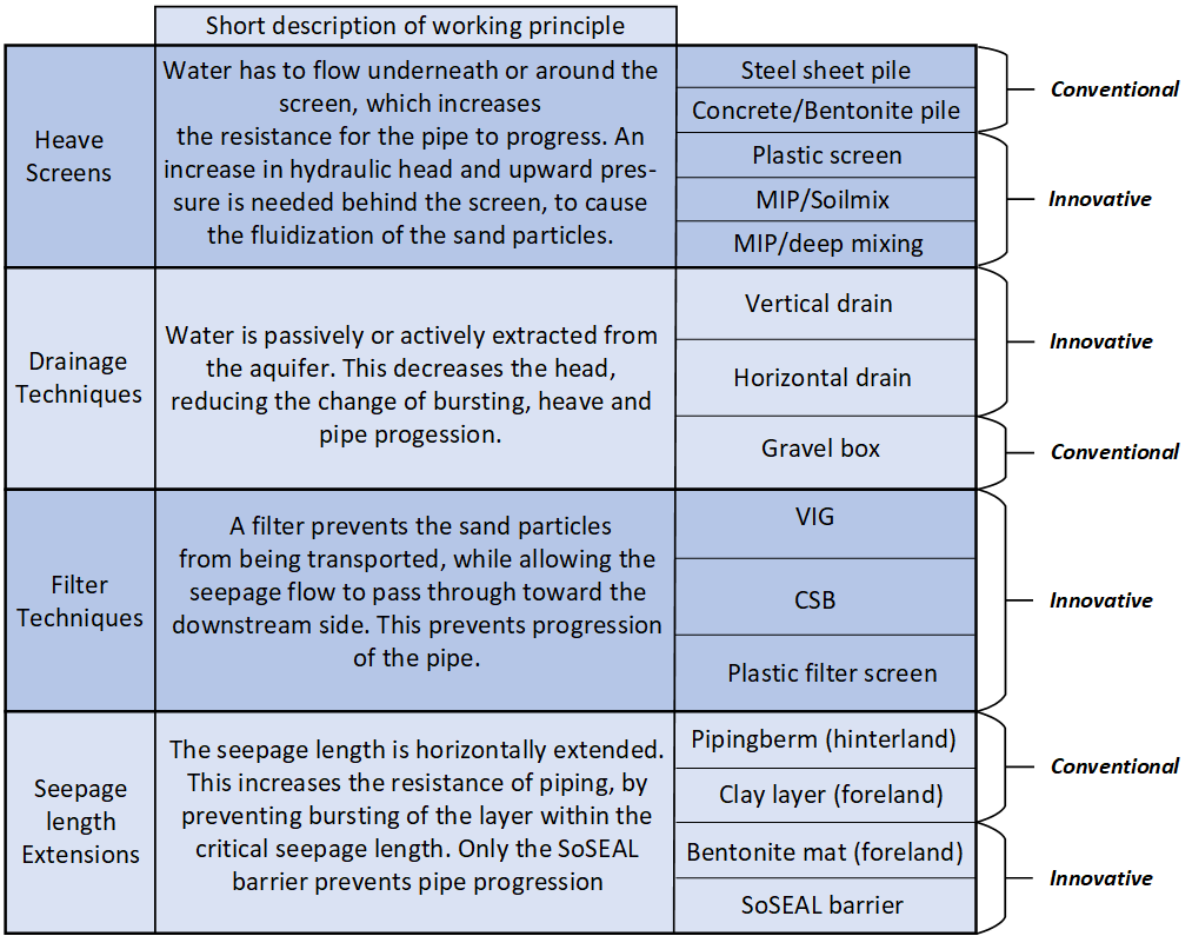

Figure 2.9: Overview of the different piping solutions and their working principles, categorized by technique.

2.3. Relevant effects and uncertainties of climate change on BEP

Since the 1800s, human activities have led to an increased use of fossil fuels. With the burning of fossil fuels, greenhouse gases are emitted and radiation is trapped. This increases the temperature on Earth and has been the start of other changing weather patterns, resulting in climate change. Climate change has caused droughts, water scarcity, wild fires, melting ice, more severe storms, increased rainfall, declining biodiversity, increased floods and sea level rise.[40]

This research focuses on piping solutions that are implemented along rivers. Therefore, this section discusses the effects of climate change that are relevant considering BEP for river dikes. Since climate change has mainly been caused by human actions, different future climate scenarios, due to different levels of human activities, are also considered in this section. Furthermore, climate change and climate scenarios are of significant importance with respect to future endeavours. However, the future is accompanied with more and increasing uncertainties. This section also elaborates on the uncertainties that come with climate change.

2.3.1. Impact of climate change on BEP

The main driving force behind BEP is the hydraulic gradient over the dike. As stated in section 2.1, an increase in the gradient can allow for the continuation of the seepage and progression of the pipe if the critical gradient is exceeded. Due to climatic changes, both soil and hydraulic conditions are affected and changes in these conditions influence the hydraulic gradient [56]. In this subsection, different impacts of climate change on BEP are discussed. Table 2.1 gives a summarized overview of the different effects and their impacts.

As stated before, increasing temperatures are one of the main driving factors behind climate change. Higher temperatures can have a significant impact on the amount of snow that is stored during the winter. When less snow is stored in the mountains, there is less melting water in summer and spring. This results in lower water levels in downstream rivers, decreasing the hydraulic gradient. Increase in mean and intense precipitation is one of the main aspects of climate change that also influences riverine water levels [56]. An increase in precipitation can cause higher discharges and elevated water levels in the river, resulting in an increase in the hydraulic gradient. However, an increase in rainfall can also cause the water levels in the channels on the downstream land side of the dike to increase faster than the levels in the river. This would result in a decrease in the hydraulic gradient. Another significant effect of climate change are droughts. Droughts can cause compaction of the soil, resulting in an increase in the subsidence of the hinterland on the downstream side [30]. This increases the hydraulic gradient over the dike.

Besides impacting BEP by influencing the hydraulic gradient, these climate changes can also influence the soil conditions. Droughts can also cause the formation of cracks in the top layer, when the clay starts to dry [56]. As described in subsection 2.1.1, such a crack, when fully developed through the top layer, causes an open exit. One of the first steps in the BEP process is then initiated. Additionally, an increase in intense precipitation can cause the soil to erode. When the top clay layer behind the dike is subdued to soil erosion, an open outlet can occur and the process of pipe formation can start as well.

Aspect of climate change	Effect	Impact on BEP
Increase in temperature	Less snow is stored during winter, resulting in less melting water and lower river levels in spring and summer.	Decrease in upstream water levels, decreasing the hydraulic gradient
Increase in precipitation	higher discharges and elevated river levels.	Increase in upstream water levels, increasing the hydraulic gradient
Increase in precipitation	Faster rising downstream water levels in the channels.	Increase in the downstream water level, decreasing the hydraulic gradient
Drought	Compaction of the soil, causing subsidence of the land on the downstream side.	Decrease in the downstream level, increasing the hydraulic gradient
Drought	Drying of the top clay layer, causing cracks to form	Formation of exit point
Increase in intense precipitation	Soil erosion of top clay layer on the downstream side.	Formation of exit point

Table 2.1: The different effects of climate change and their impact on piping.

Thus, droughts and increased mean and intense precipitation influence the hydraulic gradient and other soil conditions, impacting the processes of backward erosion. The future developments of these changes are however dependent on the amount and type of human activities. To project the different ways these climate changes can advance, different climate scenarios have been developed to give more insight. In the next section, the different scenarios and climate change developments are further discussed.

2.3.2. Climate scenarios

Human activities have been the main drivers behind the increase in global temperatures and the resulting changes in the climate. Different climate scenarios are developed and each scenarios represents a different future climate, due to human actions. In Figure 2.10, the future increase in global temperature can be seen for the different scenarios. These scenarios are developed by the IPCC and differ from each other in the amount of greenhouse gases that are emitted. Each scenario represents a different socio-economic pathway. For example; SSP5-8.5 represents a path where fossil fuels remain the main source of energy, resulting in a significant amount of emissions and thus a high increase in global temperature. Similarly, SSP1-2.6 represents a path in accordance with the Paris agreement, minimizing emissions and eventually stabilizing the change in global temperature.

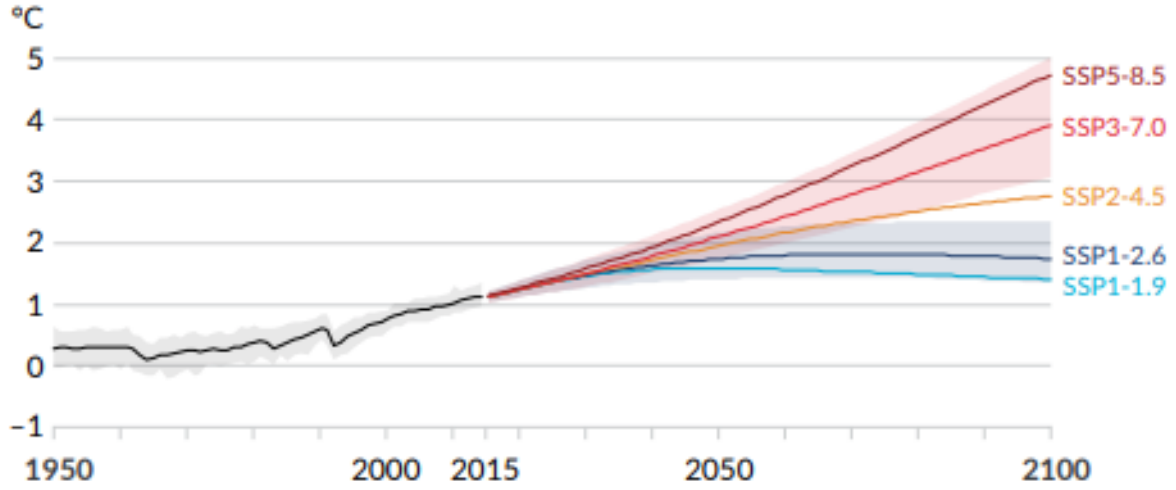

Figure 2.10: Global change in temperature for the five different SSP scenarios, relative to 1850-1900 [13].

Subsequently, each climate scenario has a different contribution to different climate change effects. With respect to the average change in annual precipitation globally, it is expected that by SSP1-1.9 there will be an increase of 2.4% in 2081-2100 compared to 1995-2014. For SSP2-4.5 this will be an increase of 4.6% and for SSP5-8.5 an increase of 8.3% [8]. Furthermore, the frequency and intensity of extreme hot events, heavy precipitation events and drought events increases for increasing global temperature.

The KNMI has partly used IPCC data and reports to address future climate change effects in the Netherlands. This is done for different climate scenarios as well. The KNMI differentiates three different emission scenarios; a high (H) emission scenario, a moderate (M) emission scenario and a low (L) emission scenario. The H scenario is according to the SSP5-8.5 pathway, the M scenario is according to the SSP2-4.5 pathway and the L scenario is according to the SSP1-2.6 pathway [55]. Additionally, the KNMI developed two different types of scenarios alongside the emission scenarios. This second type is based on the uncertainty in the regional precipitation and resulted in a dry scenario and a wet scenario. Eventually, there are six different climate scenarios developed for the Netherlands, as are outlined in Table 2.2. In this study, the low emission scenario is not considered. This is further elaborated on in section 3.3.

	Dry scenario	Wet scenario
High emission scenario	**Hd**	**Hn**
Moderate emission scenario	**Md**	**Mn**
Low emission scenario	**Ld**	**Ln**

Table 2.2: The six different climate scenario developed by the KNMI [55].

To conclude, for each scenario, the projected climate changes are different. However, the projected trend for most climate effects is the same for each scenario, showing an an increase. The main differ-

ence is the magnitude of the observed change, which is often highly depended on the scenario. Still, the different climate scenarios together with the impacts of climate change and changing weather patterns, are accompanied with many uncertainties. In subsection 2.3.3 these uncertainties are further elaborated on.

2.3.3. Uncertainties of climate change

As stated before, climate change is the resulting effect of how the climate system reacts to changes in the amount of greenhouse gases in the atmosphere. In the extent to which the climate reacts to these changes, lies a deep uncertainty. This deep uncertainty refers to the lack of being able to assign probabilities to future events because the possible outcomes or the likelihood of the different scenarios are unknown. In addition, there is still no general agreement on how to best model the climate, since many processes are difficult to predict and model. [38]
These uncertainties become even larger when looking at a more regional scale, e.g. looking to the Netherlands. Different processes, like precipitation, cloud coverage, radiation, evaporation, etc. in the summer are still less certain and less understood. By doing more research and improving climate models some of these uncertainties can be minimized. However, a significant part of the climate consists of natural variations, with sometimes big outliers as well. In addition, there are still processes that are hard to capture and simulate with a model. Volcanic eruptions and changes in the Gulf Stream, for example, are hard to predict and quantify. These natural variations occur on every timescale and are sometimes difficult to distinguish from a trend. So, even though a climate model is able to capture the processes very well, it does not necessarily mean the trend it shows is accurate [11].

Besides the scientific uncertainties in the climate system and its processes, there are thus also uncertainties in the climate scenarios. As stated in subsection 2.3.2, each SSP corresponds to a different path of human activities and the amount of emissions that come with it. The future path closest to what will become reality is still deeply uncertain. This depends largely on political and (socio-)economic developments. Climate policies are largely responsible for the amount of greenhouse gases that will be emitted. Due to these future uncertainties, there are no probabilities assigned to the different SSP and KNMI emission scenarios [11]. Additionally, each individual scenario has its own uncertainties as well. This comes partially from the previously described uncertainties and sensitivities in the climate processes. Even with a lower emission scenario, the most likely warming of a higher emission scenario can be reached. Furthermore, certain climate feedbacks can have a significant effect on the uncertainties of scenarios. For example; deforestation, emissions from the thawing of permafrost and decreasing carbon storage capacities of the oceans can influence the amount of greenhouse gases in the atmosphere. These feedbacks are currently yet to be adequately included in the SSP's [11].

So, there are deep uncertainties in the likelihood of the different scenarios and many uncertainties within each scenario as well. It is therefore important to incorporate these uncertainties into the decision-making for designs with respect to future scenarios.

3

Grebbedijk improvement project

In this thesis the Grebbedijk improvement project is used as a case study. In this chapter, an introduction and overview of the Grebbedijk project are covered first. In the following sections characteristic variables from the Grebbedijk and the river Nederrijn are defined. These variables will serve as input values and boundary conditions for the numerical model, as described in chapter 5.

3.1. Introduction to the Grebbedijk

The methodology that is used in this research to evaluate the design and life cycle of different piping solutions, can be applied in various situations and locations. However, as stated before, this research is focused on dikes along the upper rivers of the Netherlands. This means that high water levels last for a relatively long period of time. The water levels are therefore treated as stationary. Furthermore, by using a case study the different piping solutions are evaluated in representative conditions and give tangible results. The Grebbedijk improvement project is a representative case. The dike is located along the Nederrijn, which is considered to be an upper river [60]. Additionally, multiple dike sections are known to have a piping problem.

The Nederrijn is a regulated river during low and medium discharges, allowing the water level to be controlled and the flow at the IJsselkop to be directed toward the IJssel, see Figure 3.1.

Figure 3.1: The system of the Nederrijn, including the Grebbedijk.

The Grebbedijk is 5,5 km long and lies between the city of Wageningen and the Grebbeberg, see Figure 3.2. The dike protects the Gelderse Vallei from high water levels from the Nederrijn. As stated, multiple sections of the dike in this project need to be reinforced with measures against piping. (Parts of) dike sections 1D, 1E, 3A, 3B, 3C, 3D and 4B are prone to piping [58].

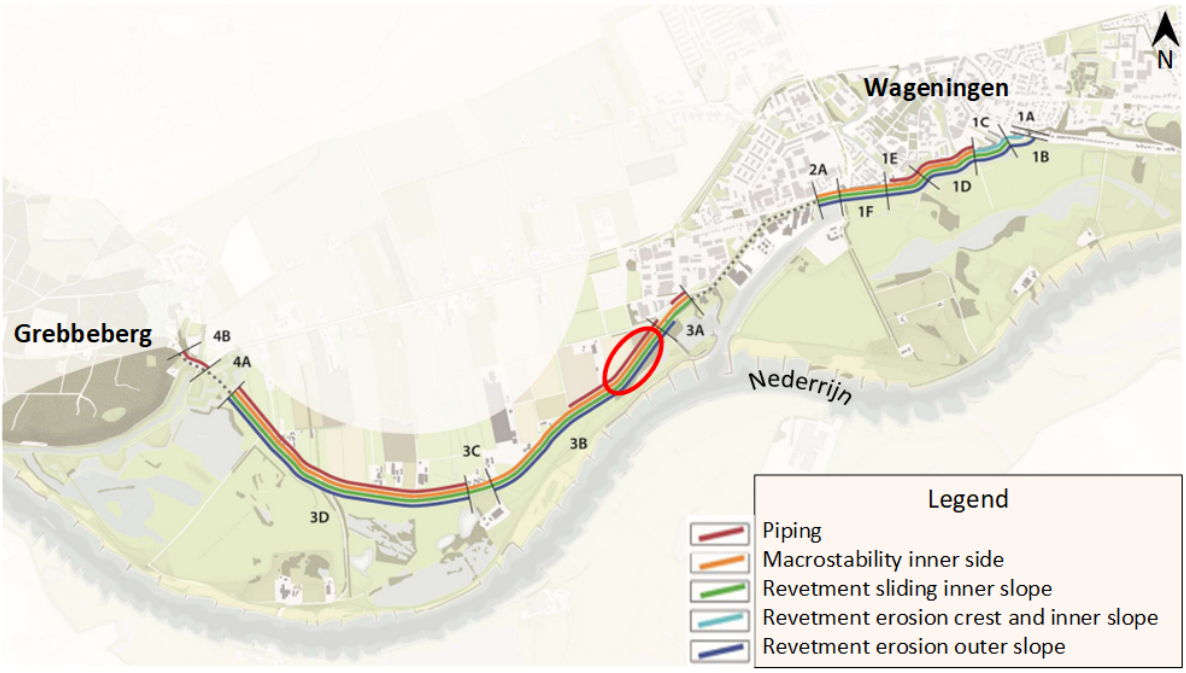

Figure 3.2: The Grebbedijk, divided in sections. Each section needs to be reinforced for the problems as defined by the legend. The critical dike profile assessed in this thesis is circled in red. (Adapted from [57])

For this research dike section 3B is chosen as the representative section to be evaluated, as the first part of this section is prone to piping, see Figure 3.2. This part of the dike has a relatively smaller foreshore and thus lies closer to the Nederrijn with respect to other dike sections. This means that there are less uncertainties and discrepancies to take into account regarding the soil profile between the dike and the river. This makes the soil characteristics that are taken as input for the model more reliable.

The Grebbedijk is denoted as dike trajectory 45-1 by the Dutch government. This dike trajectory has a relatively high safety standard that requires a failure probability of P = 1/100,000 per year [39]. When this probability is exceeded, the government has time to reinforce the dike, before the lower threshold is exceeded. Current guidelines, however, are based on the lower threshold. When designing a dike, the imposed safety standard is converted to a lower threshold, which is called the maximum allowable probability [50]. This maximum allowable probability is three times the imposed safety standard. The probability used for the design of the dike then becomes P_{norm} = 1/30,000 per year. This is used as the total maximum allowable probability for the failure of the dike. When determining the maximum allowable probability due to the piping failure mechanism, the following formulas are used [50]:

$$P_{req,sec} = \frac{\omega}{N} \times P_{norm} \tag{3.1}$$

$$N = 1 + \frac{a * L}{b} \tag{3.2}$$

- $\omega[-]$: Failure probability space for the piping failure mechanism.
- $N[-]$: Length effect factor of the piping mechanism.
- $a[-]$: Fraction of length L that is sensitive to the failure mechanism.
- $b[m]$: Length of typical independent segment for the piping mechanism.
- $L[m]$: Length of the dike section 3B.

In Table 3.1 the factors for the length effect and the reliability budget for piping can be seen.

Failure mechanism	Reliability budget (ω)	$a[-]$	$b[m]$	$L[m]$	$N[-]$
Piping	24 %	0.9	300	1240	4.72

Table 3.1: The factor N for piping based on the length effect factors and reliability budget.[48]

This results in a maximum allowable failure probability for piping of $P_{req,sec} = 1/590,000$ (or $1.695 * 10^{-6}$) for dike section 3B. Also referred to as the target probability.

3.2. Grebbedijk characteristics

In this section multiple characteristics of the dike segment from section 3B are identified and described. The identified characteristics are significant variables with respect to the backward erosion piping mechanism and have an influence on the progression of the pipe. The described characteristics also serve as input variables and/or boundary conditions in the numerical model, see section 5.4.

3.2.1. Grebbedijk cross section

The cross section and soil profile of the considered dike segment are based on a CPT probe [41], see Appendix B, a profile analysis done by RoyalHaskoningDHV (2018) and elevation data from the AHN [2]. The critical dike profile for this segment is at dike post 25, see Figure 3.2 [51].

With respect to the piping mechanism there are several important variables that need to be identified. The geometry of the dike itself determines the seepage length, and the height of the crest has a significant influence on the maximum allowable hydraulic head on the upstream side. In this thesis however, only the piping failure mechanism is considered. It is therefore assumed that the crest will most likely be heightened in the future and overtopping will not occur for the predicted water levels. The dimensions of the soil profile below the dike also have a significant effect on the development of the pipe. Since the pipe develops at the interface of the cover layer and the aquifer, the level at which this boundary lies is an important characteristic. The depth of the aquifer is an important parameter to be considered as well. In Figure 3.3 a schematised cross section of the critical dike post is presented.

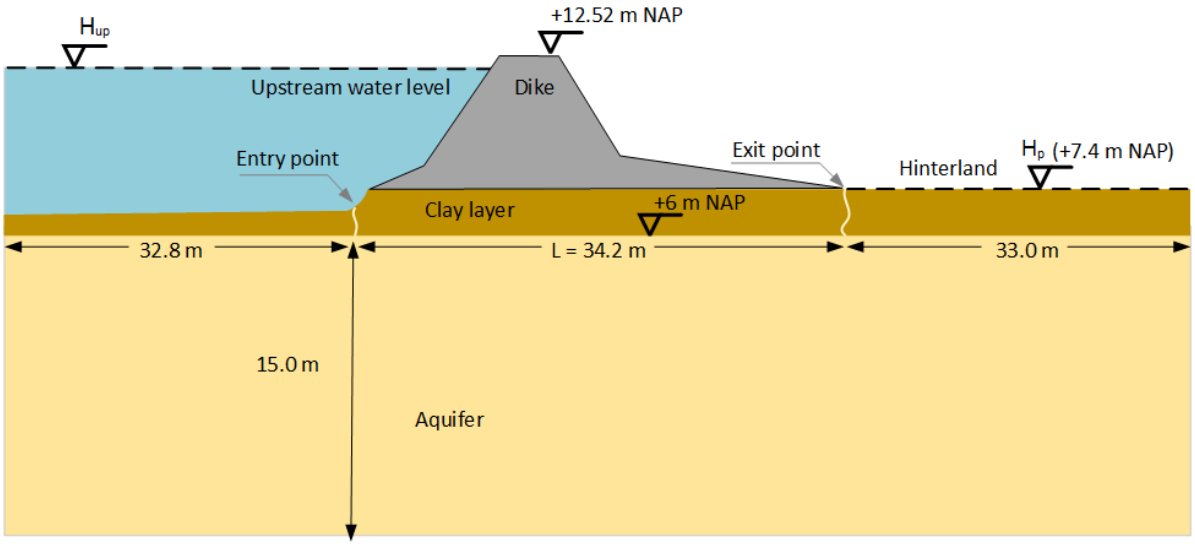

Figure 3.3: Schematized cross section of the critical dike post 25.

The locations of the entry point and exit point, as presented in Figure 3.3, are acquired from the safety analysis by Royal HaskoningDHV [51]. The foreland is relatively small at this dike post and consists of sandy layers. The location of the entry point near the outer toe of the dike is therefore assumed to be reasonable. The exit point is assumed to be near the inner toe of the dike.

3.2.2. Soil characteristics

For the progression of backward erosion piping, the groundwater flow and the size of the sand particles are important aspects. To model these aspects representatively, the 70th-percentile value of the particle size distribution (d_{70}), the hydraulic conductivity (K) and/or the permeability (k) of the soil are essential characteristics. RoyalHaskoningDHV (2018) has already performed an analysis based on particle size distributions from multiple boreholes. After statistical processing, different useful values for d_{70} were obtained. See Table 3.2.

Statistical processing	d_{70}	
Mean	430	$[\mu m]$
standard deviation	136	$[\mu m]$
Minimum	201	$[\mu m]$
Maximum	732	$[\mu m]$
Variation coefficient	0.317	$[-]$
95% Low average	307	$[\mu m]$
95% High average	552	$[\mu m]$

Table 3.2: $d70$ values after statistical processing from the particle grain size distribution analysis, following a log-normal distribution [51].

Furthermore, the hydraulic conductivity is calculated with the formula of Den Rooijen, see Equation 3.3. This resulted in a hydraulic conductivity K of 50.9 m/day or $5.89 * 10^{-4} m/s$ [51].

$$K = (c_0 - \frac{1.83 * 10^3}{m * s} ln(U)) d_{10}^2 \tag{3.3}$$

- K: the 95% high average value for the hydraulic conductivity (K_{H95}).
- c_0: packing coefficient for loose sand ($1.5 * 10^4 m/s$).
- U: uniformity coefficient is d_{60}/d_{10}. The 95% high average values for d_{60} and d_{10} are used.
- d_{10}: 10th-percentile value of the particle size distribution.
- d_{60}: 60th-percentile value of the particle size distribution.

There are no additional measurement data available for the hydraulic conductivity. The statistical processing for K is performed by assuming a variation coefficient (VC) of 0.5 [48]. The spread of the values for K is unknown, but a log-normal distribution is assumed to determine the statistical values. By performing the following steps, the mean and standard deviation are calculated.

- $\sigma_{lnK} = \sqrt{ln(1 + VC^2)} = 0.4725$
- $\mu_{lnK} = ln(K_{H95}) - 1.645 * \sigma_{lnK} = 3.1528$
- $\mu_K = e^{\mu_{lnK} + 0.5\sigma_{lnK}^2} = 26.16[m/day] = 3.03 * 10^{-4}[m/s]$
- $\sigma_K = \mu_K \sqrt{e^{\sigma_{lnK}^2} - 1} = 13.08[m/day] = 1.51 * 10^{-4}[m/s]$

Using the mean and standard deviation values after statistical processing, Table 3.3 is acquired.

Statistical processing	K	
Mean	$3.03 * 10^{-4}$	$[m/s]$
standard deviation	$1.51 * 10^{-4}$	$[m/s]$
Variation coefficient	0.5	$[-]$
95% Low average	$1.25 * 10^{4}$	$[m/s]$
95% High average	$5.89 * 10^{-4}$	$[m/s]$

Table 3.3: K values after statistical processing, following a log-normal distribution.

Subsidence is another important parameter to take into account when considering piping. Due to subsidence, the hydraulic head difference over the dike can increase. However, the analysis of Royal-HaskoningDHV and current subsidence maps of the Netherlands show that future soil settlements or subsidence are not expected at the location of the Grebbedijk [17] [47]. In this thesis, future soil subsidence is therefore not taken into consideration.

Lastly, K and d_{70} are important input parameters for the piping solutions to be modelled. It is therefore essential to consider the uncertainties associated with these parameters and their potential impact on the output.
The parameter d_{70} is derived from regional field measurements, meaning the available values form a regional dataset compiled from soil investigations conducted over a larger area and at different points in time [51]. As a result, local soil characteristics along the dike section may deviate from the regional average. Although d_{70} is applied in the model as a stochastic input parameter, its inherent uncertainty still influences the performance of the solutions and thus the outcomes of the analysis.
For very low K values, the pressure gradient may not be able to become sufficiently high for the erosion pipe to continue to develop [1]. Unlike d_{70}, K has not been determined directly from field surveys or measurements but is instead estimated using the formula of Den Rooijen. This formula takes estimated parameters for the packing coefficient (c_0) and uniformity coefficient (U). In this thesis, the hydraulic conductivity is also applied as a single value for the aquifer and does not differ in horizontal or vertical direction. Anisotropy is thus not considered. In addition, an assumption regarding the coefficient of variation was made, which significantly influences the constructed distribution of K. In reality, however, K and d_{70} are also correlated, which influences the shape of the distribution and, consequently, the generated samples. Different assumptions on K and its distribution can therefore lead to different piping behaviours being captured in the modelling.
Finally, according to Aguilar-Lopez et al., the aquifer depth has no significant influence on piping behaviour for depths greater than approximately 8 m [1]. As the aquifer in this study exceeds that depth, uncertainties in aquifer depth are expected to have no significant impact on the results.

3.3. Climate projections for the Rhine river system

In this section, the current and future conditions of the Nederrijn are discussed. These conditions depend on the developments and conditions of the Rhine. This is significantly influenced by climate projections for the whole Rhine river system. These projections and the uncertainties that come with them are also explained in more detail. Lastly, the current and future water levels at the critical dike section are discussed.

The water level at the Grebbedijk is currently regulated and kept at a minimum of 6.0 m NAP for navigational purposes. This regulation is done at the IJsselkop and through the weir at Driel. When the discharge at Lobith, which lies a little south of the IJsselkop, exceeds $3600m^3/s$, the weirs are fully opened. [62].
The maximum water level at the Grebbedijk is thus dependent on the maximum discharge at Lobith. This maximum discharge, however, is subject to uncertainties. When peak discharges of the tributaries of the Rhine and the Rhine itself coincide, they can cause an increase in the maximum discharge [59]. Incidents in the upper parts of the Rhine river system, however, can decrease the maximum discharge. A dike breach along the Rhine in Germany, depending on the location, can lead to lower discharges at Lobith. The variations of the heights of the dikes along the upper parts of the Rhine in Germany have a significant influence on potential dike breaches and thus the maximum discharge at the Grebbedijk [24]. Additionally, there is no clear maximum to the volume of water at Lobith during high water levels and the time span of high water levels is not dependent on the maximum discharge. As a result, the duration of high water levels can be underestimated when only looking at peak discharges and would undervalue piping as a failure mechanism [59]. This supports the assumption to treat the high water levels as stationary at the Nederrijn.

Climate scenarios also influence the discharges of the Rhine. For all the different climate scenarios, regarding the KNMI'23 scenarios as explained in subsection 2.3.2, the average discharges in the winter and spring season increase. However, the further these scenarios extend into the future, the greater the associated uncertainties. All scenarios project a rise in temperature. Consequently, less snow will accumulate in the mountains during winter, resulting in reduced meltwater during spring and summer and, therefore, lower Rhine discharges. In contrast, the wet scenarios, both high and moderate, predict an increase in annual average precipitation across the Rhine basin, albeit with considerable uncertainty. Additionally, all scenarios project an increase in the annual maximum discharge. [5]

To estimate the water levels at the specific dike section, they are probabilistically modelled using the Hydra-NL model. This model calculates the water levels for different return periods, based on the statistics of previously measured water levels. With Hydra-NL the different climate scenarios and discharge uncertainties at Lobith can be taken into account. The water levels can be calculated for the years 2050 and 2100 and a moderate or high emission scenario can be considered. However, the emission scenarios in Hydra-NL are based on the KNMI'06 scenarios. Future water levels are therefore not estimated using the most recent climate scenarios and a lower emission scenario was not considered back then [55]. The estimated water levels are still considered to be sufficiently accurate for future sight years. In this thesis, the future water levels are simulated for a moderate G scenario, corresponding with SSP2-4.5, and a high emission W+ scenario, corresponding with SSP5-8.5. Both scenarios are simulated with a capped discharge at Lobith of $18\,000\,\mathrm{m}^3/\mathrm{s}$ and without a cap on the discharge. The water levels are also extrapolated to 2150 for each climate scenario. The difference between the water levels of 2100 and 2050, for each return period, is added to the water levels of 2100 to get the data points for 2150. To construct the probability density functions of the water levels for the different future sight years, the data is first fitted. A composite fit of the Weibull and Generalized pareto distribution (GPD) is used, see Figure 3.4. The GPD fits the water levels of the higher return periods in the tail better than a Weibull fit alone. The Weibull fit alone overshoots the water levels for the higher return periods. In Appendix A, the calculated water levels by Hydra-NL and their composite fit for each climate scenario is presented.

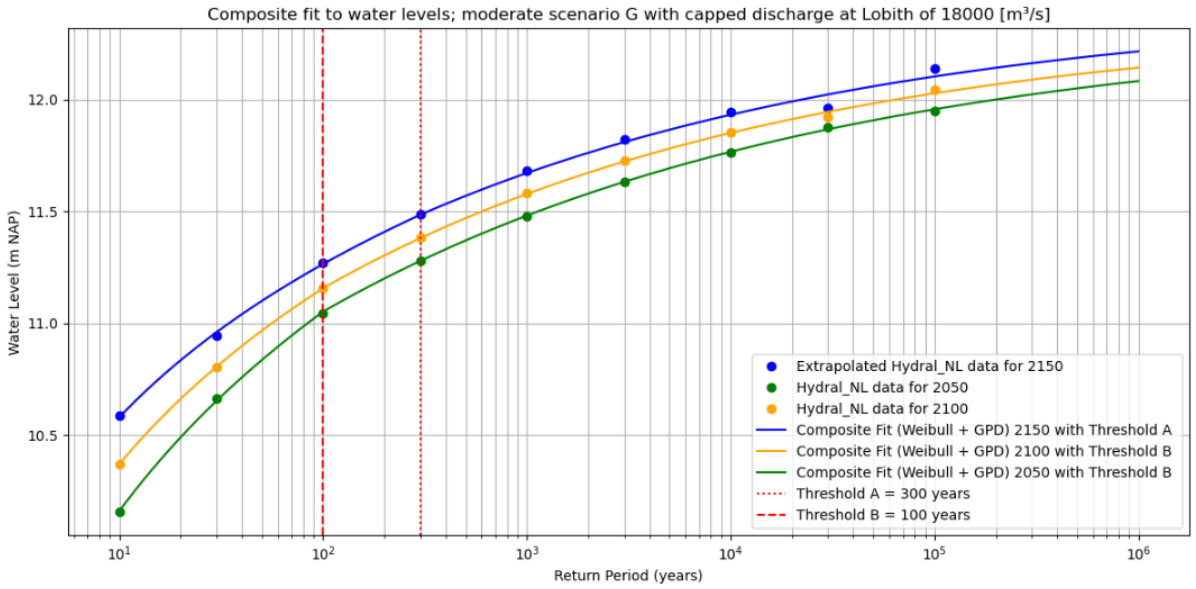

Figure 3.4: An example of the composite fit to the data of the moderate scenario G with a capped discharge at Lobith. The threshold indicates the transition between the Weibull fit (left part) and GPD fit (right part). This composite fit is also applied on the other scenarios.

In the graphs below the probability density functions of the water levels for the different scenarios and future sight years are shown.

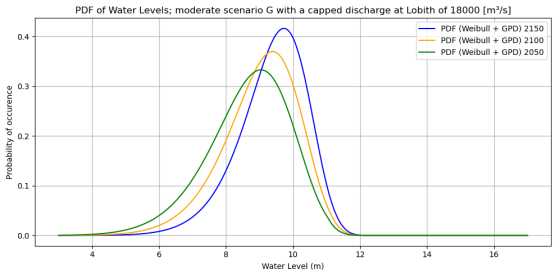

(a) PDF for scenario G with a capped discharge.

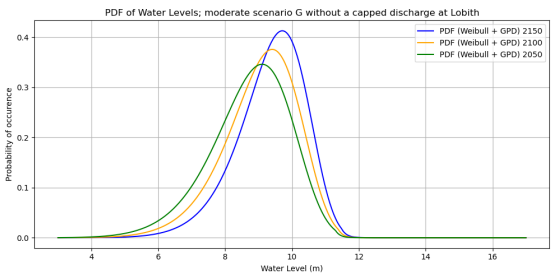

(b) PDF for scenario G with an uncapped discharge.

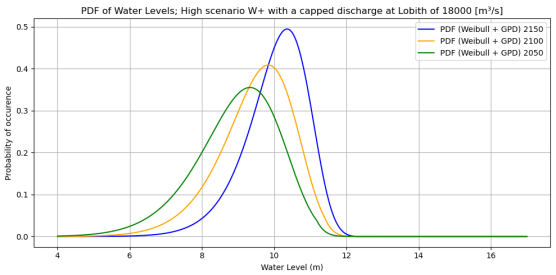

(c) PDF for scenario W+ with a capped discharge.

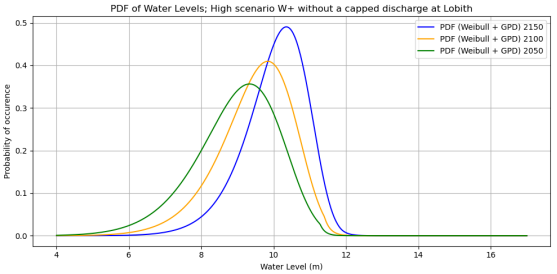

(d) PDF for scenario W+ with an uncapped discharge.

Figure 3.5: Probability density functions for the different climate scenarios and future sight years, using the composite fit.

4

Research selection of piping solutions

4.1. Introduction to the selected piping solutions

As stated in section 1.1, research has led to innovative piping solutions that differ from conventional solutions in their working principles and life cycle costs. It is uncertain how these innovative solutions perform, with respect to their design and life cycle, when compared to the conventional solutions. To make this comparison, innovative and conventional piping solutions are both researched in this thesis. The selection of piping solutions is made from the available solutions as described in subsection 2.2.2. With respect to the available time for this thesis, the number of selected solutions is limited to three.

A sheet pile and a pipingberm are two conventional solutions that have been widely implemented over the years. The sheet pile, however, is applicable in a wider range of situations than the berm. The available construction space behind a dike is often limited, due to natural areas or buildings. In these cases, the implementation of a berm is often not desired. In case the space behind the dike is sufficient, the required extension of the seepage length is often very large. As a result, the amount of expensive material needed makes a piping berm already cost-ineffective. The conventional sheet pile is considered more versatile and therefore selected to be researched.
As for the innovative solutions, many different designs and techniques are possible. In this thesis the plastic filter screen and SoSEAL barrier are selected. Both solutions show promising developments and have different working principles. Furthermore, their design, design life and costs regarding maintenance and investments are different. These aspects make the solutions interesting when comparing their performance and life cycle costs. The Prolock filter screen is a specific plastic filter screen that has promising prospects, and RPS has experience in both development and implementation. The design of the Prolock filter screen is therefore used as an initial design. The SoSEAL barrier is an innovative solution that my supervisor, Anne-Catherine, has substantial experience with and knowledge about.

The following sections describe the management and design considerations from the design guidelines for the three piping solutions in more detail.

4.2. Sheet pile

This section describes the design criteria and considerations when designing a sheet pile as a piping solution. In addition, management actions regarding maintenance and monitoring during the life time of the construction are discussed. For the working principles of the sheet pile, see subsection 2.2.1.

Witteveen+Bos has already performed an analysis on a specific type of sheet pile at multiple dike sections of the Grebbedijk [63]. In this thesis the same sheet pile design is used and modelled. The steel sheet pile is of the type AZ24-700 and has a thickness of $11.2mm$.
The position of the screen is the following step in the design process of the sheet pile. There are mainly three options; At the end of the dike near the inner toe, at the transition of the slope of the dike to the inner berm and underneath the body of the dike [4]. Placing the sheet pile underneath the body of the dike is often not preferred due to construction difficulties. At the end of the dike, the sheet pile can

be vulnerable to local instabilities on the downstream side. The sheet pile is therefore placed at the transition point of the slope. This position is also preferred from the modelling perspective, as explained in section 5.4. This placement can additionally limit the possible failure paths and the sheet pile can contribute to the macrostability of the dike as well.
The next design consideration is the depth of the sheet pile. According to the design guidelines, the design process should start with a minimum sheet pile depth of $3m$ into the aquifer [4]. This should be the minimal length to prevent hydraulic heave behind the screen and tackle pipe progression, without the occurrence of underflow. After an iterative process, the designed sheet pile depth to meet the safety standards is $3.5m$, see Figure 4.1. This process is in short explained in Appendix C.

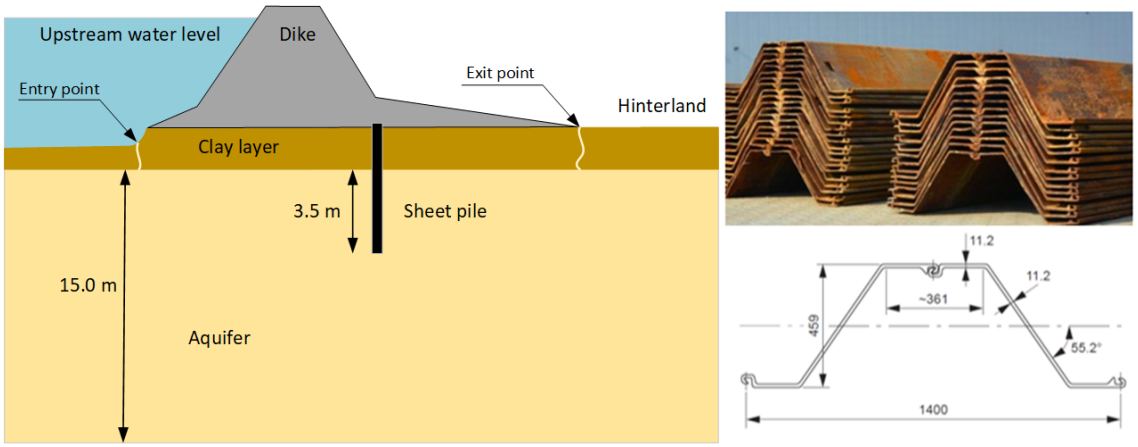

Figure 4.1: A schematisation of the sheet pile design on the left. The specific dimensions of the AZ24-700 on the right [7].

In Figure 4.2, the events that result in a piping failure when a sheet pile is implemented are shown in eight steps. The sheet pile design tackles piping by preventing the progression of the pipe at the location of the solution. By intercepting the progression at step six ($S6$), dike failure due to piping is prevented. The design is therefore tested against hydraulic heave behind the sheet pile. When the sheet pile satisfies the criteria, the acting hydraulic gradient over the length of the sheet pile should be lower than the critical gradient that allows for movement of particles. This is further described in section 5.3.

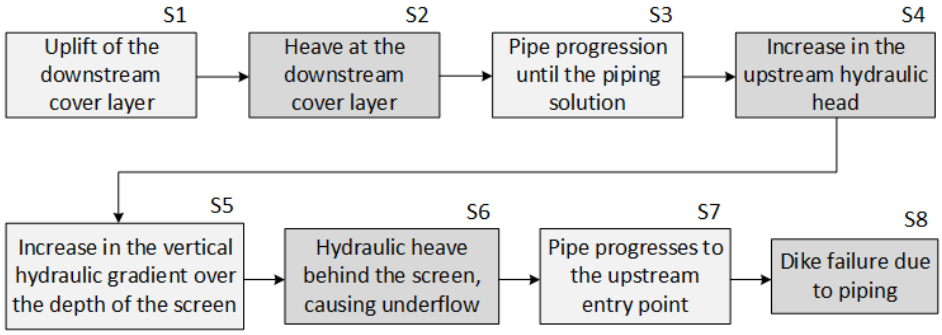

Figure 4.2: The failure steps for the sheet pile with the events that lead to failure of the dike due to piping. The sheet pile intercepts the BEP process at step $S6$.

During the lifetime of the construction it is important to monitor the performance and quality of the construction. Future dike strengthening can lead to soil deformations, which can negatively affect the integrity and stability of the sheet pile. Monitoring soil deformations is therefore important. To assess if the behaviour of the sheet pile is as expected, inspections should be made during high water levels. Possibly unexpected behaviour can then be detected. When a sheet pile is not correctly designed, the construction can be difficult and costly to repair or replace. However, a properly designed sheet pile construction requires a relatively low amount of maintenance and/or repairs. [4]

Although useful information regarding monitoring during the management phase of the sheet pile is given, climate change uncertainties are rarely mentioned by the guidelines. They are not considered in the designing process of the sheet pile.

4.3. Plastic filter screen

This section describes the design criteria and considerations when designing a plastic filter screen as a piping solution. In addition, management actions regarding maintenance and monitoring during the lifetime of the construction are discussed. For the working principles of the plastic filter screen, see subsection 2.2.1.

Similarly to the sheet pile, the design process for the plastic filter screen starts with the positioning of the screen [32]. Following the same criteria, the filter screen is placed underneath the dike at the slope transition as well. The same positioning also makes for a better comparison with the sheet pile. As stated before, the design of the Prolock screen is used as the initial design of the plastic filter screen. After testing, it was observed that placing the filter part of the Prolock design over the full depth of the screen, except the bottom $0.5m$, showed the best performance. Design guidelines state a minimal embedding depth of $1.5m$ into the aquifer. If the screen is embedded deeper in the soil, the filter part increases in length and the closed part of the filter is applied deeper into the aquifer. This ensures extra robustness in the design, as it increases resistance to hydraulic heave behind the screen [37]. After an iterative process, the designed depth of the filter screen to meet the safety standards is $2.5m$, with a $2m$ filter screen at the top and a closed screen of $0.5m$ at the bottom. This is also briefly elaborated on in Appendix C.

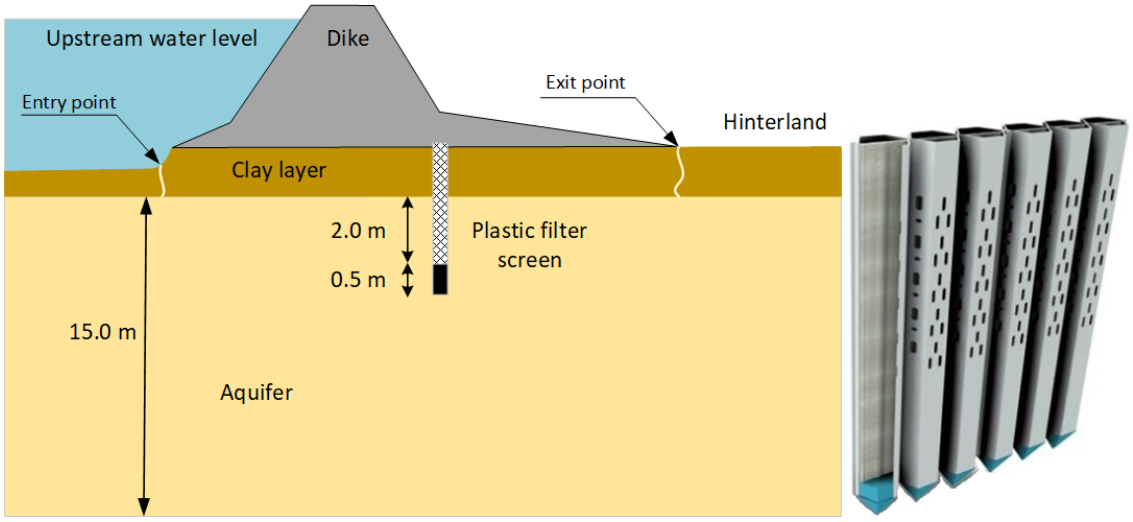

Figure 4.3: A schematisation of the plastic filter screen design on the left. The filter part is $2m$ long and the closed part is $0.5m$ long. The original Prolock filter screen is seen on the right [45].

For the plastic filter screen, the same failure steps as for the sheet pile, described in Figure 4.2, are applied. An important distinction between the sheet pile and plastic filter screen, however, is that the plastic filter screen allows water to flow through the screen. It is therefore possible that, due to uncertainties in the filter or poor design, the pipe could progress horizontally through the filter. In this thesis, this failure path is not checked and only underflow is considered. Pipe progression is thus tackled by preventing hydraulic heave ($S6$) behind the screen. This is further discussed in section 5.3. To ensure no sand is transported through the screen, the design of the perforated filter and filter sand is considered with respect to the background (aquifer) sand. The filter needs to meet multiple criteria for this assessment. The first check is the stability criterion, see Equation 4.1 [37]. With this criterion the stability of the background sand is checked. Meeting the criterion reduces the possibility of clogging of the filter.

$$C_u = d_{60}/d_{10} < 8 \tag{4.1}$$

C_u, the uniformity coefficient, is determined by the $d_{60}[\mu m]$ and $d_{10}[\mu m]$ of the background sand. From the analysis of Royal HaskoningDHV, the d_{60} and d_{10} are known [51]. This results in the following uniformity coefficient: $C_u = 375/161 = 2.33 < 8$
So the criterion is met and the stability of the background sand is sufficient.
The design of the filter screen and filter sand is based on the following two criteria:

$$d_{15F} \geq 5d_{15S} \tag{4.2}$$

$$C'_u \leq 3mm : O_F \leq 1.5(C'_u)^{0.3}d'_{85} \; or \; C'_u \geq 3mm : O_F \leq 13.5d'_{85}/(C'_u)^{1.7} \tag{4.3}$$

With criterion 4.2, the permeability of the filter is checked [37]. This criterion ensures sufficient groundwater flow through the filter sand. With d_{15F} being the d_{15} of the filter sand and d_{15S} being the d_{15} of the background sand.
To ensure the retention of the filter sand and the background sand, the width of the perforations need to meet criterion 4.3. With C'_u being the linear uniformity coefficient, d'_{85} is the linearized d_{85} of the background sand and O_F is the perforation width in mm. This criterion is based on medium compacted sand, which should be assumed after installation of the filter screen. Both the width and amount of perforations and grading of the filter sand influence the total hydraulic conductivity of the filter screen. To model the filter screen design an equivalent hydraulic conductivity is used, which takes both the perforations and filter sand into account. The correlation between the two and their impact on the equivalent hydraulic conductivity is unknown and should be determined by scale tests. This is not done in this thesis. The equivalent hydraulic conductivity is therefore based on the scale tests as described by the design guidelines [37]. The guidelines give key values for the equivalent hydraulic conductivity of the filter relative to the hydraulic conductivity of the background material for a perforation width of $0.5mm$, see Figure 4.4. It is assumed that with a perforation width of $0.5mm$ and the resulting equivalent hydraulic conductivity, both criteria 4.2 and 4.3 are met. Using the hydraulic conductivity of the in-situ sand of $50.9[m/d]$, the resulting equivalent hydraulic conductivity of the filter screen is $38[m/d]$ ($4.40 * 10^{-4}[m/s]$). This equivalent hydraulic conductivity is used as the design value for the filter of the plastic filter screen.

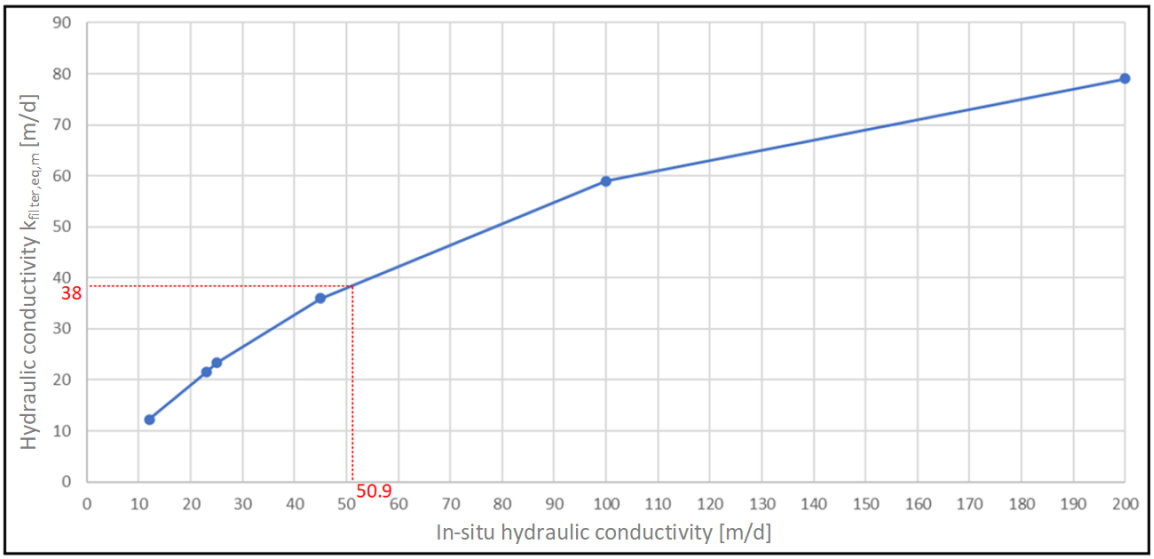

Figure 4.4: The equivalent hydraulic conductivity of the filter for a perforation width of $0.5mm$, with respect to the hydraulic conductivity of the background sand [37].

During the lifetime of the construction, the filter screen should be monitored to ensure that it functions as expected and meets safety standards. monitoring data should be compared with control data, from right after the installation of the filter [37]. This comparison should be used to assess whether further inspection or even repairs are needed. Furthermore, climate change should be considered when designing the plastic filter screen, according to the guidelines [37]. They do not expand on how to incorporate climate change in the design process. Monitoring and visual inspections should focus on checking if the filter is clogging up. The Prolock filter screen is designed so that the filter sand can be easily replaced if necessary. Furthermore, the filter needs to be vertically closed with respect to sand transport [32]. The filter sand or background sand is not allowed to be transported through the screen. This should also be monitored and checked throughout the lifetime of the screen.
Many of the monitoring inspections and repairs are considering the uncertainties in the performance of the solution. In the future, when the design is further developed and more certain, these inspections and repairs may be reduced. This also reduces the costs of the solution over its lifetime.

4.4. SoSEAL barrier

The SoSEAL barrier is an innovative design and guidelines for the design, installation and monitoring of the barrier are still in development. This section describes the current state of the art regarding the SoSEAL barrier and its guidelines.

The SoSEAL barrier is denoted as a seepage length extension measure, but mainly increases the resistance of the flow of water through and/or around the barrier. With the SoSEAL technique, aluminium (Al) and dissolved organic matter (DOM) are injected into the soil. These two components will interact and bind, creating flocs [16]. Due to the flocs, the barrier has a reduced hydraulic conductivity compared to the aquifer. With the amount of material and method of injecting, the hydraulic conductivity reduction (HCR) can be regulated. The amount of reduction influences the working principle of the barrier. Increasing the reduction of hydraulic conductivity with the SoSEAL barrier, increases the dissipation of energy of the flow of water through the barrier. This decreases the energy level of the water at the tip of the pipe, downstream of the barrier. The barrier therefore decreases the ability of the pipe to progress and an increase in the hydraulic gradient is needed to allow for progression again. It was found that reducing the hydraulic conductivity up to a factor of 40 increases the ability of the the barrier to tackle pipe progression significantly [35]. Further increasing the HCR factor, does not lead to an increase in the energy dissipation through the barrier. The hydraulic conductivity is then so low, the barrier acts as an impermeable blockade. The flow is then forced to go around the barrier and the barrier acts as a heave screen. The depth of the barrier also affects the progression of the pipe at the downstream side. By increasing the depth of the barrier, the seepage length increases. With a longer seepage length, there is an increase in energy dissipation. This increases the gradient that is needed for the pipe to branch and develop. [35]

Current analyses and laboratory tests have shown that the SoSEAL barrier intercepts the pipe formation once it reaches the barrier. This makes the solution vulnerable when local weak spots are present in the barrier. Injection tests have shown that the concentration of SoSEAL, the injection speed and injected volume significantly influence the design and performance of the barrier. The injection methods also show uncertainties with the shape and size of the barrier. A continuous SoSEAL barrier can, with current methods and knowledge, not be guaranteed. When the barrier is used to partially close of the aquifer, the continuity of the barrier is however essential. It is therefore considered that a barrier that fully closes off thin aquifers (< 10 to 15m) is currently the most robust application of SoSEAL. [33]

Additional research and tests have also shown that with the current injection techniques, problems arise with the connection between the SoSEAL barrier and cover layer. The soil pressure directly under the cover layer is relatively low with respect to deeper soil layers. The higher pressure, due to injecting, can therefore cause uplift of the cover layer or leaking of the material. The SoSEAL material is then not evenly spread along the contact area with the cover layer. This poor connection with the cover layer significantly reduces the performance of the SoSEAL barrier.

In this thesis, the SoSEAL barrier is designed as a heterogeneous barrier that fully closes of the aquifer, see Figure 4.5. The width of the barrier is designed at $2m$, since it is estimated that within a range of $2-3m$ around the injection points the hydraulic conductivity can be significantly reduced [16]. Even

though current injection techniques cause different shapes and sizes of the barrier. Additionally, spatial correlation is taken into account to represent the geological spatial variability as best as possible. A contact area directly underneath the cover layer is designed with a different hydraulic conductivity to allow for the uncertainties regarding a poor connection with the cover layer. In subsection 5.5.3, the modelling approach for this design is further discussed.

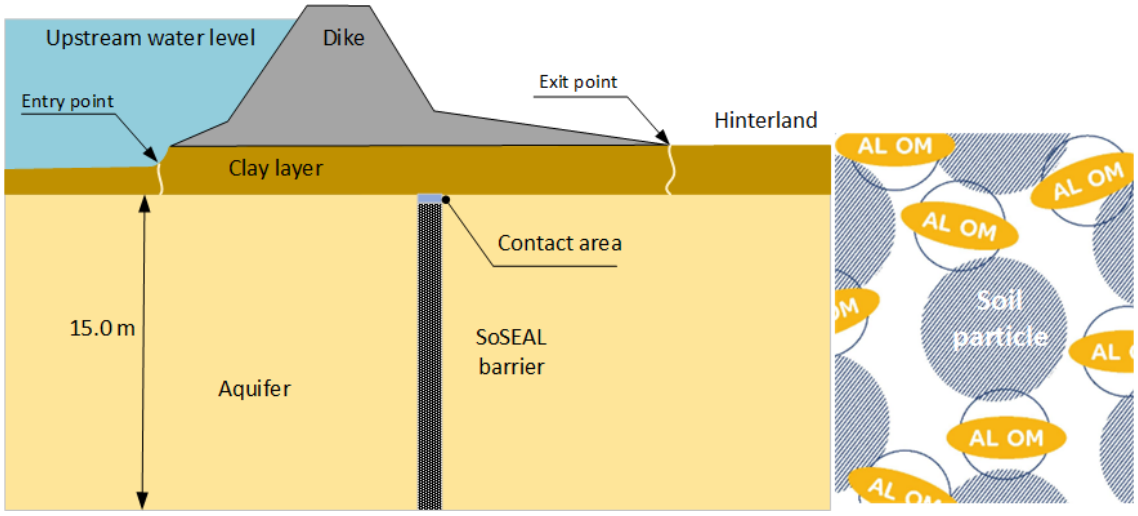

Figure 4.5: A schematisation of the designed SoSEAL barrier on the left. A simplified version of the SoSEAL technique is shown on the right [54].

Since the barrier closes the aquifer completely off, underflow is not considered a failure path. The poor connection with the cover layer and heterogeneity of the barrier itself make pipe progression through the barrier a critical failure path. In Figure 4.6, the events leading to failure are given for the SoSEAL barrier.

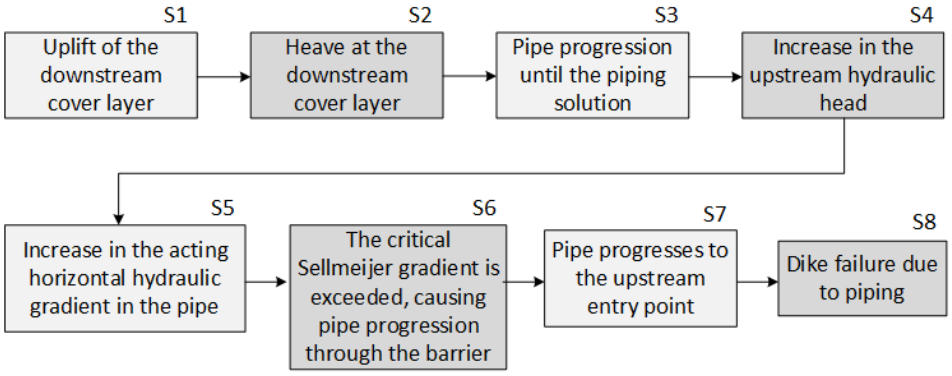

Figure 4.6: The failure steps for the SoSEAL barrier with the events that lead to failure of the dike due to piping. The SoSEAL barrier intercepts BEP at step $S6$.

By preventing horizontal pipe progression through the barrier, the SoSEAL barrier tackles piping. Consequently, step six ($S6$) is addressed by the barrier. The design is therefore tested by comparing the acting horizontal gradient in the pipe with the critical gradient according to Sellmeijer. When the SoSEAL barrier satisfies the criteria, the acting gradient should be lower than the critical gradient that allows for the horizontal progression of sand particles. In section 5.3, the criterion and critical Sellmeijer gradient are further discussed and explained.

As already stated, there are many uncertainties regarding the injection techniques and overall hydraulic conductivity of the barrier. To ensure the performance of the barrier is sufficient, monitoring the SoSEAL

barrier during its lifespan is essential. Injecting additional SoSEAL during the design life, could be necessary to ensure the needed performance of the barrier. This makes the SoSEAL barrier an expandable solution.
Since there are currently no design guidelines on the SoSEAL barrier, there are no protocols on how to take climate change into account.
Many of the uncertainties in the construction and design of the SoSEAL barrier affect the performance of the solution. In the future however, when the design is further developed, these uncertainties may be reduced. This would then also reduce the need for many monitoring and repair actions. This then subsequently lowers the costs of the solution over its lifetime.

5

Numerical model

This chapter discusses the construction of the models of the different piping solutions. In addition, it is explained how the models are tested and simulated for failure due to piping. However, a methodology overview is presented first. This methodology shows how the numerical model and its results contribute to the evaluation of the performance of the piping solutions. The methodology also shows the next evaluation steps, discussed in chapter 6 and chapter 7.

5.1. Methodology overview

In Figure 5.1, an overview of the method is presented in a methodology flow chart. The first part, in blue, consists of constructing a COMSOL model of the different piping solutions and assessing them probabilistically for different upstream water levels. A reference model is built, which is based on the Grebbedijk characteristics from chapter 3 and represents the current situation at the Grebbedijk. This reference model serves as a base model, in which the different piping solutions are implemented. Preliminary models for the piping solutions were then constructed using the design guidelines and preliminary design characteristics from chapter 4.
The sheet pile, plastic filter screen and SoSEAL barrier tackle pipe progression with different working principles. The different working principles result in different events that need to occur to result in piping failure. From these events, as explained in chapter 4, the critical step for each solution is identified. Based on this step, the failure criterion is defined to assess the ability of the solutions to tackle piping. In section 5.3, the different failure criteria are discussed. An iterative process is used to investigate the influence of the soil parameters and different design characteristics on the failure criteria. After calibrating and having confidence in the behaviour of the models, the final models were constructed. For the probabilistic assessment, the final models of the piping solutions are simulated for different water levels and generated samples of different soil characteristics.
The second part, in orange, consists of processing the model output results. The conditional failure probabilities from the probabilistic assessment are used to construct fragility curves for the piping solutions. The fragility curves and the PDF's of the water levels, see section 3.3, are used to calculate the probabilities of failure to piping for each solution. These failure probabilities are used to determine the functional lifespan of the solutions.
In the third part, shown in green, the life cycle cost analysis is performed. The calculated functional lifespans serve as input for the LCC analysis. A specific life cycle method to analyse the costs is adopted. By means of this analysis, the solutions are evaluated for various uncertainties for different scenarios. See chapter 7 for the life cycle cost analysis.

This chapter thus discusses the construction of the models in COMSOL and their probabilistic assessment, corresponding to the first (blue) part of the methodology.

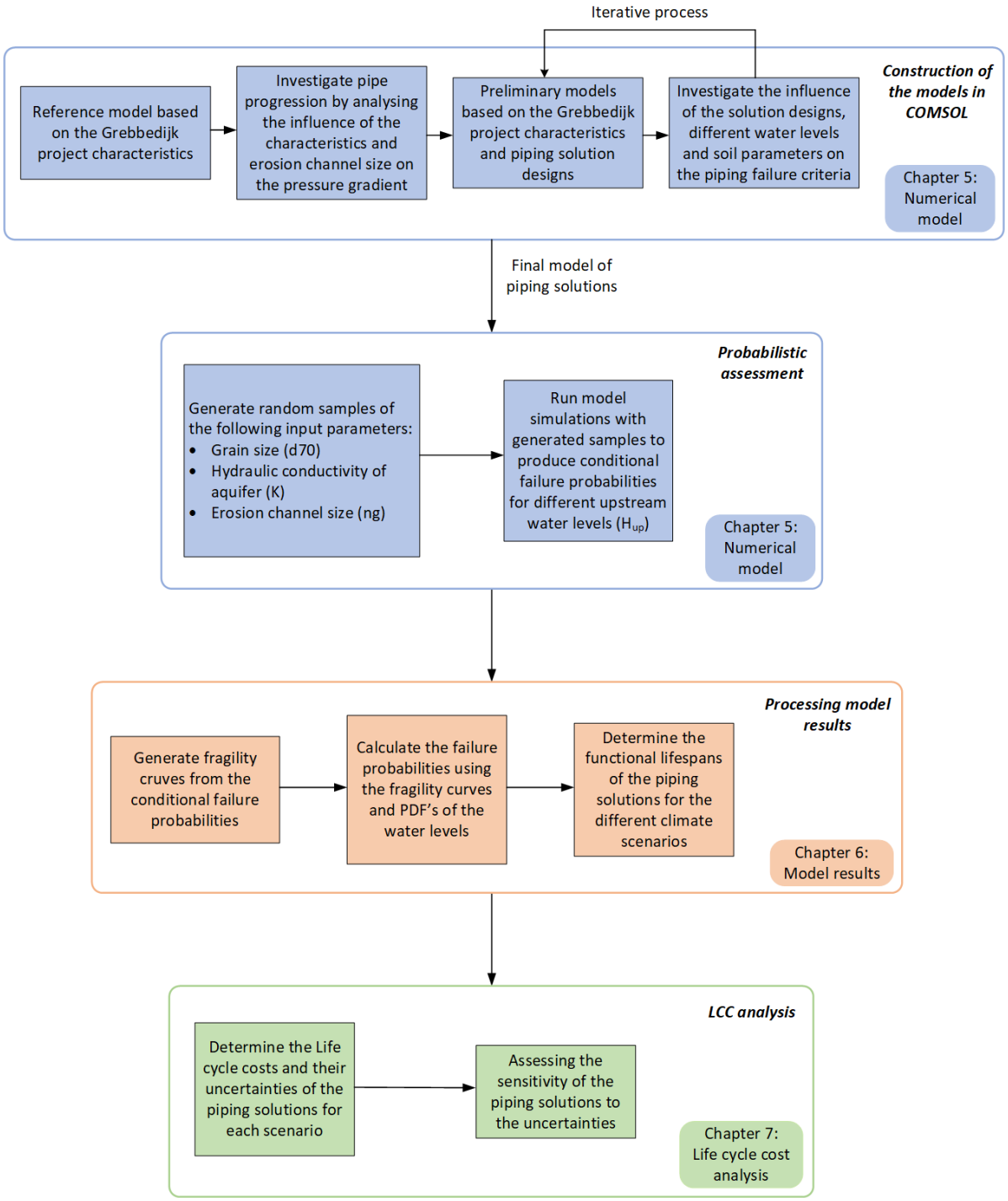

Figure 5.1: Flow chart of the methodology

5.2. Introduction to COMSOL

To investigate the effect of the relevant uncertainties and to evaluate the performance of the different piping solutions, a numerical model is built using COMSOL Multiphysics 6.2. With COMSOL, a 2D finite element model (FEM) is built, using the Subsurface Flow module. With this module, the groundwater flow through a porous medium, in this case the aquifer, can be simulated. The model represents a system along an upper river and as such, the conditions are not time dependent. The model is therefore solved for stationary situations, using Darcy's law.

$$u = -\frac{k}{\mu} \cdot \rho g \Delta H \tag{5.1}$$

- $u[m/s]$: flow velocity.
- $k[m^2]$: soil permeability.
- $\mu[kg/ms]$: dynamic viscosity.
- $\nabla H[-]$: hydraulic gradient.

The model consists of different domains, that represent different parts of the system. For example, the sheet pile, aquifer and erosion pipe are modelled as different domains. Each domain has a representative hydraulic conductivity or permeability. With Equation 5.1, the flow velocity of the water through the domains is modelled. To correctly model the turbulent flow of the water through the erosion pipe channel, Navier-Stokes should be used. However, for a coupled Navier-Stokes-Darcy problem it becomes difficult to solve the model at the boundary conditions, especially for small values of the hydraulic conductivity [25]. Since Navier-Stokes and Darcy's law depend on each other at the boundaries, solving the system becomes a heavy iterative computational process [1]. Therefore, the pipe is modelled with a fictitious material that has a much higher fictitious permeability ($k*$) than the permeability of the aquifer. In section 5.4 the approach of the fictitious permeability is further elaborated on. Using this approach, Darcy's Law can also be applied on the pipe domain, preventing the iterative process [61]. This method has proven to give similar results to the coupled Navier-Stokes-Darcy approach [1].

5.3. Failure criteria

For the piping mechanism to cause dike failure without the presence of a piping solution, the processes, as described in section 2.1, need to occur. When a piping solution is implemented, the processes change. In chapter 4, these processes leading to failure are presented with the steps for each solution. The piping solutions address a specific step, leading to specific failure criteria. This section discusses the failure criteria that are checked with the COMSOL model for each piping solution. Whether piping will occur depends on the ability of the piping solutions to meet the criteria.

5.3.1. Fault tree

The mechanism of preventing the progression of the pipe depends on the critical seepage path [22]. The design of the piping solution, causes the critical seepage path to be either horizontal or vertical. The sheet pile forces the water to flow underneath the screen, creating a vertically critical seepage path along the length of the screen. The design of the plastic filter screen allows water to flow through, but sand particles still need to be transported underneath the screen to cause pipe progression. The critical seepage path for the plastic filter screen is thus also vertical. Both the plastic filter screen and sheet pile are consequently checked for hydraulic heave behind the screen (see $S6$ in Figure 4.2).
In the reference situation, the pipe progresses horizontally under the cover layer, as explained in section 2.1. The horizontal seepage path is thus critical. The SoSEAL barrier is designed to vertically close off the aquifer, preventing the water from flowing around and/or underneath it. The barrier does have potential weak spots, but mainly a weak connection with the cover layer. The potential danger lies in the pipe progression through the contact area of the barrier, which makes the critical seepage path horizontal as well. The reference situation and SoSEAL barrier are consequently checked for the horizontal gradient in the pipe.

The resulting criteria for the piping solutions, depending on the critical seepage path, can be seen in Figure 5.2. These criteria are further discussed in the next subsections.

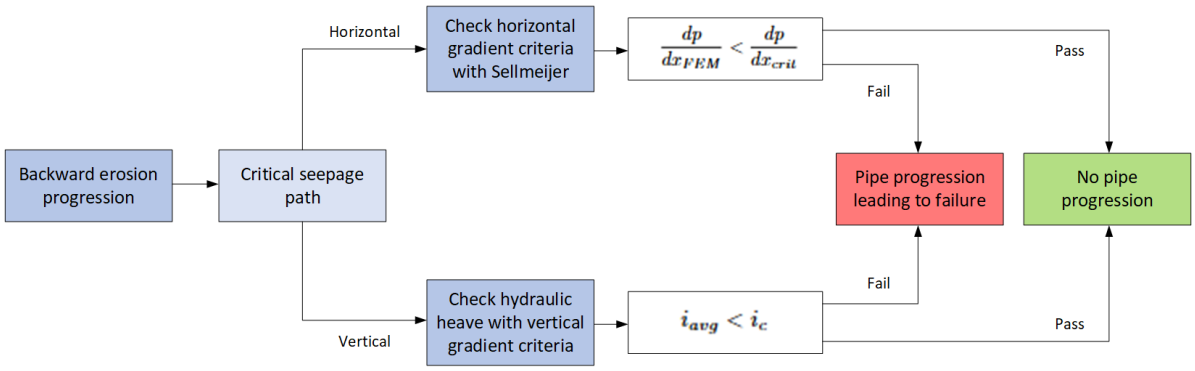

Figure 5.2: The different failure criteria based on the critical seepage path.

5.3.2. Criterion SoSEAL barrier

The implementation of the SoSEAL barrier reduces the flow of water. This lowers the acting horizontal gradient in the erosion channel to below the critical gradient needed for the sand particles to move. The SoSEAL barrier therefore tackles pipe progression by addressing $S6$ from the event tree in section 4.4. For the SoSEAL barrier to tackle this critical step, the following criterion must be met.

$$\frac{dp}{dx_{FEM}} < \frac{dp}{dx_{crit}} \tag{5.2}$$

The model computes the hydraulic gradient over the whole system using the physics of Darcy's Law. The computed gradient ($\frac{dp}{dx_{FEM}}$) of the erosion channel is subsequently checked with the critical gradient ($\frac{dp}{dx_{crit}}$), to check whether the acting gradient is high enough to move the grain particles inside the pipe and therefore cause pipe progression [1]. This critical gradient is based on the two-forces method by Sellmeijer [18]. The downward force of the weight of the particle is compared to the horizontal drag force by the flow of water through the channel. When the horizontal force is bigger than the downward force, the particles start to move [61]. When the two forces are in equilibrium, the critical gradient can be expressed by Equation 5.3. With η being White's sand packing coefficient, θ the bedding angle of the sand grains for which Sellmeijer is calibrated and a the channel height of the erosion channel.

$$\frac{dp}{dx_{crit}} = \frac{\pi\gamma'_s}{3\gamma_w} * \frac{d_{70}\eta\, tan(\theta)}{a} \tag{5.3}$$

5.3.3. Criterion plastic filter screen & sheet pile

By implementing the sheet pile or plastic filter screen, pipe progression is addressed by preventing the hydraulic heave failure directly downstream of the screen, as shown in Figure 4.2. To ascertain whether hydraulic heave can occur, the vertical gradient directly downstream of the screen is checked with the model. When the acting vertical gradient behind the screen (i_{avg}) is lower than the critical vertical gradient (i_c), see Equation 5.5, the pipe will not progress.

$$i_{avg} < i_c \tag{5.4}$$

The critical gradient (i_c) has a value of 0.5, as imposed by design guidelines [22] [49].

The vertical gradient (i_{avg}) directly downstream of the screen is expressed as follows.

$$\begin{aligned} i_{avg} &= \frac{\Delta\varphi}{s} \\ \Delta\varphi &= \varphi_{b,screen;avg} - \varphi_{pipe} \end{aligned} \tag{5.5}$$

With:

- $\Delta\varphi[m]$: The average acting hydraulic head difference downstream of the screen over the length of the embedded depth.
- $s[m]$: The embedded depth of the screen.
- $\varphi_{b,screen;avg}[m]$: The computed average hydraulic head at the bottom of the screen on the downstream side.
- $\varphi_{pipe}[m]$: The imposed average hydraulic head in the erosion pipe on the downstream side of the screen.

5.4. Reference model

As stated in section 5.1, the reference model is based on the Grebbedijk characteristics and serves as a base model for the piping solution models. The reference model consists of two domains; the aquifer and the erosion pipe. Before implementing the Grebbedijk characteristics in the model, the expression for the fictitious permeability of the pipe is obtained. This expression is needed to define the permeability of the pipe domain in the model.

The pressure gradient of the head loss in the pipe channel is given by the Darcy-Weisbach equation, with D_h representing the hydraulic diameter and f representing the friction factor of the flow.

$$\frac{dh}{dx} = \frac{fu^2}{2gD_h} \tag{5.6}$$

The friction factor can be expressed by Equation 5.7, with the factor β_f depending on the shape of the cross section of the erosion channel. The Reynolds number (Re) is expressed by Equation 5.8 and besides the flow velocity and hydraulic diameter, also depends on the density (ρ) and dynamic viscosity (μ) of the water in the aquifer. [1]

$$f = \frac{\beta_f}{Re} \tag{5.7}$$

$$Re = \frac{u\rho D_h}{\mu} \tag{5.8}$$

In the model used in this thesis, it is assumed that resistance of the flow of water inside the pipe is only significant in horizontal (x) direction. This is due to the high aspect ratio of the length of the pipe versus its height. Combining 5.7 and 5.8 inside 5.6, the equation for the flow velocity inside the pipe can be rewritten to Equation 5.9 [1]. By comparing this equation to the equation of Darcy's Law (5.1) and assuming laminar and incompressible flow inside the pipe, the fictitious permeability of the pipe domain can be expressed by Equation 5.10 [61].

$$u = (\frac{2D_h^2}{\beta_F}) * (\frac{g\rho}{\mu}) * \frac{dh}{dx} \tag{5.9}$$

$$k^* = -\frac{2D_h^2}{\beta_f} \tag{5.10}$$

To implement this fictitious permeability on the pipe domain, the D_h and β_f need to be known. Both depend on the shape and size of the erosion pipe. The most correct way to model the pipe would be according to the fracture flow approach. The pipe is then modelled with a significantly larger width relative to the height. Due to the fact that piping is a 3D phenomenon, the resulting loss of pressure over such a wide pipe is in reality much higher than what is modelled in 2D. However, with the fictitious permeability the pipe can be modelled with a geometry that has a height and width with an aspect ratio close or equal to one. This way, the additional loss of pressure over the pipe can be accounted for and allows the model to capture the piping process. The erosion channel in this model is therefore shaped as a square cross section, with a channel height of a and shape factor β_f of 56.92. The hydraulic diameter D_h of the pipe is equal to a for a square cross section. [1]

$$a = ng * d70 \tag{5.11}$$

As can be seen from Equation 5.11, the channel height a, depends on the number of grains (ng) and the representative grain size ($d70$). Since the size of the pipe is not known beforehand, ng is also taken as a stochastic input parameter. Lastly, the length of the pipe is assumed to be from the exit point on the downstream side, until the middle of the dike body. It is assumed that once the pipe reaches half the length of the dike and the acting gradient is larger than the critical gradient, the pipe progression cannot be stopped [1]. The pipe will then progress until it reaches the upstream side, resulting in the failure of the dike. This pipe length is also assumed in the models for the piping solutions.

An overview of the input parameters, including the characteristic parameters of the Grebbedijk, can be seen in Table 5.1. These parameters also serve as input for the models of the piping solutions. For more elaboration on the hydraulic conductivity K and d_{70} grain size, see section 3.2.

Parameter		Representative value	Distribution
d_{70}	$[m]$	$3.07 * 10^{-6}$	log-normal
L_{dike}	$[m]$	34.20	-
L_{pipe}	$[m]$	17.10	-
$D_{aquifer}$	$[m]$	15.00	-
H_{up}	[m NAP]	11.77[1]	-
H_{down}	[m NAP]	7.40	-
ΔH	$[m]$	4.37[1]	-
0.3d	$[m]$	0.66	-
μ	$[Pa\ s]$	$1.0 * 10^{-3}$	-
η	[-]	0.25	-
θ	$[deg]$	37	-
g	$[m/s^2]$	9.81	-
K	$[m/s]$	$5.89 * 10^{-4}$	log-normal
γ'_s	$[kN/m^3]$	16.19	-
γ_w	$[kN/m^3]$	9.81	-
ng	[-]	4 [2]	uniform

Table 5.1: Characteristic input parameters from the Grebbedijk for the numerical model.

In Figure 5.3, the meshed reference model with its boundary conditions can be seen. The model is built with a domain for the aquifer and a domain for a predefined pipe. Since the height of the pipe is significantly smaller with respect to the dimensions of the aquifer, refined meshing is applied around the pipe. The pressure head boundaries allow the water to flow in the porous media domains. At the no flow boundaries, the imposed flow velocity is zero, meaning there is no inflow of water. A probe is placed in the middle of the pipe. This probe measures the acting gradient ($\frac{dp}{dx_{FEM}}$) and the critical gradient ($\frac{dp}{dx_{crit}}$) inside the pipe.

[1] The representative value is from Royal HaskoningDHV [51]. The model uses different upstream water levels as input parameters; see section 5.6.

[2] To investigate the influence of the number of grains, a range of values is taken into account in the model; see section 5.6.

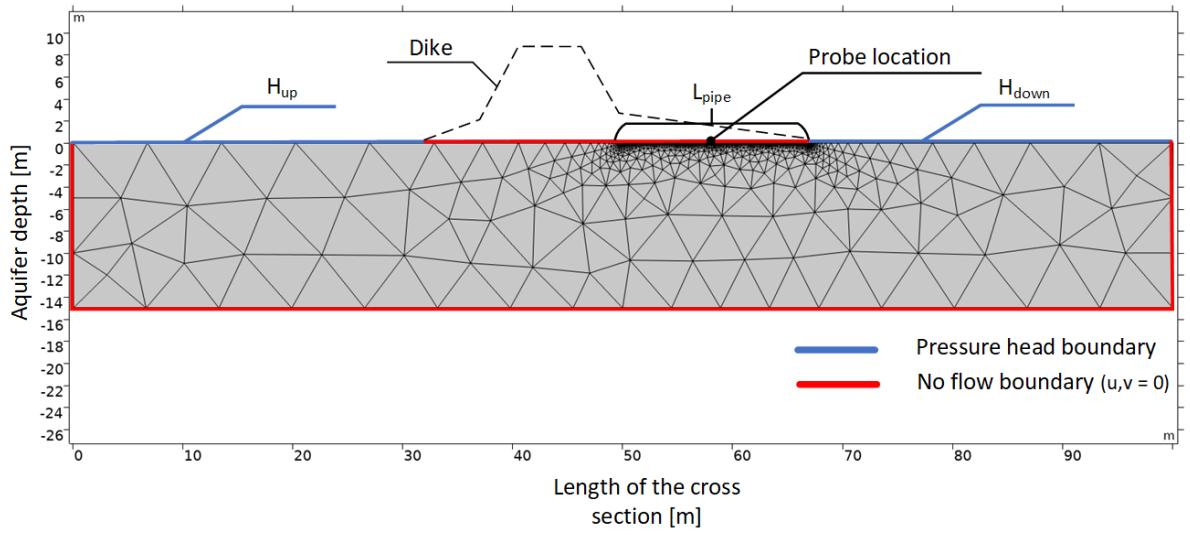

Figure 5.3: The modelled reference situation and applied boundary conditions

The exit point of the pipe is, as stated previously, assumed to be directly on the downstream side of the dike. The end of the pipe and its exit point are presented in Figure 5.4.

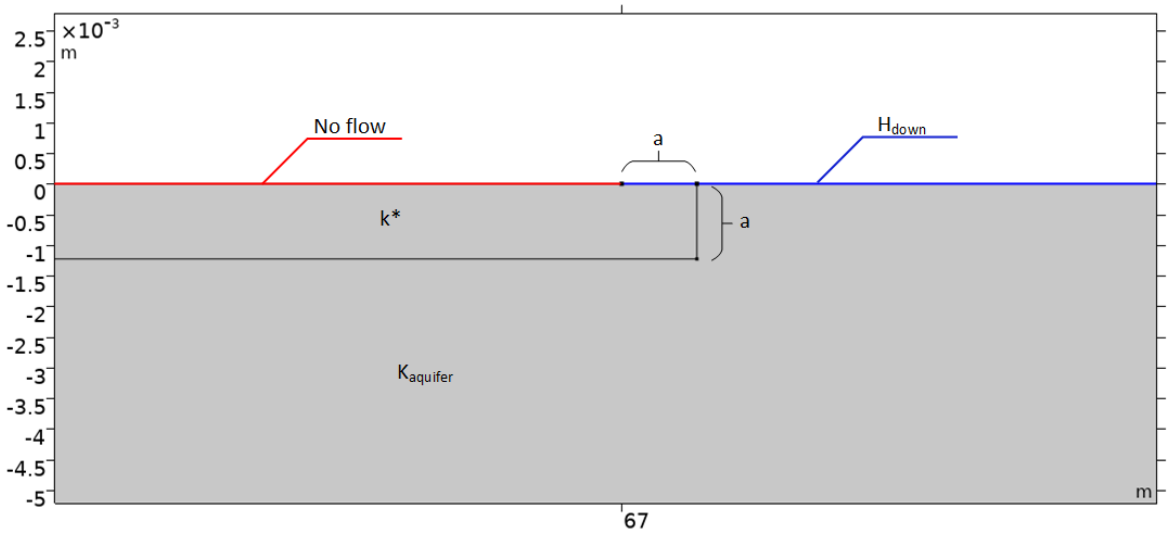

Figure 5.4: A zoomed in image of the end of the pipe with the outlet. The fictitious permeability k^* is applied to the pipe domain and the hydraulic conductivity $K_{aquifer}$ applied to the aquifer domain.

5.5. Model of piping solutions

In this section the models of the different piping solutions are discussed. The reference model, Grebbedijk characteristics and contents of chapter 4 serve as input for the models.

5.5.1. Sheet pile model

The steel sheet pile is an impermeable screen that forces the flow to change direction. Therefore, no flow through the screen is allowed. To model this in a representative way, a domain is added to the reference model with a hydraulic conductivity close to zero. This makes the domain of the sheet pile (almost) impermeable, preventing groundwater flow through the screen.

In Figure 5.5 below the meshed FEM model for the sheet pile can be seen. The mesh is refined between the domains, due to the difference in the dimensions of the sheet pile, the pipe and the aquifer,

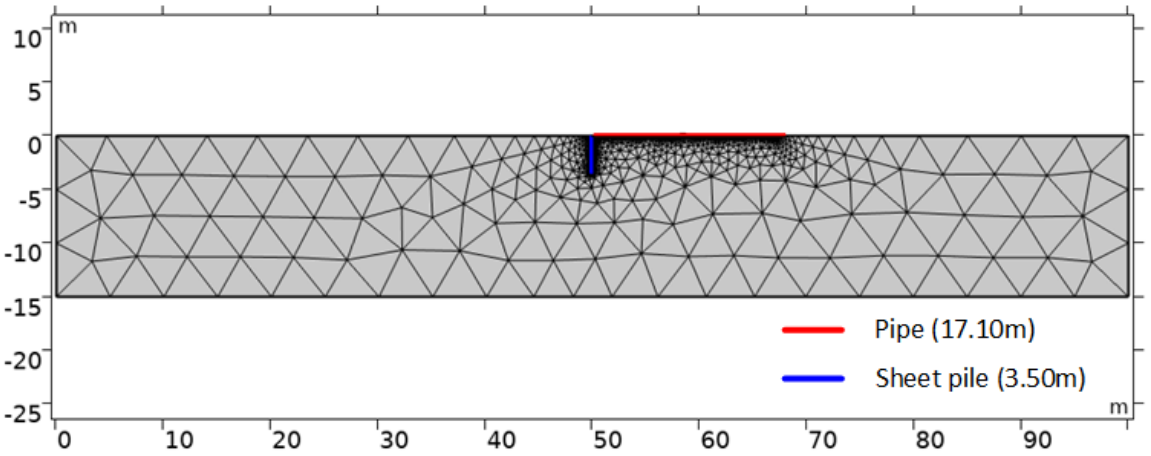

Figure 5.5: the FEM model of the sheet pile.

To check the criteria for hydraulic heave, the average vertical gradient directly behind the sheet pile is checked. This is done by assuming a prism behind the screen over which the gradient is evaluated, see Figure 5.6. This prism has the length of the embedded depth of the sheet pile and a width of $0.25m$ [4]. At the bottom of this prism, the average hydraulic head ($\varphi_{b,screen;avg}$) is evaluated by the model. The hydraulic head at the top of the prism (φ_{pipe}) is imposed and equal to the ground level of the hinterland [4].

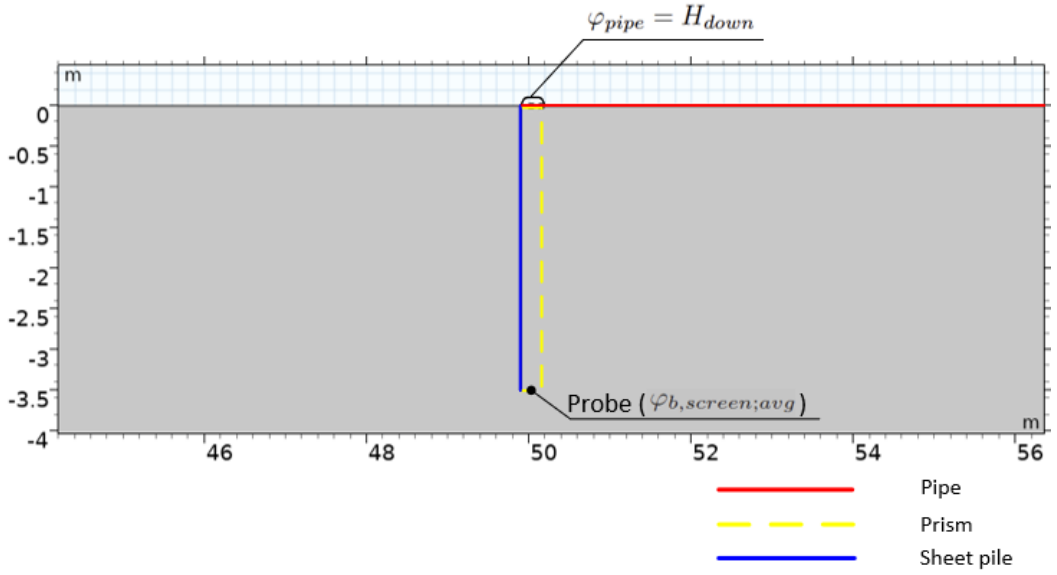

Figure 5.6: The prism is modelled directly downstream of the sheet pile. At the bottom of the prism a probe is placed at midpoint to get the $\varphi_{b,screen;avg}$. At the top of the prism, φ_{pipe} is set equal to the downstream water level, which is equal to the ground level of the hinterland

In addition to the parameters listed in Table 5.1, the input parameters shown in Table 5.2 are required for the model of the sheet pile.

$L_{sheet}[m]$ (depth)	$B_{sheet}[mm]$ (width)	$K_{sheet}[m/s]$
3.50	11.20	$1.00 * 10^{-20}$

Table 5.2: Additional input parameters for the domain of the sheet pile.

5.5.2. Plastic filter screen model

The plastic filter screen consists of two parts; an impermeable part and a filter part. These two parts are modelled as two different domains. The impermeable lower part of the design is modelled in the same way as the domain of the sheet pile. The upper filter screen part is modelled with the equivalent hydraulic conductivity, taking both the perforations and the filter sand into account.

In Figure 5.7 below the meshed FEM model for the filter screen can be seen. The mesh is refined around the pipe and the plastic filter screen, especially the perforated part, to accurately capture the groundwater flow.

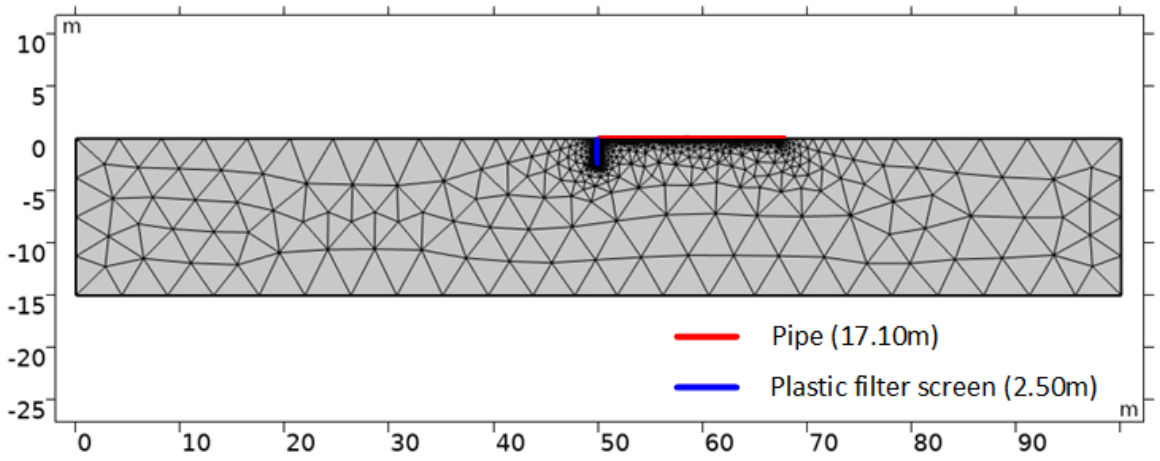

Figure 5.7: the FEM model of the plastic filter screen.

To check the criteria for hydraulic heave, the average vertical gradient directly behind the plastic filter screen is checked. This is done similarly to the sheet pile model, see Figure 5.8

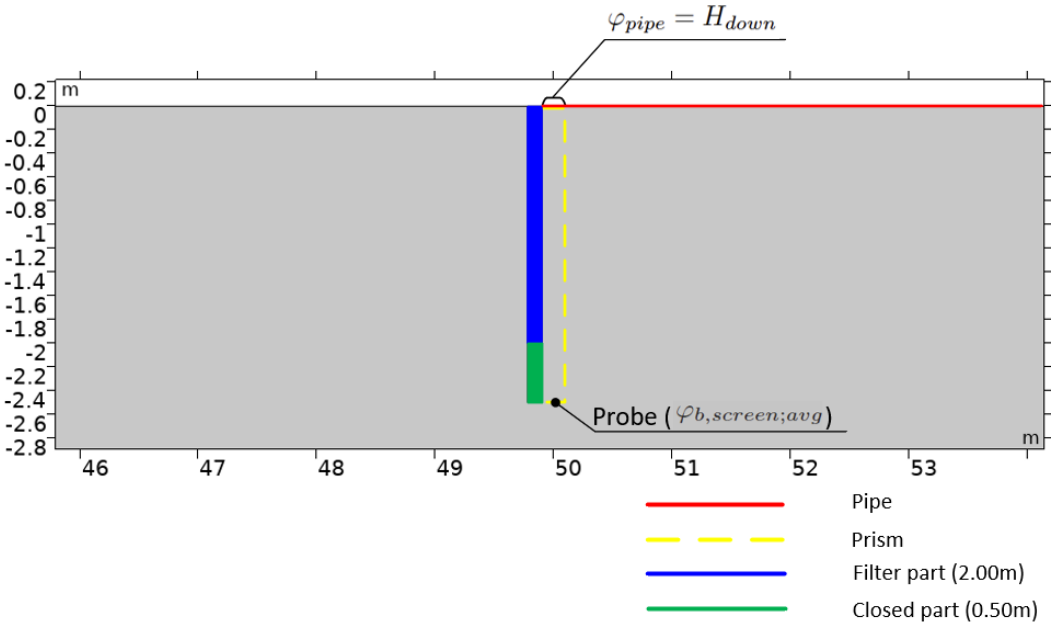

Figure 5.8: The model of the plastic filter screen with the prism directly downstream of the screen, similarly to the sheet pile model.

The additional input parameters for the plastic filter screen are defined in Table 5.3 below. In addition to the parameters listed in Table 5.1, these input parameters are required for the model of the plastic filter screen.

$L_{filter}[m]$	$L_{closed}[m]$	$B_{screen}[mm]$	$K_{closed}[m/s]$	$K_{filter}[m/s]$
2.00	0.50	120	$1.00 * 10^{-20}$	$4.40 * 10^{-4}$

Table 5.3: Additional input parameters for the domains of the plastic filter screen.

5.5.3. SoSEAL barrier model

The meshed FEM model for the SoSEAL barrier can be seen in Figure 5.9 below. The mesh is refined around the pipe and the top of the barrier beneath the boundary. This refinement is done to capture the flow through the contact area in more detail.

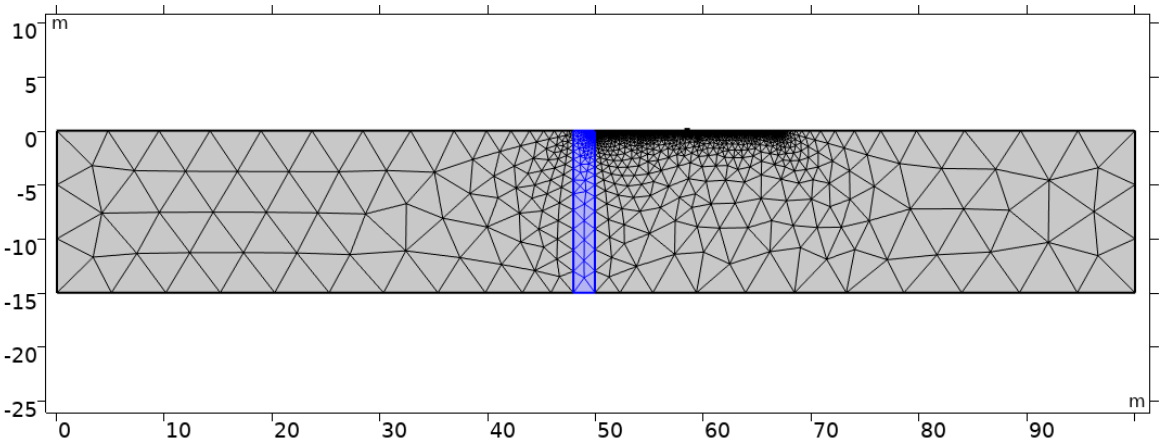

Figure 5.9: the FEM model of the SoSEAL barrier with a length of $15m$. The SoSEAL barrier is highlighted in blue.

As stated in section 4.4, by increasing the HCR factor to around 40, the SoSEAL barrier's ability to tackle pipe progression increases significantly. However, a barrier with continuous HCR cannot be guaranteed with current injection methods. In this thesis the SoSEAL barrier is therefore modelled as a heterogeneous barrier. To account for the heterogeneity, random HCR factors are sampled from a normal distribution. The random samples are taken for a grid of 50x150 points. Since a HCR factor of 40 can be seen as the desired reduction factor, 40 is taken as the mean factor. An assumption is taken regarding the precision of the current injecting technique and therefore the standard deviation is set to 10. To represent the geological spatial variability as best as possible, the random samples across the grid are smoothed to introduce spatial correlation. Lastly, outliers are discarded for HCR values lower than 15 and higher than 75. Figure 5.10 shows the modelled SoSEAL barrier with the spatially varying HCR values. This grid of HCR factors is then applied on the hydraulic conductivity of the aquifer to achieve the actual hydraulic conductivity field for the domain of the SoSEAL barrier, see Equation 5.12. Since $K_{aquifer}$ is a stochastic input parameter in this study, $K_{field,soseal}$ is different for each simulation.

$$K_{field,soseal} = \frac{K_{aquifer}}{HCR_{field}} \tag{5.12}$$

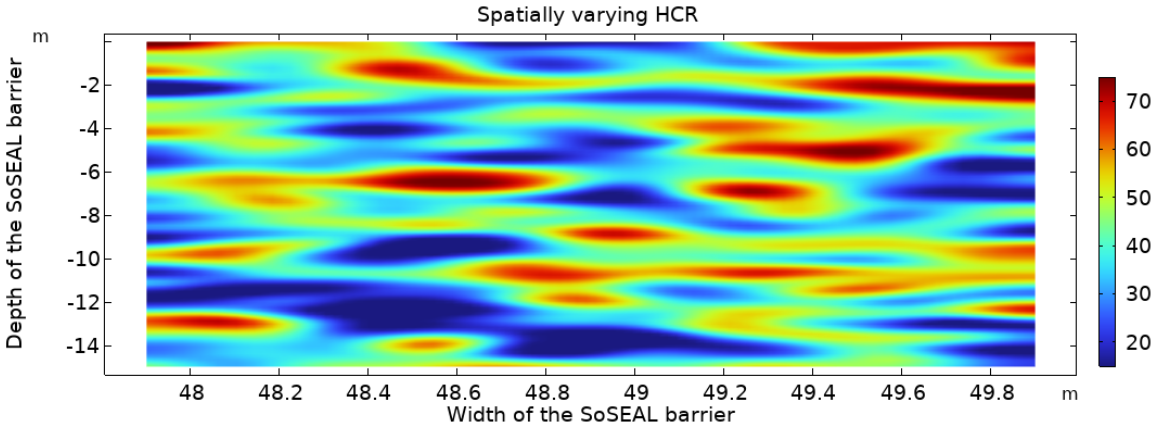

Figure 5.10: The heterogeneous SoSEAL barrier with spatially varying HCR over a depth of $15m$.

The contact area is modelled as a separate domain to represent the imperfect connection between the cover layer and the top of the barrier, see Figure 5.11. To capture the potential flow of water through this contact zone into the pipe, its hydraulic conductivity was set higher than that of the aquifer by applying a scaling factor (f). Despite this increase, it was made sure that the resulting conductivity remains within the typical range for a sand layer. To incorporate the uncertainty associated with the connection between the barrier and the cover layer, random samples of this factor are drawn from a log-normal distribution. Based on an analysis of the flow behaviour across different values, a factor of 10 was selected as the 95th percentile of the distribution. This analysis is also briefly discussed in Appendix C. Unlike the barrier, the contact area is not modelled as a heterogeneous zone. The domain of the area has a single hydraulic conductivity. The value of which is determined by the scaling factor, that is drawn from the log-normal distribution for each simulation.

$$\begin{aligned} K_{contact} &= K_{aquifer} * f \\ f_{95} &= 10 \end{aligned} \tag{5.13}$$

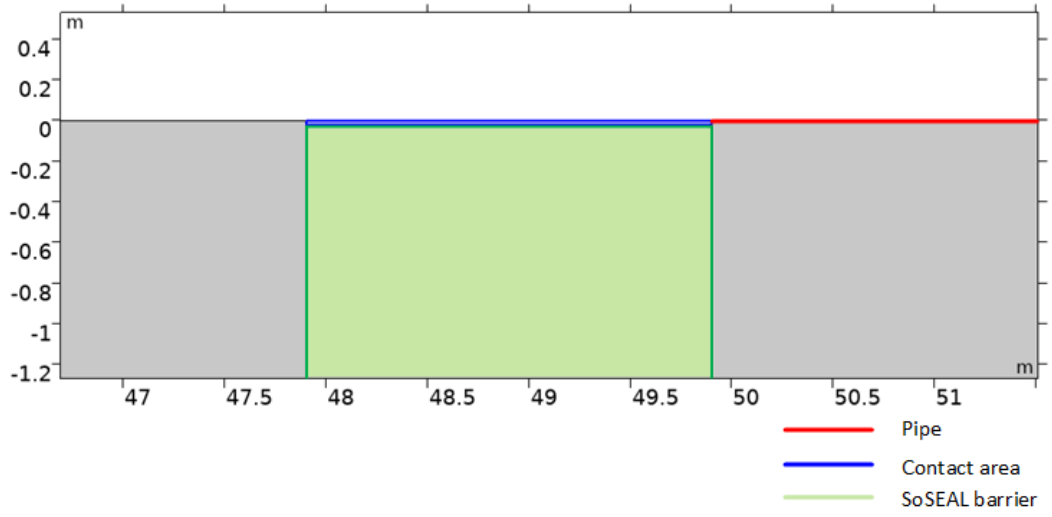

Figure 5.11: A zoomed in image of the top of the SoSEAL barrier with a contact area modelled as a separate domain

In addition to the parameters listed in Table 5.1, the input parameters shown in Table 5.4 are required for the model of the SoSEAL barrier.

$L_{barrier}[m]$	$L_{contact,zone}[m]$	$B_{soseal}[m]$	$K_{barrier}[m/s]$	$K_{contact,zone}[m/s]$
15.00	a	2.00	$K_{field,soseal}$ (5.12)	$K_{contact}$ (5.13)

Table 5.4: Additional input parameters for the domains of the SoSEAL barrier.

5.6. Sampling approach

As described in section 5.1, simulations are performed for the different piping models to generate output, which is then used to determine conditional failure probabilities for various upstream water levels. Several parameters are subject to uncertainty and are therefore randomly sampled according to their respective probability distributions. The models are subsequently simulated using these uncertain input parameters across different upstream water levels. This section outlines the upstream water levels considered in the analysis and the sampling approach used for the stochastic parameters.

5.6.1. Upstream water levels

Conditional failure probabilities for different upstream water levels are required to construct fragility curves for the piping solutions. However, running a sufficient number of simulations to obtain reliable estimates for these probabilities across the water levels is computationally demanding. To reduce time and computational effort, the number of simulated water levels is kept to a minimum. This is achieved by first identifying a lower bound water level at which the dike has already demonstrated sufficient safety. From this 'proven strength' of the dike, a limited set of higher water levels is selected for the simulations. The conditional failure probabilities for intermediate water levels are then determined through interpolation, see section 6.3.

To determine the lower bound water level, historical water level data for the Grebbedijk from 1950 to 2025 was analysed [46]. The highest recorded water level during this period, which occurred in 1995, is taken as the lower bound. At this level, $10.52m$ NAP, the dike has proven sufficient strength. For the model simulations, the following additional upstream water levels relative to NAP are selected: $11.00m$, $11.50m$, $12.00m$, $12.50m$, $13.00m$, $13.50m$, $14,00m$. Increments of $0.5m$ are applied to adequately cover the relevant range of water levels. The planned crest height of the dike after renovations is $12.70m$ NAP. It is expected that in the future the dike will be further heightened to prevent overflowing. Water levels up to $14.00m$ NAP are therefore considered the most relevant and critical. For water levels exceeding this range, extrapolation is applied. This is further explained in section 6.3

5.6.2. Latin hypercube samples

In this thesis, Latin Hypercube Sampling is used to sample the uncertain input parameters. Latin Hypercube Sampling (LHS) is a statistical method used to efficiently sample values from multiple uncertain parameters while ensuring good coverage of their entire range [53]. Simple random sampling can leave large gaps or clusters in the parameter space. LHS divides the cumulative distribution of each parameter into n equally probable intervals, where n is the desired sample size. From each interval, one value is randomly selected, while applying the target distribution. These sampled values are then combined so that each interval for every parameter is used exactly once, forming n unique parameter sets. This approach reduces sampling bias and ensures that all portions of each parameter's distribution are represented, making LHS particularly effective for uncertainty analysis and sensitivity studies. In addition, with LHS the coverage of the entire range of the distribution of each parameter is achieved with much fewer samples than with random sampling. This allows for less needed simulation and reduces computational time.

LHS is performed for the following parameters:

- Grain size, d_{70}, according to the log-normal distribution as described in section 3.2.
- Hydraulic conductivity of the aquifer, $K_{aquifer}$, according to the log-normal distribution as described in section 3.2.
- Hydraulic conductivity of the contact area of the SoSEAL barrier, f, as described in subsection 5.5.3.
- Number of grains for the erosion channel height, ng, according to a uniform distribution.

Findings from a study by van Esch et al. [18] have shown that the number of grains ranges from 0 to 30. A uniform distribution with bounds 0 and 30 is adopted for the parameter ng.
Adjusting the pipe height a in the model based on ng and d_{70} would normally require re-meshing the erosion channel domain for each simulation, which significantly increases computational time. To avoid this, the pipe height is not modified directly in the geometry. Instead, a scaling factor is introduced in the permeability formula of the pipe ($k*$), which incorporates the sampled values of ng and d_{70}. This approach accounts for changes in pipe height within the model physics while eliminating the need for re-meshing. This approach is explained in more detail in Appendix D.

Each water level is simulated with a different number of runs. At lower water levels, the probability of piping is smaller, requiring more simulations to obtain a sufficient number of failures. The table below summarizes the number of simulations per water level. To reduce computational time, these numbers are kept as low as possible while maintaining reliability.

Upstream water level [m NAP]	Number of simulations
11.00	25,000
11.50	15,000
12.00	10,000
12.50	5,000
13.00	2,500
13.50	1,000
14.00	500

Table 5.5: Number of simulations for each upstream water level. Performing more simulations for lower water levels to capture the low failure probabilities.

5.7. Modelling uncertainties

It is important to emphasize that the piping models contain several input uncertainties, which are accounted for to varying degrees. These uncertainties affect the results of this study and must therefore be considered. They arise from assumptions, design choices, and model characteristics.

As previously discussed, according to Sellmeijer's two-forces equilibrium assumption, once a pipe has progressed to half of the dike body, its further progression will irreversibly continue until dike failure. The solutions are positioned at this critical location, halfway the seepage length. Subsequently, it can be implied that failure of the solution directly results in failure of the dike. However, because the solutions differ in their working principles, this location may be more optimal for some solutions than for others. In this study the influence of other locations is not researched.

In addition, each solution is modelled for a single set of design dimensions. Exploring alternative depths or geometries could provide better insight into the sensitivity of performance to design parameters. For instance, the current depth of one solution may be relatively more effective than that of another. Furthermore, the performance of one solution may be more sensitive to changes in the depth than the other. Besides the dimensions, there are uncertainties in the input parameters regarding the working principles of the solutions. These input uncertainties differ significantly between the plastic filter screen, the SoSEAL barrier, and the sheet pile. The equivalent hydraulic conductivity of the filter screen is derived from the aquifer's K, which carries uncertainties as discussed in subsection 3.2.2. Consequently, the screen's performance is directly influenced by these uncertainties. For the SoSEAL barrier, assumptions and estimations had to be made regarding the contact area and the heterogeneous hydraulic conductivity field, as detailed in section 4.4. These strongly affect the barrier's working principle and behaviour. This input is relatively conservative in this study, due to current uncertainties with the composition of the SoSEAL barrier and current injection techniques. The performance of the barrier could thus be enhanced by adjusting the composition of the SoSEAL material and/or by improving injection techniques.

Beyond design related uncertainties, the characteristics and dimensions of the COMSOL model also contribute to uncertainty. As noted in subsection 3.2.2, aquifer depth has only a limited impact beyond a certain threshold. In contrast, the aquifer width plays a more significant role: a wider aquifer allows

larger groundwater volumes and flows, reducing the critical gradient in the pipe [43]. Since the aquifer width was based on the critical dike profile from the Royal HaskoningDHV safety analysis [51], its choice directly influences the potential for pipe progression.

The representation of the pipe itself introduces further uncertainty. In this study, the erosion channel is modelled with a square cross-section, which produced representative results. However, as shown by Aguilar-Lopez et al., alternative cross-sectional shapes may also be appropriate, potentially yielding different gradients while still producing results within the expected range [1].

Finally, discretization uncertainties arise from the meshing process. Since every numerical model requires a mesh, the choice of resolution and element type can influence the outcomes. In this thesis, no dedicated mesh convergence study was performed, and therefore some variability due to discretization cannot be excluded.

6

Model results

6.1. From model output to functional lifespan

After constructing the models for the piping solutions and running the simulations, the model output is processed to determine the different functional lifespans of the solutions, see Figure 6.1. The conditional failure probabilities, computed from the output of the model simulations, are used to generate fragility curves for each piping solution. Using the fragility curves and probability density functions of the water levels for the different climate scenarios, the failure probability due to piping is determined. By comparing the failure probabilities with the imposed required safety standard, the lifespans of the different piping solutions are determined for each climate scenario.

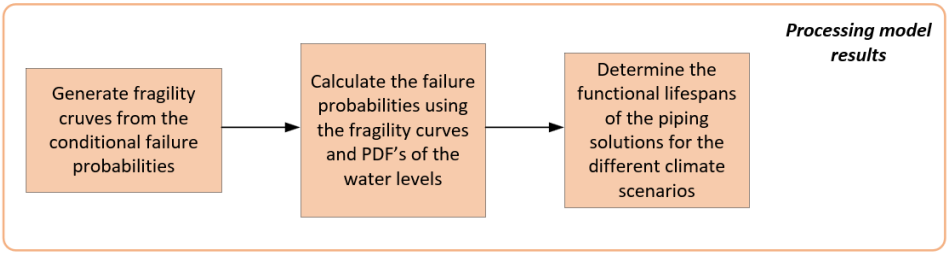

Figure 6.1: Methodology for processing the model results to determine the functional lifespans of the piping solutions for different scenarios.

The fragility curve ($F_f(h_i)$) is composed of all the conditional failure probabilities, according to Equation 6.1 [28]. With Z being the limit state function for the piping solution. This limit state function is based on the failure criteria for the solutions. When the solution does not meet the criterion, it is denoted as a failure. The limit state function is checked for each simulation, mounting to a certain amount of failures for each water level.

$$F_f(h_i) = P\{Z(H_1, ..., H_n) < 0 | H_i = h_i\} \tag{6.1}$$

By multiplying the fragility curve with the PDF of the water levels, a probability contribution curve (PCC) is created [28] [52]. Integrating the PCC gives the total failure probability due to piping.

$$PCC(h) = f_h(h) * F_f(h) \tag{6.2}$$

$$P_f = \int PCC(h_i)dh \tag{6.3}$$

In Figure 6.2, an example of the different curves is displayed to give a visual interpretation.

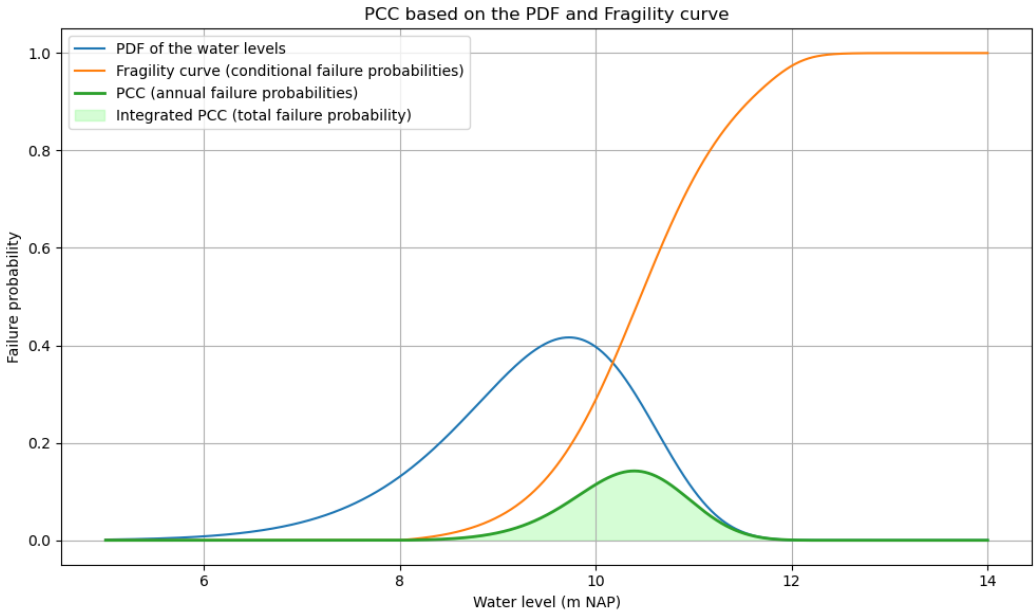

Figure 6.2: A graphical example to illustrate the different curves clearly. Multiplying the fragility curve with the PDF gives the PCC. Integrating the PCC gives the failure probability for piping. The shown curves are set as an example.

The failure probabilities due to piping are calculated for different future sight years; 2050, 2100, 2150. By integrating the PCC for each sight year and interpolating log-linearly between those failure probabilities, the failure probability for each future year is determined. When the failure probability crosses the maximum allowable failure probability, the piping solution does not fulfil the safety standard any more. The functional lifespan of the piping solution is considered until the year this exceedance takes place.

6.2. Reference model

As already discussed in section 5.4, a probe in the middle of the pipe measures the acting hydraulic gradient and critical hydraulic gradient for each simulation. When the acting gradient is higher than the critical gradient, the pipe can progress. This is considered as a failure of the dike due to piping. As already investigated by Royal HaskoningDHV, the current situation does not meet the criteria for heave and uplift of the cover layer [51]. Their analysis has also shown that the acting gradient for the critical water level is significantly higher than the critical gradient for pipe progression. The current dike does therefore not meet the required safety standard regarding piping.
The reference model also shows that the current situation does not meet the safety standard based on the criteria for pipe progression. This is presented in Figure 6.3, by showing the failure probabilities for the moderate scenario G with a capped discharge. As can be seen, do the failure probabilities of the current situation significantly exceed the maximum allowable failure probability for the current and future years.

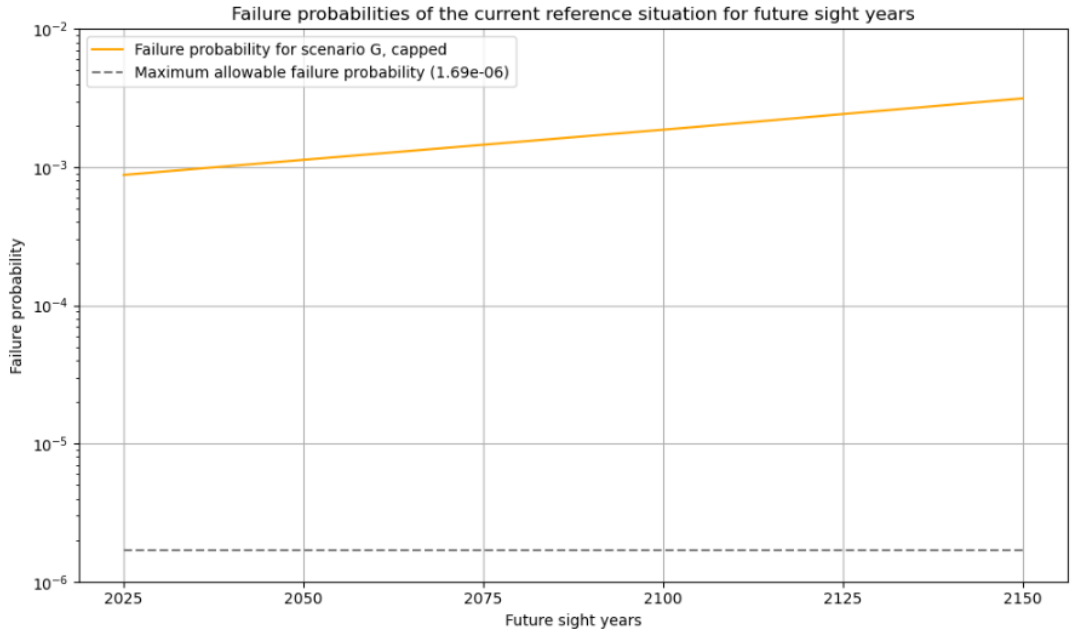

Figure 6.3: The failure probabilities of the current reference situation for future sight years, exceeding the maximum allowable failure probability significantly.

6.3. Model results of piping solutions

In this section the model results of the piping solutions are presented. Using the fragility curves and PDF's of the water levels, the failure probabilities and functional lifespans for the different climate scenarios are determined.

To construct the fragility curves, linear interpolation is applied between the conditional failure probabilities for the simulated water levels from Table 5.5. Other interpolation methods (using log-normal and log-linear correlations) have been tried and resulted in smoother curves. However, the fitting with those methods caused under- or overestimations of the conditional failure probabilities for the modelled water levels. Additionally, the shape parameters for these curves had to be estimated, adding extra uncertainty. Small fitting errors for these low probabilities cause significant deviations. Linear interpolation between the known conditional failure probabilities is therefore considered. For higher water levels (above 14 m NAP) the curve is log-linear extrapolated with a maximum value of 1, since the probability cannot be higher. This is however not necessary, since water levels higher than simulated do not occur for any of the scenarios and future sight years. It is still done to give a complete impression and visualisation of the behaviour of the solution.

6.3.1. Results of the sheet pile model

To determine the conditional failure probabilities for the designed sheet pile, the criterion for hydraulic heave behind the screen is checked with each simulation. When the sheet pile does not meet the criterion, it is considered a failure due to piping, since the pipe will continue to progress. After running the simulations as described in Table 5.5, the results are used to construct the fragility curve for the sheet pile. However, no failures were recorded for the water levels of $11.00m$, $11.50m$ and $12.00m$. At these levels, the probability of failure is very low, and the number of simulations performed was insufficient to capture any failures. As noted earlier, increasing the number of simulations to obtain failures would substantially increase computational time. Therefore, the conditional failure probabilities for these water levels are estimated. They are based on the observed behaviour of the sheet pile and the failure probabilities at higher water levels. Additionally, the conditional failure probabilities need to be lower than what could have been detected with the number of simulations used.

With this approach, the sheet pile shows a jump in the performance at around $12m$ NAP. The sheet pile fails significantly more for increasing water levels above $12m$ NAP. Below $12m$ NAP, failures were difficult to capture, even with very conservative values of soil parameters and the number of simulations

used (no failure is recorded in 10,000 simulations). This shows that the hydraulic head difference, caused by the upstream water level, has a significant influence on the hydraulic heave behind the screen. The estimated conditional failure probabilities are therefore significantly lower for water levels below $12m$ NAP. All conditional failure probabilities are presented in Table 6.1.

Upstream water level	Conditional failure probability
11.00	$5.0 * 10^{-6}$*
11.50	$2.0 * 10^{-5}$*
12.00	$6.67 * 10^{-5}$*
12.50	0.018
13.00	0.052
13.50	0.076
14.00	0.092

Table 6.1: Conditional failure probabilities for different upstream water levels. Estimated failure probabilities are denoted by *.

In Figure 6.4, the fragility curve of the sheet pile is presented. Since the failure probabilities are relatively small, the curve is shown on a log scale to give a better visual interpretation. From this fragility curve, the jump in performance can be seen more clearly. The fragility curve also shows the 'proven strength' level is at $10.5m$ NAP, since the conditional failure probability goes to zero.

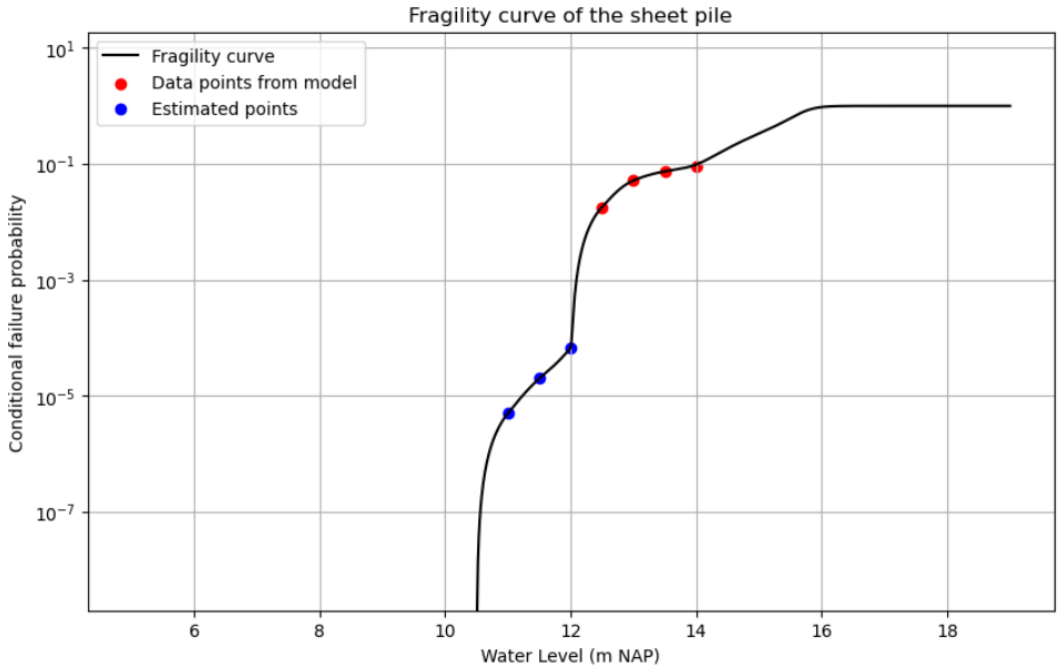

Figure 6.4: The fragility curve of the sheet pile plotted on a log scale.

This fragility curve is multiplied with the PDF's of the water levels for the different climate scenarios as described in section 3.3. After integration of the resulting PCC's, the failure probabilities for piping for each scenario and future sight year are calculated. In Figure 6.5, the year of exceeding the maximum allowable failure probability is shown.

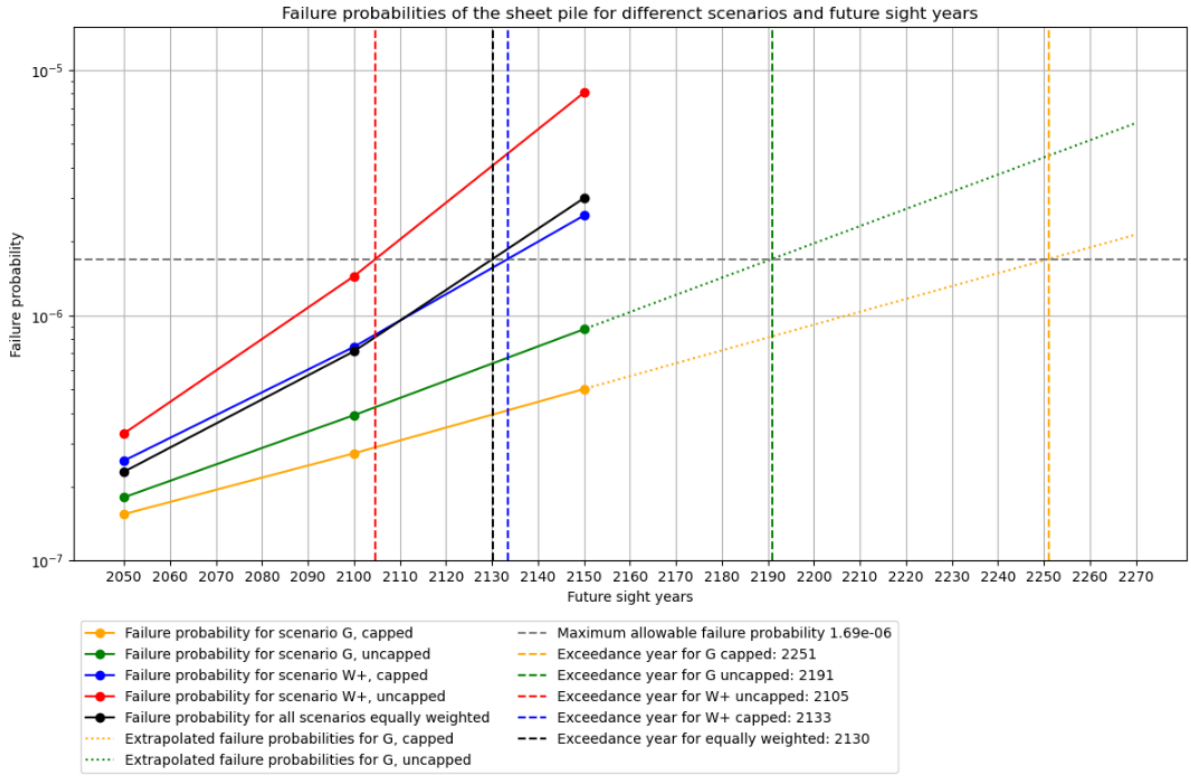

Figure 6.5: The failure probabilities and resulting lifespan for the sheet pile for each climate scenario.

Since it is uncertain which climate scenario becomes reality in the future, the lifespan for a combined future scenario has also been calculated. For this combined future scenario, each climate scenario has been taken into account equally (25% each). The failure probabilities and exceedance year for this equally weighted scenario is also shown in Figure 6.5. It can be seen that the equally weighted scenario is similar to the capped W+ scenario.
Furthermore, the uncapped scenarios give higher water levels for the higher return periods. Since the sheet pile shows increasing conditional failure probabilities for higher water levels, the uncapped scenarios give higher failure probabilities.
It is also observed that the difference in failure probabilities between scenarios increases over time.

In Table 6.2, an overview of the resulting exceedance years is given for each scenario. These years indicate the end of the functional lifespan of the sheet pile for each scenario. These lifespans are used for the LCC analysis in chapter 7.

Scenario G capped	Scenario G uncapped	Scenario W+ capped	Scenario W+ uncapped	Scenario Equally weighted
2251	2191	2133	2105	2130

Table 6.2: The calculated years of exceeding the maximum allowable failure probability for the sheet pile for the different climate scenarios.

6.3.2. Results of the plastic filter screen model

As stated in subsection 5.3.3, the hydraulic heave criterion is used to assess the performance of the plastic filter screen against the progression of the pipe. When the plastic filter screen does not meet the criterion, it is considered a failure, as is the case with the sheet pile. After running the simulations, the plastic filter screen showed no recorded failures for the water levels of $11.00m$ NAP and $11.50m$ NAP, indicating the probabilities are lower than 1/25,000 and 1/15,000 respectively. Similarly to the sheet pile, the probability of failure is very low for these water levels and the number of simulations

was insufficient to capture any failures. A jump in the performance is also seen at $12m$ NAP, however not as steep as for the sheet pile. Using expert judgement, conditional failure probabilities have been assumed that follow the expected shape of the curve. The plastic filter screen shows a similar shape of the curve for the higher water levels as the sheet pile. However, the plastic filter screen did fail for $12m$ NAP, contrary to the sheet pile. In addition, the other conditional failure probabilities are closer to each other. The conditional failure probabilities for $11.00m$ NAP and $11.50m$ NAP are therefore slightly higher, while keeping a similar shape in the curve. All conditional failure probabilities are presented in Table 6.3.

Upstream water level	Conditional failure probability
11.00	$6.67 * 10^{-6}$*
11.50	$3.0 * 10^{-5}$*
12.00	$2.0 * 10^{-4}$
12.50	0.018
13.00	0.044
13.50	0.063
14.00	0.076

Table 6.3: Conditional failure probabilities for different upstream water levels. Estimated failure probabilities are denoted by *.

In Figure 6.6, the fragility curve of the plastic filter screen is presented. Since the failure probabilities are relatively small, the curve is shown on a log scale to give a better visual interpretation. From this fragility curve, the jump in performance can be seen more clearly.

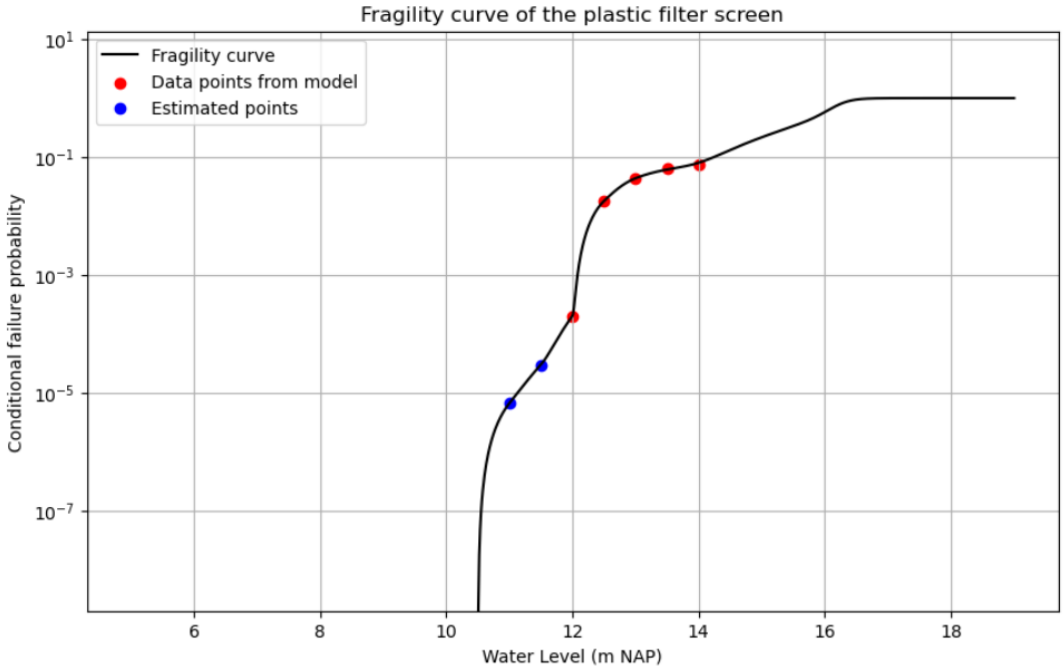

Figure 6.6: The fragility curve of the plastic filter screen plotted on a log scale.

This fragility curve is multiplied with the PDF's of the water levels for the different climate scenarios as described in section 3.3. After integration of the resulting PCC's, the failure probabilities for piping for each scenario and future sight year are calculated. In Figure 6.7, the year of exceeding the maximum allowable failure probability is shown.

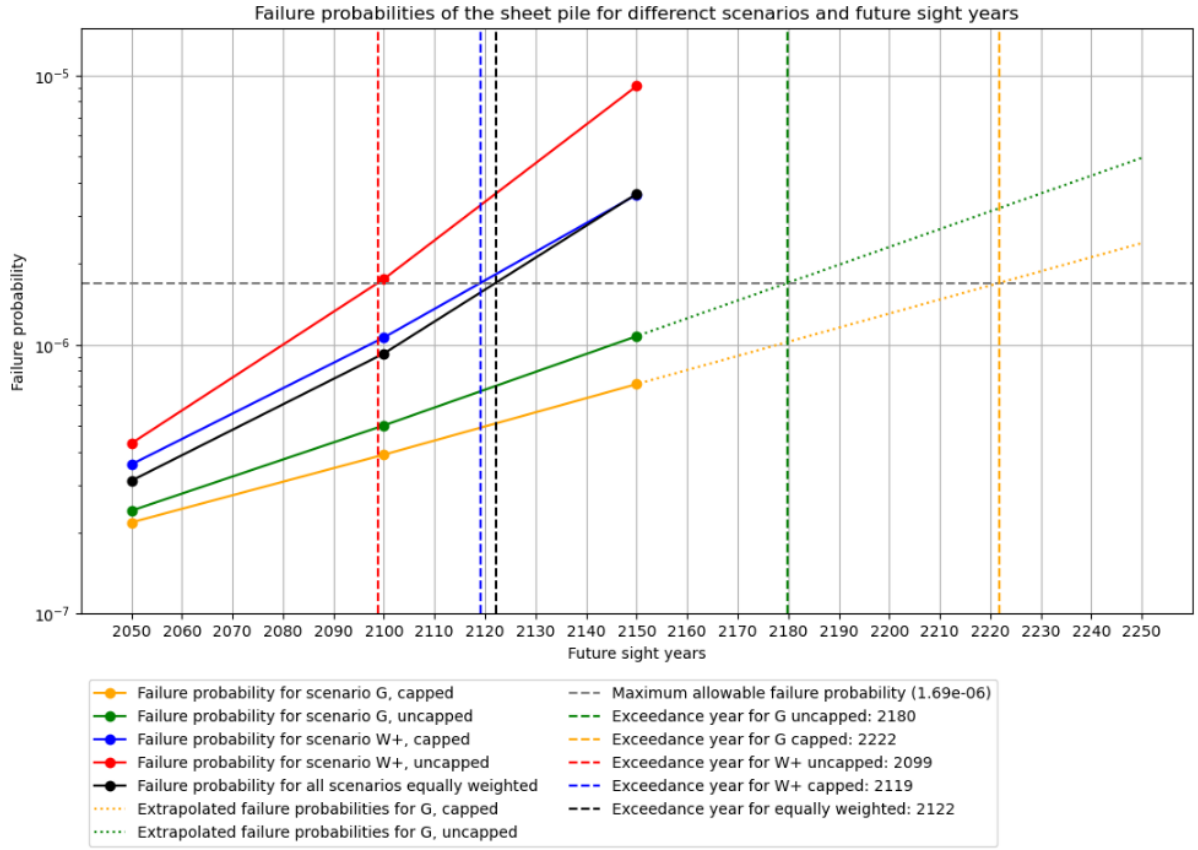

Figure 6.7: The failure probabilities and resulting functional lifespan for the plastic filter screen for each climate scenario.

A combined future scenario, where each climate scenario is equally taken into account, is also evaluated for the plastic filter screen. The failure probabilities and exceedance year for this equally weighted scenario is also shown in Figure 6.7.

In Table 6.4, an overview of the resulting exceedance years is given for each scenario. These years indicate the end of the functional lifespan of the plastic filter screen for each scenario. These lifespans are used for the LCC analysis in chapter 7.

Scenario G capped	Scenario G uncapped	Scenario W+ capped	Scenario W+ uncapped	Scenario Equally weighted
2222	2180	2119	2099	2122

Table 6.4: The calculated years of exceeding the maximum allowable failure probability for the plastic filter screen for the different climate scenarios.

6.3.3. Results of the SoSEAL barrier model

To calculate the conditional failure probabilities for the SoSEAL model, the criterion of Equation 5.3 is checked for each simulation. If the SoSEAL barrier does not meet the criterion, pipe progression cannot be prevented. Not meeting the criterion is considered as a failure due to piping. However, no failures were recorded for upstream water levels of $11.00m$ NAP and $11.50m$ NAP. This is attributed to the limited number of simulations, which was insufficient to capture the very low failure probabilities at these levels. To address this, the probabilities for these water levels were estimated based on the observed behaviour of the SoSEAL barrier at higher water levels. The results for higher water levels indicate that an increase in upstream water level has only a limited effect on the failure probability, since the failure probabilities stay relatively low. The conditional probabilities for $11.00m$ NAP and

$11.50m$ NAP have therefore been estimated to lie relatively close to each other and to the probability for $12.00m$ NAP. All conditional failure probabilities are presented in Table 6.5.

Upstream water level	Conditional failure probability
11.00	$1.0 * 10^{-5}$*
11.50	$6.0 * 10^{-5}$*
12.00	$7.0 * 10^{-4}$
12.50	$8.0 * 10^{-4}$
13.00	0.0020
13.50	0.0060
14.00	0.010

Table 6.5: Conditional failure probabilities for different upstream water levels. Estimated failure probabilities are denoted by *.

In Figure 6.8, the fragility curve of the SoSEAL barrier is presented. Since the failure probabilities are relatively small, the curve is shown on a log scale to give a better visual interpretation. From this fragility curve, it can be seen that the failure probabilities slightly increase with increasing upstream water levels.

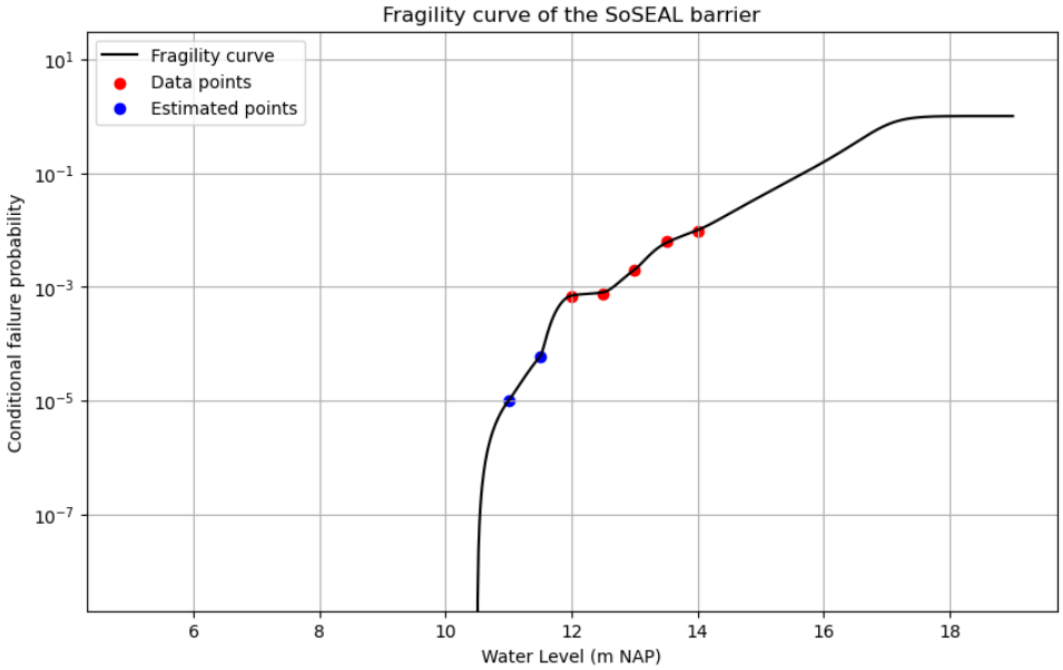

Figure 6.8: The fragility curve of the SoSEAL barrier plotted on a log scale.

This fragility curve is multiplied with the PDF's of the water levels for the different climate scenarios as described in section 3.3. After integration of the resulting PCC's, the failure probabilities for piping for each scenario and future sight year are calculated. In Figure 6.9, the year of exceeding the maximum allowable failure probability is shown. The combined future scenario, in which each climate scenario is taken equally into account, is presented as well.

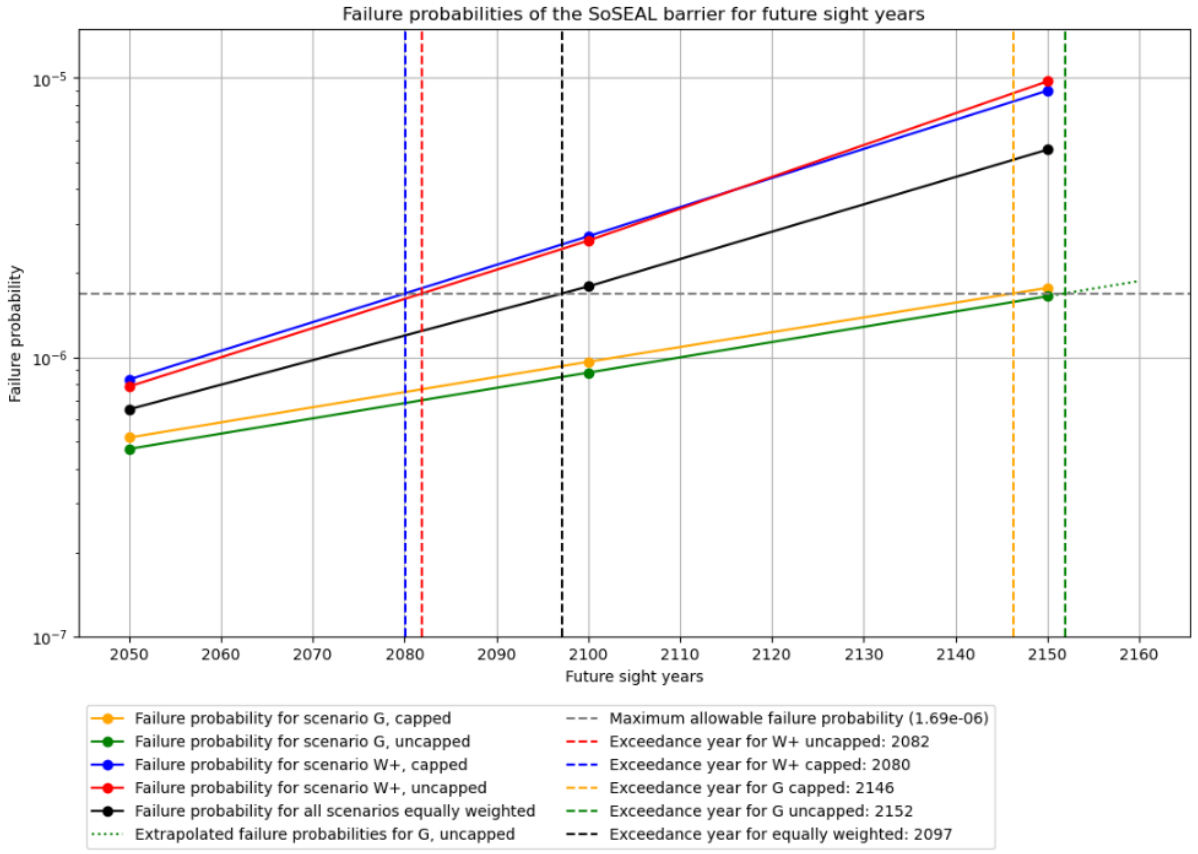

Figure 6.9: The failure probabilities and resulting functional lifespan for the SoSEAL barrier for each climate scenario.

From Figure 6.9, it is observed that the SoSEAL barrier shows relatively similar behaviour for the capped and uncapped scenarios. These scenarios are relatively similar to each other for the lower water levels (up to approximately $12.00m$). The water levels up to $12.00m$ NAP have a considerably higher probability of occurring compared to water levels above $12.00m$ NAP. Only for the return periods of 10,000 and above, equalling low probabilities, are the water levels in the uncapped scenario significantly higher than the capped scenario. Since the conditional failure probabilities of the SoSEAL barrier remain relatively low even at higher water levels, the overall failure probabilities for both the capped and uncapped scenarios show similar trends across future sight years. Additionally, Hydra-NL results indicate slightly higher water levels for capped scenarios at lower return periods compared to uncapped scenarios. Because these lower return periods dominate the overall water level probabilities, capped scenarios yield marginally higher conditional failure probabilities.

In Table 6.6, an overview of the resulting exceedance years is given for each scenario. These years indicate the end of the functional lifespan of the SoSEAL barrier for each scenario. These lifespans are used for the LCC analysis in chapter 7.

Scenario G capped	Scenario G uncapped	Scenario W+ capped	Scenario W+ uncapped	Scenario Equally weighted
2146	2152	2080	2082	2097

Table 6.6: The calculated years of exceeding the maximum allowable failure probability for the SoSEAL barrier for the different climate scenarios.

6.3.4. Comparison of the model results

Based on the fragility curves and failure probabilities for the different scenarios, the behaviour and performance of the different solutions are compared. In Figure 6.10, the fragility curves of the solutions are shown together.

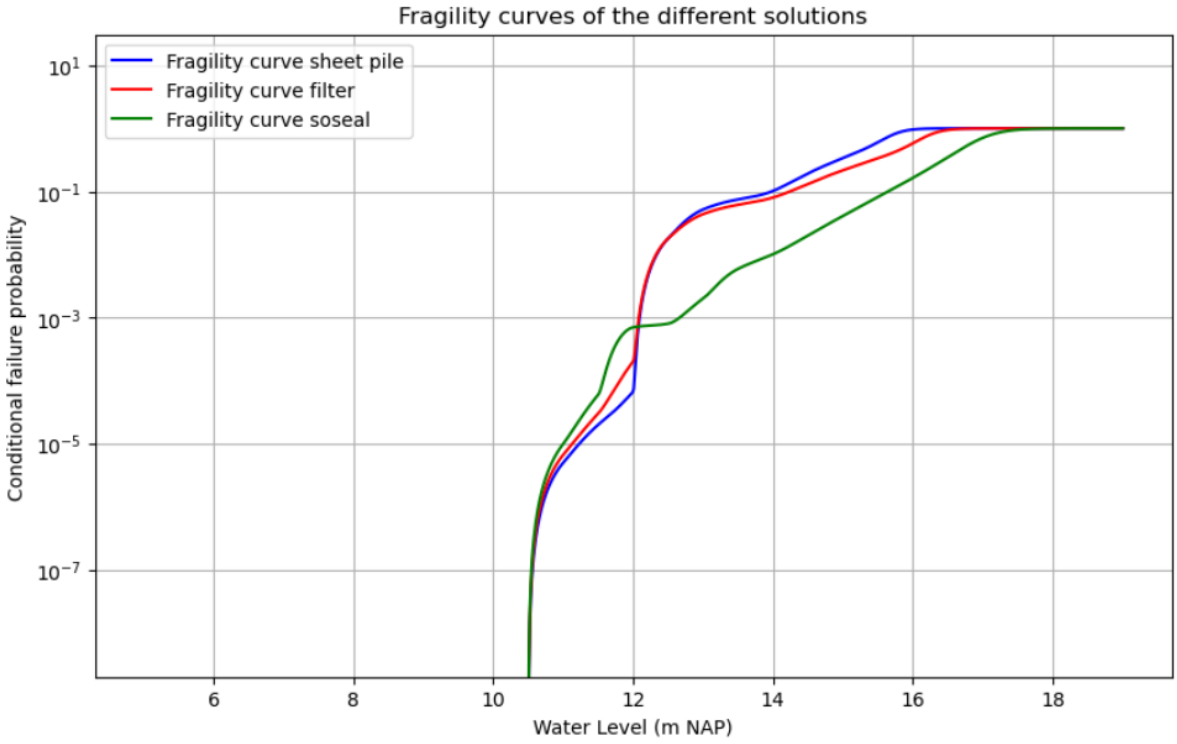

Figure 6.10: The fragility curve of each solution is plotted together to allow for a clear comparison.

The plastic filter screen and sheet pile exhibit similar behaviour in mitigating hydraulic heave behind the screen. Both solutions show a sharp increase in the conditional failure probability at approximately 12.00 m NAP. For higher water levels, the plastic filter screen demonstrates lower conditional failure probabilities than the sheet pile, suggesting that to a certain degree it is less sensitive to increasing water levels. This is due to its filter structure, which allows water to pass through a significant portion of the screen. Notably, the plastic filter screen achieves comparable conditional failure probabilities despite being one meter shorter than the sheet pile.

In contrast, an increase in upstream water levels has only a limited effect on the conditional failure probability of the SoSEAL barrier. However, for lower water levels (below approximately 12.00 m NAP), its failure probabilities are estimated to be higher than those of the plastic filter screen and the sheet pile. This is likely caused by the barrier's heterogeneity and the relatively higher hydraulic conductivity at the contact area. Nonetheless, by completely sealing the aquifer over its full depth, the SoSEAL barrier exhibits greater independence from increasing water levels compared to both the plastic filter screen and the sheet pile.

Lastly, modelling and simulating the solutions revealed that small design adjustments can greatly impact the functional lifespan. These adjustments change the fragility curve by affecting the conditional failure probabilities. These probabilities are very small and the overlay of the fragility curve with the PDF's is minimal. Even slight changes in the design can therefore significantly influence the failure probabilities and the year when the maximum allowable failure probability is exceeded. Consequently, the functional lifespan is highly sensitive to such design modifications. Even more so than considering a different climate scenario.
This also shows that the uncertainties and assumptions in the input for the design, as described in section 5.7, affect the performance of the solutions significantly, especially regarding the innovative solutions.

7

Life cycle cost analysis

7.1. Introduction to the LCC analysis

To evaluate the different piping solutions for various scenarios and uncertainties, a life cycle cost (LCC) analysis is performed. This section provides a short introduction to what is considered when evaluating the life cycle. This evaluation is done quantitatively by assessing the life cycle in costs. The solutions are further investigated and compared for under changing scenarios to evaluate their performance and sensitivity under varying uncertain (future) conditions.

7.1.1. The life cycle

The life cycle of a structure extends from its implementation phase to the end of its lifetime. Since structures differ in design, performance and lifespan, each life cycle is unique. Furthermore, throughout the lifetime of the structure, the loading and environmental conditions can change. This influences the structure and its performance and, consequently, the overall life cycle. When assessing a life cycle, it is therefore important to consider these evolving conditions and the aspects of the structure they influence.
Additionally, the structural aspects are significantly affected by the design of a structure. The design is defined by specific needs, but also involves uncertainties. These must be taken into account and monitored throughout the lifespan when conducting a life cycle evaluation. In addition, the loading and environmental conditions are also subject to future uncertainties, which can influence the total lifetime of the structure. When evaluating the life cycle, these conditions need to be monitored as well and adequate actions need to be considered to ensure sufficient performance during the lifetime of the structure.

In this study, the life cycle of the different piping solutions is evaluated and compared. The different piping solutions have different designs and working principles. Additionally, different lifetimes have been acquired from the model results for each solution. It is currently unclear how the different piping solutions compare when considering their total life cycle. To make a comprehensive evaluation and comparison, all these aspects must be considered and addressed. To be able to quantitatively compare the life cycle of the solutions for different lifetimes, an LCC analysis is performed using the EAC method. This method is explained in more detail in the following subsection.

7.1.2. The method of equivalent annual cost

As mentioned, the equivalent annual cost (EAC) analysis is used to analyse and assess the life cycle costs of the piping solutions. The EAC represents the costs over a certain time frame (i.e., lifespan) as a constant annual cash expense, see Equation 7.3 [52]. The future costs (C) are discounted to the present value using a discount factor. This accounts for the devaluation of money in the future, due to factors such as inflation. By discounting and summarizing all the costs that are made over the entire time frame (t^*), the total present value (PV) is calculated, see Equation 7.2. This total present value can be divided by an annuity factor, to determine the EAC of the considered solution. This annuity factor

is a summation of the discount factors, that are used over the entire time frame, see Equation 7.1 [52].

$$A_{t^*} = \frac{1-(1+r)^{-t^*}}{r} \tag{7.1}$$

$$PV_{tot} = I + \sum_{t=1}^{t^*} \frac{C}{(1+r)^t} \tag{7.2}$$

$$EAC = \frac{PV_{tot}}{A_{t^*}} \tag{7.3}$$

- PV_{tot}: The total present value (€)
- I: The investment costs (€)
  These costs do not need to be discounted as they are implemented at the start of the time frame.
- t: The considered year within the lifespan (year)
- t^*: The total lifespan and last considered year (year)
- C: The costs implemented each year during the lifespan (€)
- r: The discount rate (%)
- $(1+r)^t$: This is considered the discount factor

As stated before, the piping solutions differ in their design and working principles, which influences their performance. This results in different lifespans for the different scenarios. The method of the EAC enables a consistent and representative comparison when considering different lifespans. By determining the EAC for each solution and scenario, the different solutions can be quantitatively evaluated. Using the EAC method, the different degrees of uncertainty in the designs and scenarios, are expressed in costs as well. This results in a range of EAC values for a certain scenario and lifespan. By applying the EAC analysis to various uncertainties for different future scenarios, the total EAC and changes in its range can be assessed. In Figure 7.1, the application of the EAC method in this study is presented graphically over time.

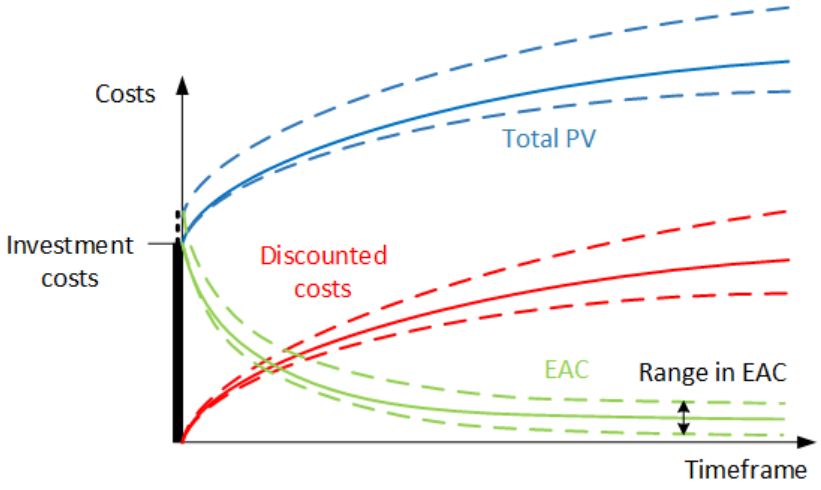

Figure 7.1: The application of the EAC method in this thesis with constant yearly costs over the time frame. Different investment and future costs results in different EAC values. This graph shows a range of EAC values that is determined for a solution and scenario. By considering a different scenario and solution the range is different.

The different future costs, to account for different degrees of uncertainties, result in different discounted costs and total present value for each solution. This results in a range of EAC for each scenario. These future uncertainties are further explained in subsection 7.1.3 below.

7.1.3. Future uncertainties

When assessing the uncertainties for various future scenarios and their corresponding lifespans, different ranges of EAC are acquired for each scenario. By comparing the ranges and changes in the range of the EAC, the sensitivity of the solutions to future uncertainties and different lifespans is assessed. This allows for a quantitative evaluation of the design and performance of the solutions under various future uncertainties. In Figure 7.2, this LCC analysis using EAC is concisely depicted.

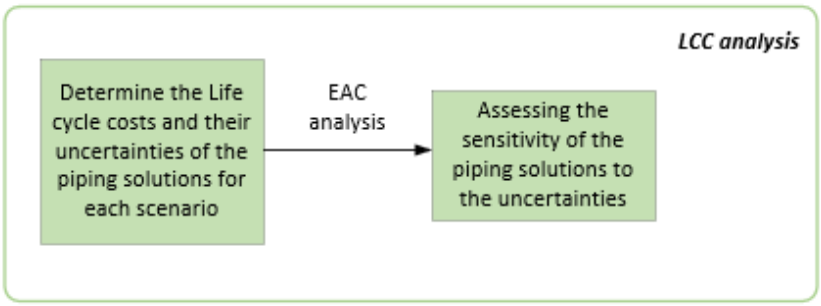

Figure 7.2: Methodology flow chart of the LCC analysis, using the EAC method.

In this study various uncertainties in the future climate, the design and the performance are included. By addressing five different climate scenarios, climate uncertainties are considered. As discussed in section 6.3, from the model results, different lifespans for these climate scenarios are derived. Uncertainties in the design and performance are accounted for with variability in the costs and different technical lifespans. The piping solutions require an initial investment and additional costs that are made during the considered lifespan. By also taking into account economic uncertainties, such as inflation, for prices of materials and construction work, a range of possible costs over the lifespan can be determined. This enables a comparison, independent of differences in lifespans and timing of investments. In section 7.2 the various uncertainties that influence the EAC are discussed further.

7.2. Input variables

In this section the different uncertainties that are used as input variables in the EAC analysis to assess the sensitivity of the solutions are discussed. Each uncertainty addresses the design, performance and/or lifespan of the solution. The variability in different cost expenses reflects the uncertainty in the performance and design of the solutions. The climate scenarios have resulted in different functional lifespans, influencing the time frame of the life cycle. By assessing the variability in the technical lifespan, the uncertainty in the performance and future conditions is taken into account as well. With the EAC analysis the sensitivity to these future uncertainties are assessed.
Most of the costs are based on expert judgement and discussions with my supervisor Yoeri Jongerius

7.2.1. Climate scenarios

The future climate change uncertainties are represented by the different climate scenarios. From the results of the simulated models, the functional lifespans have been determined for each climate scenario. These lifespans are shown in the Table 7.1 for each solution.

	Scenario G capped	**Scenario G uncapped**	**Scenario W+ capped**	**Scenario W+ uncapped**	**Scenario Equally weighted**
Sheet pile	226	166	108	80	105
Plastic filter screen	197	155	94	74	97
SoSEAL barrier	121	127	55	57	72

Table 7.1: The functional lifespans of the different piping solutions for each climate scenario.

7.2.2. Investment costs

The investment costs comprise of three parts; groundwork, materials and installation. The costs of groundwork consider the preparation costs regarding the site before installation procedures can start. The material costs are the expenses necessary to make the piping solution. The costs of installation consist of the delivery, unloading and installing costs of the piping measure.
As stated before, economic uncertainties have been taken into account in the determination of the costs. The volatility in the market prices of raw materials over the last 20-25 years have been considered, as well as fluctuations in costs for construction labour in the civil engineering sector. By estimating the low, average and high points in these prices, a range of costs can be predicted for the piping solutions.

In the determination of the investment costs for the sheet pile, the dimensions of the design and the used AZ24-700 profile are considered. To estimate the range of possible investments costs, the index factors for the market prices of steel and for the civil engineering sector have been analysed [19] [14] [15]. Steel prices are highly volatile. This resulted in a significant change between the lowest and highest steel prices. These steel prices were used to estimate the low and high costs for the materials. The index factors for work in the civil engineering sector have been used to calculate low and high costs for the groundwork and installation.

For the plastic filter screen, the average investment costs have been estimated. Using the index factors for the civil engineering sector, the low and high costs for the groundwork and installation have been determined. Based on the average material costs, it is estimated that the lowest and highest material costs are 20% lower and 20% higher than the average costs, respectively.
This same approach is also used to estimate the range of investment costs for the SoSEAL barrier.

In Table 7.2 the range of investment costs for each solution is given.

Investment costs [€]	Sheet pile	Plastic filter screen	SoSEAL barrier
Low costs	1,080,896.40	1,065,329.81	1,226,702.17
	871.69 [$/m$]	859.14 [$/m$]	989.28 [$/m$]
Average costs	1,676,851.94	1,244,005.36	1,510,396.38
	1,352.30 [$/m$]	1,003.23 [$/m$]	1,218.06 [$/m$]
High costs	2,272,807.49	1,422,680.90	1,794,090.58
	1,832.91 [$/m$]	1,147.32 [$/m$]	1,446.85 [$/m$]

Table 7.2: The variability in investment costs for each solution that is used in the EAC analysis. The costs are also expressed in costs per meter.

7.2.3. Replacement costs

At the end of the time frame of the investigated life cycle, a replacement of the solution can be considered. The costs of replacement are the expenses that are made when the piping solution has reached the end of its technical lifespan and is replaced.
The technical lifespan of the sheet pile is estimated to be a 100 years, while for for the plastic filter screen a lifespan between 50-100 years is estimated by different design guidelines [37] [32]. This study considers an average technical design life of 75 years for the plastic filter screen and for the SoSEAL barrier as well. The piping solutions also have a certain functional lifespan, that runs until it exceeds the maximum allowable failure probability. From Table 7.1, it is evident that under certain climate scenarios, the functional lifespan exceeds the technical design life of the solutions. When the functional lifespan exceeds the technical lifespan, a replacement can be considered. In this analysis a replacement of the solution is therefore also considered as a separate scenario. The replacement costs are for all solutions estimated to be the same as the initial investment costs [27]. So, for the range of replacement costs, see Table 7.2.

It is important to note that the replacement costs are a future investment. These costs need to be discounted to represent them as a present value. In Equation 7.4, the used formula to account for the replacement costs is presented.

$$PV_{replace} = \sum_{k=1}^{m} \frac{C_{replace}}{(1+r)^{k \cdot \Delta t_{rep}}} \tag{7.4}$$

With:

- $PV_{replace}$: Present value of the replacement costs (€)
- $C_{replace}$: Replacement costs, which are equal to the investment costs (€)
- Δt_{rep}: Replacement interval (75 or 100 years)
- $m = [\frac{t^*}{\Delta t_{rep}}]$: Number of replacements within the time frame t^*
- k: The considered replacement within the total amount of replacements

The present value of the replacement costs is added to the total present value (PV_{tot}) of the solution for the considered scenario.

7.2.4. Restoration costs

Restoration costs are implemented for the innovative solutions. Uncertainty can be taken into account, regarding the performance of the plastic filter screen and SoSEAL barrier over an increasing time period. The plastic filter screen can possibly become clogged, while the injected SoSEAL material could dissipate or not reach the desired hydraulic conductivity reduction. It could therefore be necessary to renew the filter sand and re-inject the SoSEAL material, to guarantee sufficient performance. The associated costs with renewing the filter sand and re-injecting SoSEAL are considered with the restoration costs.

The restoration costs for renewing the filter sand are based on a percentage of the original material and installation costs. The plastic filter screen, according to the Prolock design, is constructed so that the filter sand can easily be replaced if necessary. Additionally, sand is a relatively cheap raw material. The costs are therefore only a small percentage, keeping the range of possible costs relatively small. The restoration costs for re-injecting extra SoSEAL material are also based on a percentage of the original investment costs. The costs of the material and injection of SoSEAL are a relatively large part of the investment costs. It is estimated that re-injecting extra SoSEAL material would therefore account for a significant part of these costs, resulting in a wide range of relatively high expenses. In Table 7.3 below, the restoration costs for the plastic filter screen and SoSEAL barrier are shown.

Restoration costs [€]	Plastic filter screen	SoSEAL barrier
Low costs	73,409.76	460,986.13
	59.20 [$/m$]	371.76 [$/m$]
Average costs	95,325.89	667,907.51
	76.88 [$/m$]	538.64 [$/m$]
High costs	119,930.47	912,500.16
	96.72 [$/m$]	735.89 [$/m$]

Table 7.3: The variability in restoration costs for each solution. The costs are also expressed in costs per meter.

the costs for the restoration operations of the plastic filter screen and the SoSEAL barrier are accounted for every 30 years. This interval is estimated to adequately consider potential clogging of the filter screen and degradation of the SoSEAL barrier. Incorporating these restoration costs ensures that the solutions maintain their intended performance throughout the entire considered lifespan. In Equation 7.5, the used formula to account for the restoration costs is presented.

$$PV_{restoration} = \sum_{k=1}^{n} \frac{C_{restoration}}{(1+r)^{k \cdot \Delta t}} \tag{7.5}$$

With:

- $PV_{restoration}$: Present value of the restoration costs (€)
- $C_{restoration}$: Restoration cost per interval (€)
- Δt: Restoration interval (30 years)
- $n = [\frac{t^*}{\Delta t}]$: Number of restoration investments in the time frame t^*

The present value of the restoration costs is added to the total present value (PV_{tot}) of the solution for the considered scenario.

7.2.5. Maintenance & monitoring costs

The maintenance & monitoring costs are applied as a yearly expense over the duration of the lifespan. For this expense item, two separate scenarios are considered. The maintenance & monitoring costs are used as a constant yearly input in the EAC analysis for the default scenario. For the other scenario the maintenance & monitoring costs are applied as a yearly increasing expense. With the solutions possibly degrading faster over time and the possibility of more extreme events occurring during the lifespan, a yearly increase in the costs is considered as realistic input for the sensitivity assessment as well.

The maintenance & monitoring costs of the sheet pile are estimated to be 2% of the investment costs each year [12]. The low and high end are based on the low and high investment costs, respectively.
For the plastic filter screen, a range of 2 to 10% of the average investment costs has been applied for the maintenance & monitoring costs. This wider range of costs is considered appropriate, to account for the uncertainties in the innovative design of the solution. For the SoSEAL barrier, a range of 2 to 10% of the average investment costs has been applied for the maintenance & monitoring costs as well. This results in a relatively wide range of costs. Since the SoSEAL barrier has certain significant uncertainties in the design as well, see section 4.4. This range is considered fitting.
For the yearly increase in costs for each solution, 2% of the average yearly maintenance & monitoring costs is estimated for each scenario. No high and low costs are estimated for the yearly increase. In Table 7.4, the maintenance & monitoring costs for both the yearly constant and increasing scenario are presented for each solution.

Maintenance & Monitoring (M&M) [€/y]	**Sheet pile**	**Plastic filter screen**	**SoSEAL barrier**
Low costs	21,617.93	24,880.11	130,207.93
	17.43[$/m$]	20.06 [$/m$]	24.36 [$/m$]
Average costs	33,537.04	62,200.27	75,519.82
	27.05 [$/m$]	50.16 [$/m$]	60.90[$/m$]
High costs	45,456.15	124,400.54	151,039.64
	36.66[$/m$]	100,32 [$/m$]	121.81 [$/m$]
Yearly increase in M&M costs [€/y]	670.74	1244.01	1510.40
	0.54[$/m$]	1.00 [$/m$]	1.22 [$/m$]

Table 7.4: The variability in the constant maintenance & monitoring costs for each solution. The yearly increase in the costs for each solution is shown as well. The costs are also expressed in costs per meter.

Depending on whether the costs are constant or yearly increasing, they are implemented differently as input in the EAC analysis. Equation 7.6 is used to calculate the costs when the scenario with constant yearly maintenance & monitoring is evaluated and Equation 7.7 is used when the scenario with yearly increasing maintenance & monitoring costs is evaluated.

$$C = C_{constant} \tag{7.6}$$

$$C = C_{constant} + (t-1)c_{incr} \tag{7.7}$$

With:

- C: The yearly maintenance & monitoring costs (€)
- $C_{constant}$: Constant amount of yearly maintenance & monitoring costs (€)
- c_{incr}: the yearly increase in maintenance & monitoring costs (€)

7.2.6. Technical lifespan

A scenario with varying technical lifespans is also considered, to take uncertainty into the performance of the design into account. As stated earlier, the sheet pile is assumed to have a lifespan of 100 years, while the plastic filter screen and SoSEAL barrier are estimated at 75 years. However, these estimates are uncertain. Conditions may be harsher than anticipated or the design of solutions may underperform. It is also possible that the solutions may last longer if their design proves to be more resilient or conditions are more favourable. To account for this uncertainty, both lower and upper bounds of technical lifespan are included in the analysis. Because the plastic filter screen and SoSEAL barrier have greater design and performance uncertainties than the sheet pile, a wider range is applied to those lifespans. Since the design guidelines suggest a range of 50–100 years for the filter screen [31][36], this range is used for the varying technical lifespans. This range is also adopted for the SoSEAL barrier. For the sheet pile, a smaller uncertainty is taken into account, leading to a smaller range: 85–115 years. In Table 7.6, an overview of the range of technical lifespans is given.

Technical lifespans	Sheet pile	Plastic filter screen	SoSEAL barrier
High estimate	115	100	100
Average estimate	100	75	75
Low estimate	85	50	50

Table 7.5: The estimates of the different technical lifespans of the piping solutions to account for future uncertainties.

7.2.7. Discount factor

To calculate the discount factors ($(1+r)^t$), various discount rates are possible to be used. In this study, the discount rate for fixed costs that are largely independent of its use and less affected by economic growth is considered. According to Steunpunt Economische Expertise and the HWBP programme, a rate of $r = 1.6\%$ is therefore used [20] [27]. However, the discount rate can change significantly in the future. Approximately ten years ago the rate for fixed costs was 2.5% and the rate for considering societal costs 5.5% [52].

The discount rate is an important parameter in the EAC analysis. It influences the present value by regulating how much future costs are discounted. Additionally, it influences the total EAC by altering the annuity factor for the considered lifespan. In section E.1, the effect of different discount rates on the EAC of the solutions for the different scenarios is further elaborated and discussed.

7.3. Results EAC analysis

In this section, the results of the EAC analysis for the different scenarios are presented. By comparing the differences in the EAC for the different scenarios, an evaluation is performed. This evaluation addresses the sensitivity and performance of the solutions under the given uncertainties.

7.3.1. Default scenario

The first EAC analysis covers the default scenario. The default scenario consists of a range that covers nine combinations of low, average and high cost regarding the investment, restoration and constant yearly maintenance & monitoring expenses. These costs are considered for the functional lifespans (see Table 7.1) of each climate scenario.

In Figure 7.3, the full range of the EAC is shown for each solution and scenario.

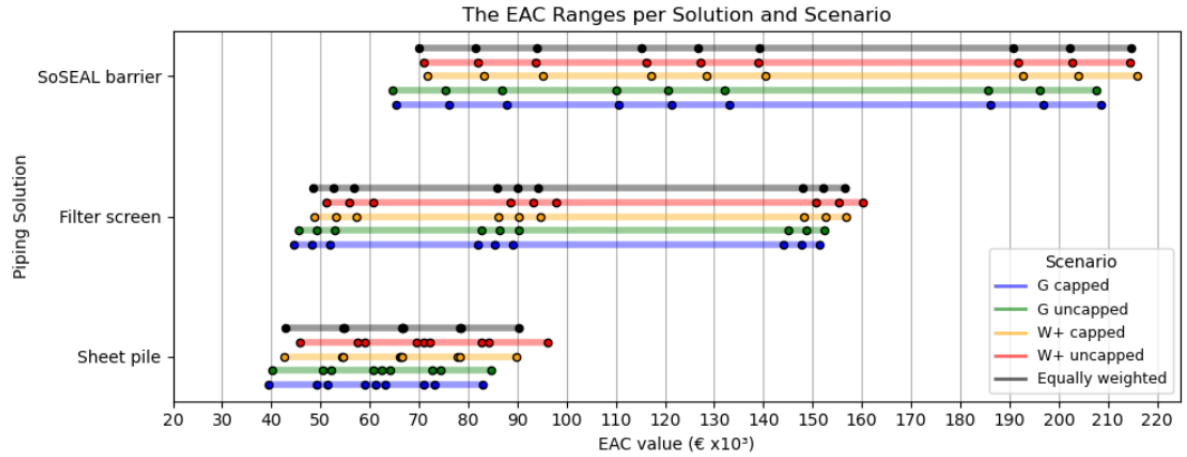

Figure 7.3: The EAC ranges for each solution and scenario, with constant maintenance & monitoring costs. The range consists of the combinations of the lowest, average and highest costs options from the cost tables of each solution. The replacement costs are not considered.

Figure 7.3 shows that for the different climate scenarios the EAC stays in a similar range. With the G scenarios, the time frames increase compared to the W+ scenarios. With increasing time frames, i.e. longer lifespans, the total present value increases, but the annuity factor as well. Consequently, the resulting EAC values for different climate scenarios stay in similar ranges. However, the ranges of the more extreme W+ scenarios, are shifted more to the right, resulting in slightly higher EAC values. Furthermore, it is clear that the ranges for the SoSEAL barrier and plastic filter screen are both significantly larger than the ranges for the sheet pile. This shows that the sheet pile has less design and performance uncertainties compared to the plastic filter screen and SoSEAL barrier. Additionally, the ranges for the SoSEAL barrier are larger than those of the plastic filter screen and start at higher EAC values. The higher starting EAC values of the SoSEAL barrier, are mainly due to the considerably higher restoration costs, compared to those of the sheet pile and plastic filter screen. From Table 7.1, it can be seen that these costs are implemented at least twice for the moderate and weighted scenarios, and once for the W+ scenarios, adding considerable costs over the total lifespan.
From Figure 7.3, it is also evident that the costs for the plastic filter screen and SoSEAL barrier are clustered into three groups, while the costs for the sheet pile are more uniformly distributed. The cluster behaviour and significantly larger EAC ranges for the SoSEAL barrier and plastic filter screen are due to the uncertainty in their yearly maintenance & monitoring costs. Since these costs are implemented every year, its value influences the total range the most. The left cluster corresponds to all options with low maintenance & monitoring costs, the middle cluster to the options with average m & m costs and the right cluster to the options with high m & m costs. This is more clearly illustrated with Figure 7.4 below.

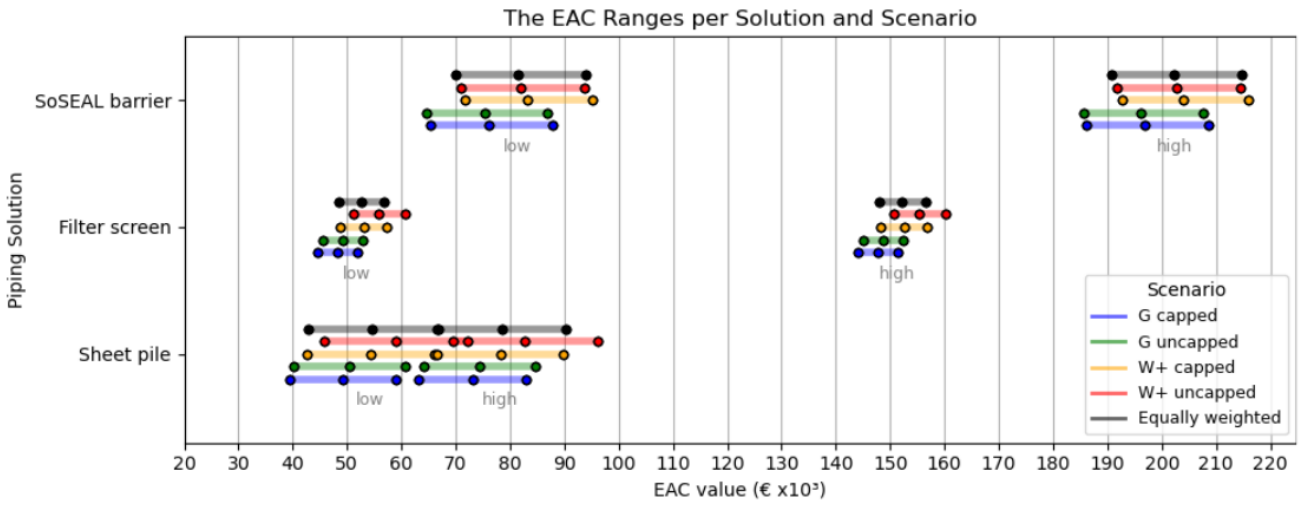

Figure 7.4: The different EAC ranges for low and high maintenance & monitoring costs. The options with average maintenance & monitoring costs are excluded from this figure. In both the low and high range are still the low, average and high costs for the other expenditure items considered.

This figure shows that the yearly maintenance & monitoring costs are the key factor in determining the EAC range for the plastic filter screen and SoSEAL barrier. Even though the lowest and highest costs for the other expense items are still incorporated, the low and high range are significantly further apart than for the sheet pile. Since the sheet pile has more certainty in its maintenance & monitoring costs, the ranges are closer together. However, this also shows that there is less room for improvement. For the plastic filter screen and SoSEAL barrier, it can be seen that if the maintenance & monitoring costs would become more certain, the total width of the EAC range would be substantially smaller. The innovative solutions would then become a more attractive and economically viable option to implement. However, they could still be more expensive than the sheet pile.

7.3.2. Sensitivity to increasing maintenance & monitoring costs

As shown in subsection 7.3.1, the maintenance & monitoring costs play a crucial role in the EAC analysis. It is also a realistic scenario that the maintenance & monitoring costs increase each year over time, as stated in subsection 7.2.5. It is therefore considered valuable to take the yearly increasing maintenance & monitoring costs into account as a separate scenario as well.
In Figure 7.5, the EAC ranges for yearly increasing maintenance & monitoring costs with the functional lifetime as the considered time frame, are presented. The EAC values have increased compared to the scenario with constant maintenance & monitoring costs. This is expected because each year more costs are added to the total present value. Since the yearly increase is significantly higher for the SoSEAL barrier and plastic filter screen, those EAC values have increased the most. Furthermore, all solutions show higher EAC values for the moderate scenarios compared to the W+ and equally weighted scenarios. This shows that with increasing yearly costs, a longer lifespan results in higher EAC values. This is interesting, since for constant yearly maintenance & monitoring costs a shorter lifespan resulted in higher EAC values. This indicates that the increase in the present value over the years has a relatively larger impact than the discounting and the increase in annuity factor.

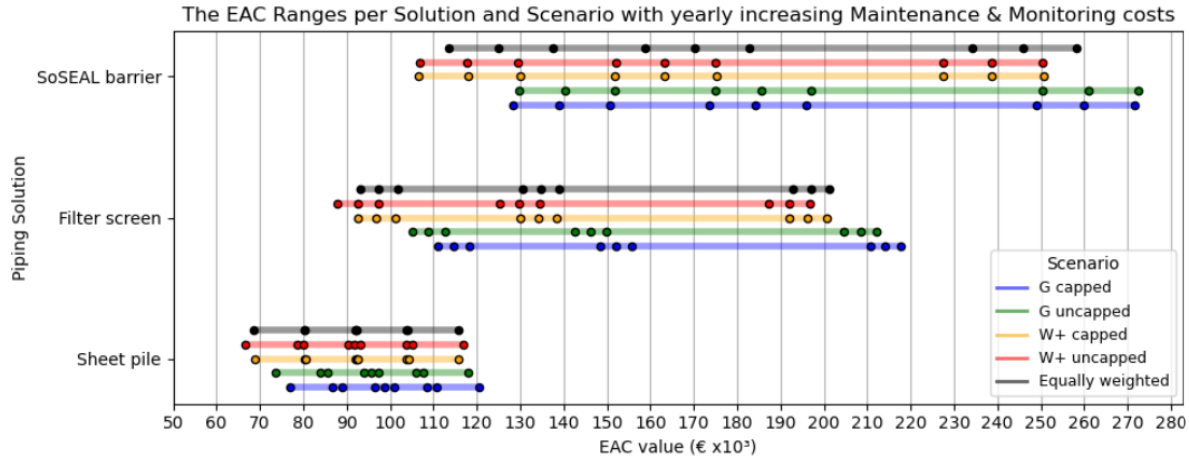

Figure 7.5: The EAC ranges for the functional lifespan with yearly increasing maintenance & monitoring costs.

7.3.3. Sensitivity to different lifespans

Since many of these functional lifespans exceed the technical lifespan of the solutions, another EAC analysis is performed with the technical lifespans as the time frame. In Table 7.6 the new time frames are presented. When the technical lifespan is not exceeded, the functional lifespan is still considered for that scenario.

	Scenario G capped	**Scenario G uncapped**	**Scenario W+ capped**	**Scenario W+ uncapped**	**Scenario Equally weighted**
Sheet pile	100	100	100	80	100
Plastic filter screen	75	75	75	74	75
SoSEAL barrier	75	75	55	57	72

Table 7.6: The total lifespans (t^*) of the different piping solutions for each climate scenario.

When comparing the lifespans to those from Table 7.1, the time frames for the moderate G scenarios have become significantly smaller, while the lifespans for the W+ and equally weighted scenarios changed relatively little.

Constant yearly maintenance & monitoring costs

First, the EAC of the solutions for constant yearly maintenance & monitoring costs is evaluated. In Figure 7.6 the EAC ranges when considering the technical lifespans are presented. The ranges for the different scenarios become very similar due to the similar time frames.

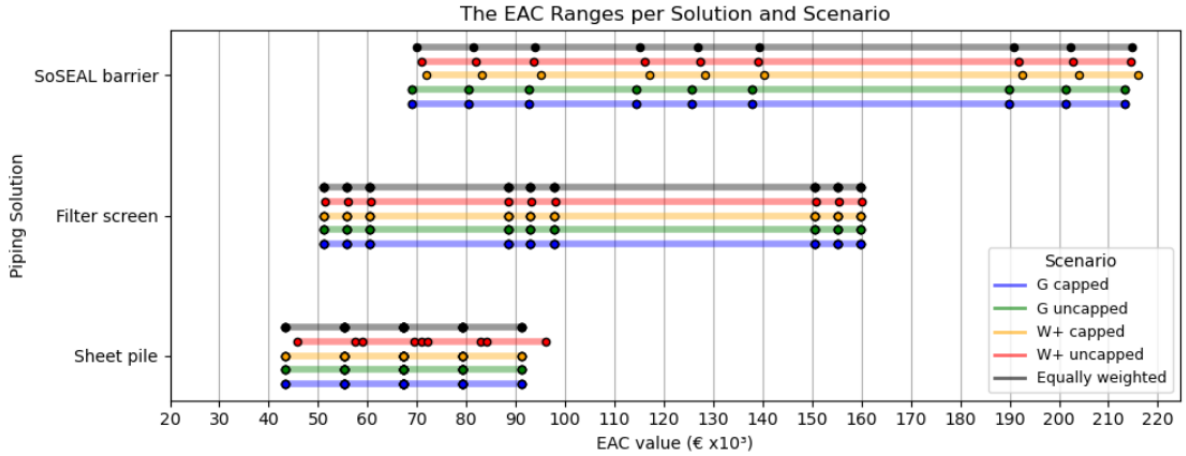

Figure 7.6: The EAC ranges for the different solutions and climate scenarios, considering the lifespans form Table 7.6 and constant yearly maintenance & monitoring cost.

The differences in EAC for the technical lifespan and functional lifespan are relatively small. To be able to compare the differences with Figure 7.3 more clearly, the difference between the two ranges is plotted in Figure 7.7. The total ranges are subtracted from each other for each scenario to show the increase or decrease at both ends of the ranges. An increase in EAC on either end of the range thus shows a shift to the right (higher EAC values), whereas a decrease in EAC on either end shows a shift to the left of the (lower EAC values).

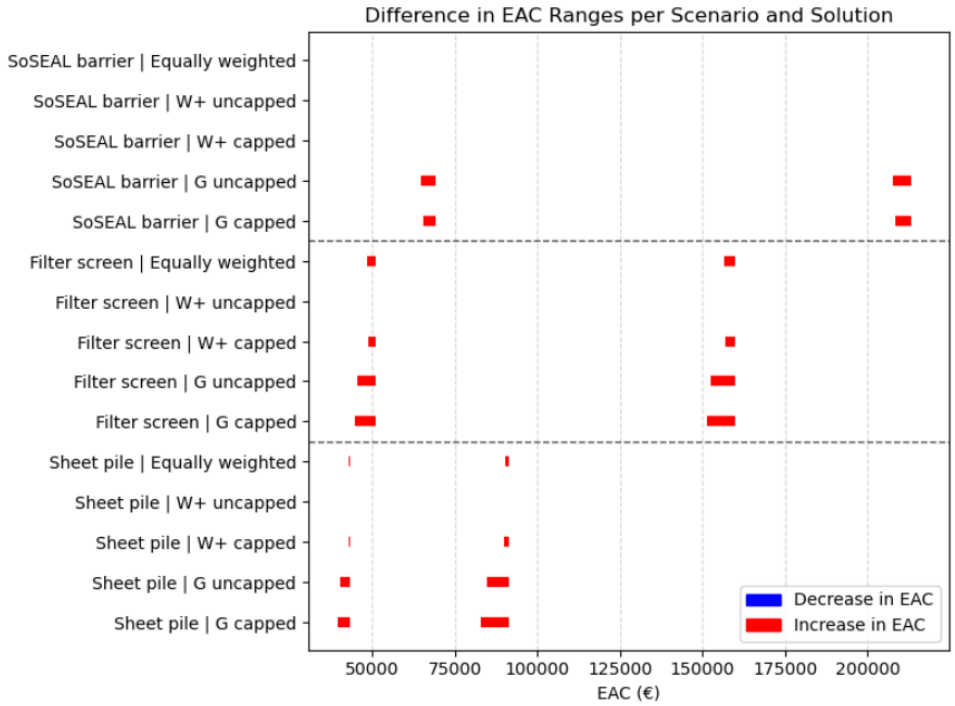

Figure 7.7: The difference in the EAC ranges over the technical lifespan compared to the functional lifespan, with constant maintenance & monitoring costs. The visualisation shows that the EAC values have stayed the same or have increased when considering the technical lifespan.

When the technical lifespan is not exceeded and the functional lifespan is thus still considered, there is no change in EAC. Figure 7.7 shows that for the technical lifespan, the EAC ranges have shifted to higher EAC values. This increase is the most for the moderate G scenarios. This shows again that for longer time frames and constant maintenance & monitoring costs, the annuity factor has a greater impact than the increasing total present value. This is due to the fact that the maintenance & monitoring costs do not increase over time, but are increasingly discounted. Since the time frames for the G scenarios have decreased significantly more compared to the W+ scenarios, when considering the technical lifespan, these EAC values have increased more. The differences in the EAC ranges are in similar ranges for each solution.

To evaluate the influence of a replacement cycle an additional time frame is considered. Since the technical lifespan for the plastic filter screen and SoSEAL barrier is estimated to be 75 years, a maximum life cycle of 150 years is considered. The replacement costs are implemented after 75 years in 2100. With a technical life span of a 100 years, the maximum considered life cycle for the sheet pile is 200 years. Replacement costs are implemented after a 100 years in 2125. The functional lifespan of a solution is still considered, if the 150 or 200 year time frame exceeds their respective functional lifespan. In Figure 7.8, the differences in EAC ranges are displayed between the functional lifespan without considering replacement and the life cycle with replacement.

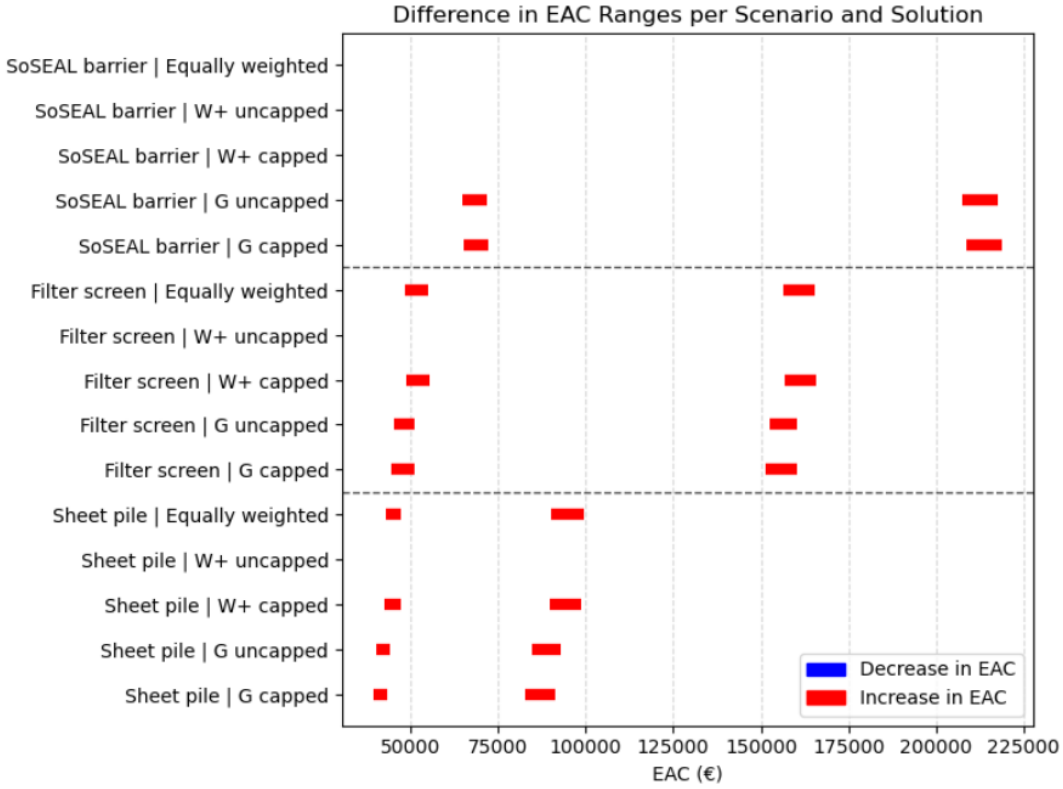

Figure 7.8: The difference in the EAC ranges over a life cycle with a replacement is compared to the functional lifespan (without replacement). Constant maintenance & monitoring costs are considered. The visualisation shows that the EAC values have increased when considering a replacement cycle. Only when the time frame stayed the same for a scenario, the EAC values did not change.

Since the replacement costs are a relatively large investment, they cause a jump in the total present value of the solution, increasing the EAC. It can be seen that mainly for the relatively long time frames of the moderate scenarios, the EAC values increase when considering the replacement costs of the solution. This is to be expected, since for longer time frames a replacement needs to be implemented. While for the more extreme climate scenarios the functional lifespan is often shorter than the technical lifespan. For the W+ scenario with an uncapped discharge, none of the solutions perform well enough to reach beyond their technical lifespan. A replacement is then not implemented, resulting in the same

EAC. Although the replacement costs differ between the solutions, the increase in EAC is relatively similar for scenarios that need a replacement.

Increasing yearly maintenance & monitoring costs

The sensitivity to different lifespans is also considered for yearly increasing maintenance & monitoring costs. When comparing the EAC values and ranges with the technical lifespan as the time frame, a decrease is observed, see Figure 7.9. This is expected since the time frames are shorter. Additionally, the bigger the difference between the technical lifespan and functional lifespan, the higher the decrease in EAC values. This shows it is important to consider the technical lifespan when comparing the solutions, since it causes significant differences. Furthermore, the decrease is significantly smaller for the sheet pile compared to the plastic filter screen and SoSEAL barrier. Besides the smaller difference in lifespans for each scenario, this is also due to the sheet pile's lower yearly costs. The differences in EAC additionally show that a different lifespan has especially impact on the plastic filter screen and SoSEAL barrier, since their yearly increase is relatively high.

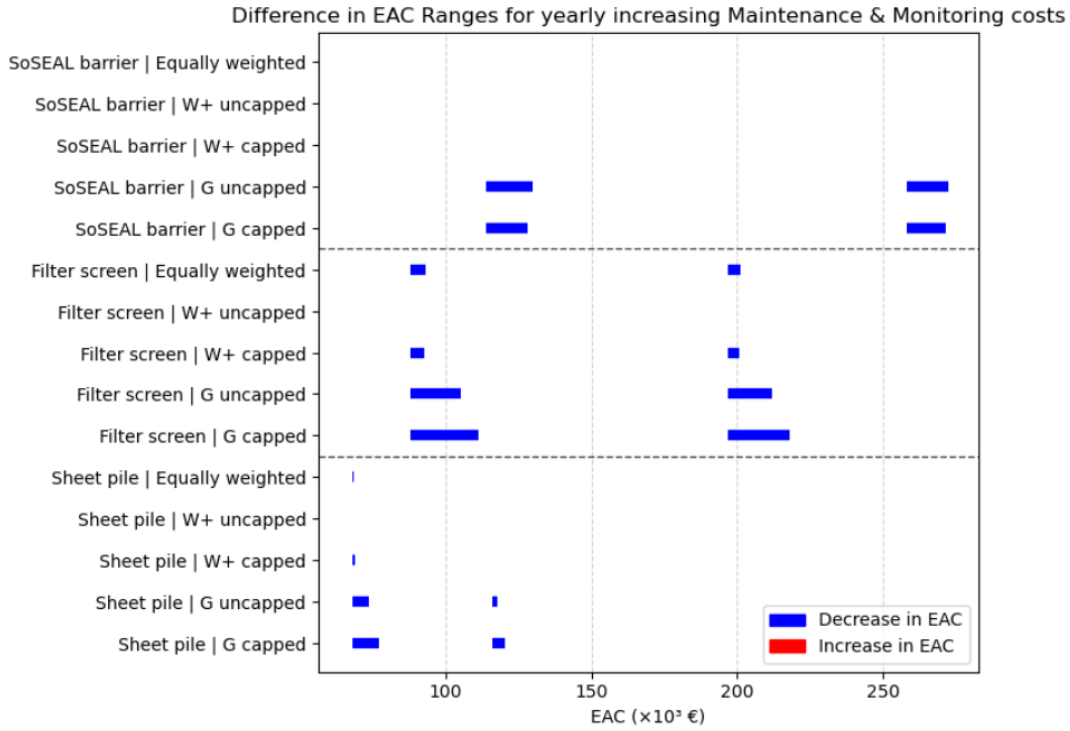

Figure 7.9: The EAC differences between considering the functional lifespan and the technical lifespan, both with yearly increasing maintenance & monitoring costs. The shorter technical lifespan shows a decrease in EAC for most scenarios compared the time frame of the functional lifespan.

Lastly, the scenario with varying technical lifespans is considered. In this EAC analysis the high and low estimates for each solution, from Table 7.5 are compared. Since a different lifespan has a greater impact on the scenario with increasing yearly costs compared to constant yearly costs, the evaluation for different technical lifespans is done for the scenario with increasing yearly costs. In Figure 7.10 the differences between a longer and a shorter technical lifetime are shown.

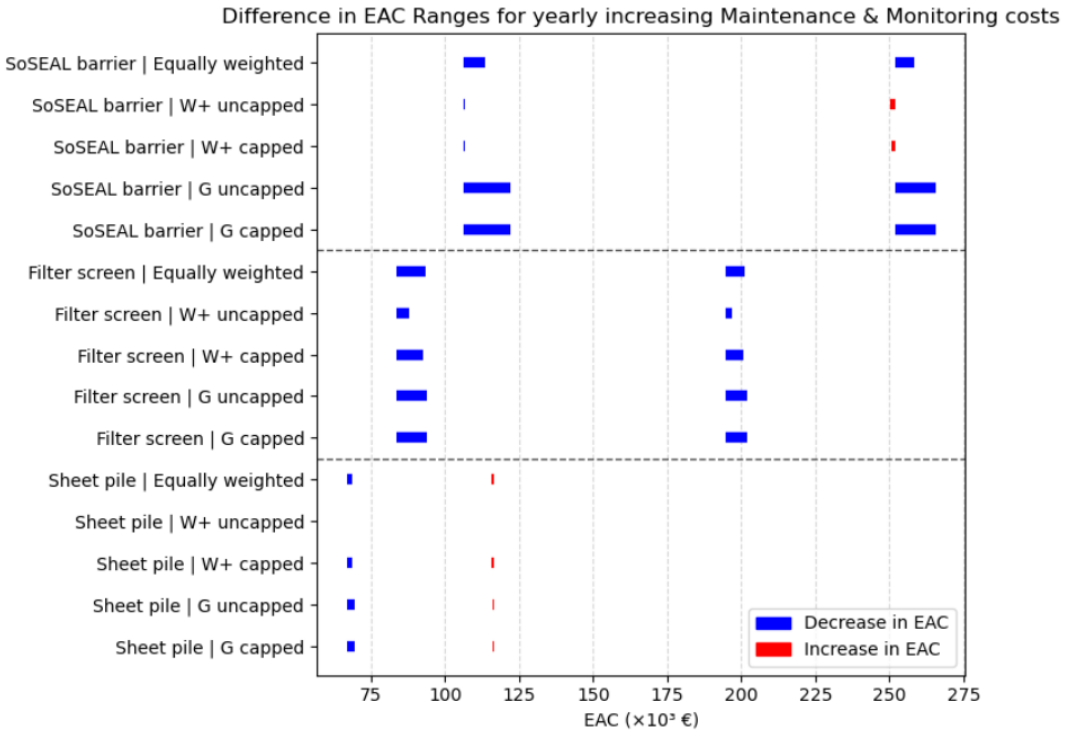

Figure 7.10: The difference in EAC ranges between different technical lifespans with yearly increasing maintenance & monitoring costs. A comparison between a technical lifespan of 100 and 50 years is made for the plastic filter screen and SoSEAL barrier. For the sheet pile the comparison is made between a technical lifespan of 115 and 85 years. If the technical lifespan exceeds the functional lifespan, the functional lifespan is considered.

A shorter technical lifespan shows a decrease in the EAC of the plastic filter screen for all scenarios. For the SoSEAL barrier, a decrease is observed with a shorter lifespan for the moderate scenarios and equally weighted scenarios. However, for the W+ scenarios there is a small decrease on the left and increase on the right, meaning the range is wider for a shorter lifespan. The solution becomes thus more sensitive to the costs uncertainties. It is important to note that for the W+ scenarios of the SoSEAL barrier the difference between the 50 year lifespan is small, because the functional lifespan for the capped and uncapped scenario are 57 and 55, respectively. For the sheet pile, similar behaviour is seen. For all scenarios except the W+ uncapped scenario (since the functional lifespan is only 80 years), the range becomes wider for a shorter lifespan. This is interesting since it was observed in Figure 7.9 that a 100 year technical lifespan decreases the EAC compared to the higher functional lifespans. This suggests that the effect of shorter lifespans leading to lower EAC values and shorter ranges, only holds up to a certain point. By investigating more lifespans this effect could be further analysed for all solutions.
However, as discussed, the increase and decrease in the range of EAC is different for each solution and scenario. This shows that for the investigated designs and current costs, each solution has a different (optimal) lifespan for which this range is minimal. More importantly, each solution is a different number of years away from their optimal lifespan. Since one solution may thus be closer to the optimum then the other, a direct comparison is difficult to perform.

7.4. Key findings

By assessing the uncertainty in the costs for different climate scenarios, it shows that the economic and design uncertainties have a greater influence on the amount and range of EAC, compared to the climate uncertainties. It was found that especially the uncertainty in the maintenance & monitoring costs contribute the most to the range and uncertainty in the EAC of the solutions. Furthermore, with constant yearly maintenance & monitoring costs, the EAC values are lower for shorter lifespans. With yearly increasing maintenance & monitoring costs, the EAC values increase for shorter lifespans.
Since the range of these costs is the smallest for the sheet pile, this piping solution shows the least

uncertainty in the EAC. Additionally, for increasing maintenance & monitoring costs the sheet pile showed little sensitivity to changing lifespans (i.e. future uncertainties), while the plastic filter screen and SoSEAL barrier showed a significant decrease. For constant maintenance & monitoring costs all solutions are similarly sensitive to changing conditions.
It is also found that all solutions are less sensitive to different lifespans for the W+ scenarios. This is because the functional lifespans are already shorter compared to the more moderate scenarios. Considering the technical lifespan, does therefore not yield a (significant) difference in the time frame.

So, according to these differences, the sheet pile is the least sensitive to uncertainties in the lifespan under yearly increasing costs compared to the plastic filter screen and SoSEAL barrier. With increasing time, however, the knowledge on the innovative solutions and certainty in their design will increase. The amount and range of yearly costs of the innovative solutions will then decrease with time. This would make the plastic filter screen and SoSEAL barrier less sensitive to the future uncertainties and could potentially make them a competitive alternative to the sheet pile.

Another key finding from Figure 7.10 shows that there may be an optimal lifespan for the solutions when yearly increasing costs are considered. In this thesis, however, only one design and a limited number of lifespans for each solution is evaluated. Since the solutions differ in costs and performance, each solution has a different optimal lifetime. Additionally, it is unclear how close the considered lifespans are to their optimum lifetime. This makes a comparison of the changes in the values and range of the EAC between the solutions difficult.

Lastly, in this EAC analysis, the increasing risk of dike failure over time is not taken into account. The failure probabilities considered in this study relate exclusively to piping of a certain section of the dike trajectory. Furthermore, failure due to piping represents only one aspect of the overall dike failure probability. Other failure mechanisms, such as macro-stability and overtopping, must also be considered to determine the critical failure mode. Therefore, attributing the total risk of dike failure solely to the performance of the piping solutions of this dike section would not be accurate or representative without accounting for the other failure mechanisms.
Nevertheless, it is of interest to examine how incorporating risk affects the EAC. As risk increases over time, this is represented by adding a non-constant, annually increasing expenditure to the analysis. The impact of this adjustment is demonstrated in section E.2.

8

Conclusions & recommendations

8.1. Conclusions

This study evaluates the design and life cycle performance of different piping solutions under climate change uncertainties. The aim was to address the knowledge gap regarding how (innovative) solutions with distinct working principles compare in their performance under varying climate change uncertainties, and how these differences affect the costs of their associated life cycle. The research was guided by the following main question:
How does the design and life cycle of different piping solutions compare under climate change uncertainties?

To answer this question, the following sub-questions are addressed in this study:

1. What are the effects and uncertainties of climate change on the different piping solutions, and how are these currently considered in the design guidelines?
2. How can the different solutions be modelled to investigate their performance under climate change uncertainties, using COMSOL?
3. What are the effects of the different designs and climate change uncertainties on the failure probabilities due to piping for each solution, according to the COMSOL model?
4. How does the sensitivity of the different solutions to the design and climate change uncertainties compare, based on a life cycle cost analysis?

Changes in temperature, precipitation, and drought conditions do influence the hydraulic gradient, a key driver of backward erosion piping. An increase in precipitation and extreme discharges raise upstream water levels and gradients, while drought related subsidence can increase the gradient as well. These effects carry uncertainty due to the amount of human activities, which is represented by different climate scenarios. In this thesis a moderate G and high emission W+ scenario from the KNMI [55], for a capped and uncapped discharge have been considered. Furthermore, a combined scenario with all four scenarios taken into account equally (25% each) is considered. The likelihood of each scenario is uncertain as well. It is important to account for these future uncertainties in the design decisions. Current design guidelines however, rarely consider climate change in relation to the design and lifetime of the structure. Where mentioned, they lack explicit methods on how to incorporate the relevant uncertainties into the design.

The different working principles of each solution determines their sensitivity and performance under varying hydraulic gradients. These aspects were evaluated by assessing the representative failure criteria using COMSOL models. All models were built with the fictitious permeability approach for the erosion pipe. The failure criterion for each solution is based on the critical event in the steps leading to piping failure. The hydraulic heave criterion is analysed for the sheet pile and plastic filter screen, while the SoSEAL barrier was assessed using the Sellmeijer horizontal gradient criterion. The sheet pile was modelled as an impermeable domain and the plastic filter screen using an equivalent

hydraulic conductivity for the filter section. A heterogenous field of normally distributed HCR factors and a weakened contact area are used to model a representative SoSEAL barrier. Climate change effects were represented in the model by varying upstream water levels. The models were simulated for these water levels, and the performance was quantified using conditional failure probabilities.

From the models and resulting conditional failure probabilities for piping, it is concluded from this study that the plastic filter screen and sheet pile exhibit similar performance; besides both preventing hydraulic heave, they show a sharp increase in failure probability beyond 12.0 m NAP. This threshold is specifically for the designs modelled in this thesis. From the threshold value it is concluded that from a certain water level the sheet pile and filter screen are more prone to piping. Although, the plastic filter screen proved slightly less sensitive to rising water levels, likely due to its permeable structure. The SoSEAL barrier, when fully sealing the aquifer, demonstrated low sensitivity to higher water levels compared to the other solutions. However, for relatively low water levels, its estimated failure probabilities were higher, likely due to the heterogeneity of the barrier and elevated hydraulic conductivity at the contact interface. Overall, the SoSEAL barrier showed similar trends for capped and uncapped scenarios, as its failure probabilities remained low even for extreme events.
The results and piping failure probabilities of each solution are significantly influenced by the model input. This input is subjected to assumptions, design choices and model characteristics. Especially the plastic filter screen and the SoSEAL barrier have inherent uncertainties due to their innovative designs. The performance of the barrier depends heavily on the injection technique and SoSEAL material, which influence the contact area and the amount of reduction in hydraulic conductivity. The performance of the plastic filter screen is dependent on the modelled equivalent hydraulic conductivity, which is subjected to the uncertainties in the filter screen, filter sand and the hydraulic conductivity of the aquifer. Improving these aspects by decreasing the uncertainties in the future or taking different estimations could significantly increase the performance of the innovative solutions.

Using the Equivalent Annual Cost (EAC) analysis, the life cycle costs under different design and climate uncertainties have been determined. By analysing and comparing the amount and range in costs for different scenarios, the sensitivity of the solutions to the uncertainties is assessed.
The sheet pile demonstrated the lowest values and range in EAC, followed by the plastic filter screen and the SoSEAL barrier. The range of EAC values, was most sensitive to the uncertainty in the maintenance & monitoring costs, highlighting the importance of accurate cost estimations. While differences between the climate scenarios are observed, climate-related uncertainties had significantly less influence on the costs than uncertainties in design-related expenses. In the future the knowledge on the innovative solutions and certainty in their design will increase. The amount and range of the yearly costs will then decrease with time. This would make the plastic filter screen and SoSEAL barrier less sensitive to the future uncertainties and could potentially make them a competitive alternative to the sheet pile.

Under constant annual maintenance & monitoring costs, longer lifespans resulted in lower EAC values for all solutions. However, when the costs increase annually, longer lifespans produce higher EAC values, emphasising the need to compare technical lifespans and functional lifespans in design decisions. Additionally, including replacement costs resulted in similar proportional increases in EAC for each solution.
Investigating the uncertainty in technical lifespan under yearly increasing costs, showed a shorter life cycle does not for all climate scenarios always yield lower EAC values and a shorter range. It suggested that for each solution, there is a different optimal lifespan for which the sensitivity is minimal. However, the increase and/or decrease in the range of EAC for each solution is design dependent. In this thesis, however, only one design and a limited number of lifespans for each solution is evaluated. In addition, it is unclear how close the considered lifespans are to their optimal lifetime. A direct comparison is therefore difficult to perform.

To conclude, the performance of the different piping solutions is influenced by both design and climate change uncertainties. Changes in the lifespan and yearly costs significantly affect the performance of the solutions across different scenarios, even more than the uncertainties of climate change. This study underscores the importance of considering design uncertainties and incorporating cost variability into current decision-making. By Reducing these current uncertainties in innovative solutions, they could prove to be suitable alternatives when evaluating and comparing different solutions.

8.2. Recommendations

Based on the findings of this study, several recommendations are proposed to improve the design evaluation under climate change uncertainties.

Recommendations are made for improving the current study and for conducting future research.

- Due to time limitations, the number of simulations was limited. The conditional failure probabilities for the relatively lower water levels could unfortunately not be captured. When enough time is available, the models should be run for significantly more simulations to obtain more accurate conditional failure probabilities. The needed number of simulations for accurate results should be determined.
- The current analysis focuses primarily on economic performance and sensitivity to cost and design uncertainties. While climate change is considered, the environmental impact of the solutions is not. However, environmental impact is an increasingly important criterion in construction decision-making. It is recommended to integrate environmental indicators, such as the MKI (Milieukostenindicator) factor, into life cycle assessments of piping solutions.
- The present study evaluated the solutions as stand-alone measures. In practice, sequential implementation (e.g., applying a solution followed by a more robust measure in the next reinforcement cycle) may provide cost and risk advantages. Future research should explore hybrid strategies, where solutions are combined and the next increment is considered. In these strategies, the innovative solutions may present themselves as a more suitable alternative.
- Current design evaluations assume a constant safety standard over the life cycle. However, as economic growth progresses, societies often demand higher safety levels in the future. Future studies should investigate the influence of increasing safety standard over time. Adaptive design strategies could be determined that account for the increasing safety requirements over time.
- The analysis revealed that the Equivalent Annual Cost (EAC) is strongly influenced by the chosen lifespan of the solution, particularly when maintenance & monitoring costs increase over time. An optimal lifespan for which the EAC values are lowest and the range in EAC the smallest could be found. As stated, in this study only one design for each solution is investigated. It is thus unclear how far the considered lifespan for the design is from the optimal lifespan. Future research could therefore focus on optimizing the functional lifespan for each solution, considering both technical and economic factors. An adaptation of the currently used EAC method can be used to identify the lifespan that results in the lowest EAC.
- The solutions are the most sensitive to the uncertainty in maintenance & monitoring, restoration and replacement costs. These costs had a larger impact on the solutions than climate-related uncertainties. To increase the reliability of life cycle cost assessments, more accurate cost estimates and forecasting methods can be developed. This should include collecting empirical data on long-term maintenance requirements and failure repair costs. Establishing standardized cost databases for innovative solutions can significantly reduce uncertainty in economic evaluations. Reducing these uncertainties over time could also potentially lead to better performing innovative solutions in design evaluations.

References

[1] JP Aguilar-López et al. “Piping erosion safety assessment of flood defences founded over sewer pipes”. In: *European Journal of Environmental and Civil Engineering* 22.6 (2018), pp. 707–735. DOI: 10.1080/19648189.2016.1217793.

[2] AHN. *AHN viewer*. 2025. URL: https://www.ahn.nl/ahn-viewer.

[3] A. Wiggers et al. *Publicatie Heaveschermen*. Tech. rep. HWBP, 2023.

[4] A. Wiggers et al. *Publicatie Heaveschermen*. Tech. rep. HWBP, 2025.

[5] J. Buitink et al. *Implications of the KNMI’23 climate scenarios for the discharge of the Rhine and Meuse*. 2023.

[6] J. Tournier et al. *Internal Erosion of Existing Dams, Levees and Dikes, and their Foundations Volume 1: Internal Erosion Process and Engineering Assessment*. Tech. rep. ICOLD, 2013.

[7] ArcelorMittal. *Profile: AZ 24-700*. 2025. URL: https://projects.arcelormittal.com/foundations/products/steel-sheet-piles/z-sections/profile-az-24-700.

[8] P.A. Arias et al. “Technical Summary”. In: *Climate Change 2021: The Physical Science Basis. Contribution of Working Group I to the Sixth Assessment Report of the Intergovernmental Panel on Climate Change*. Ed. by V. Masson-Delmotte et al. Cambridge, United Kingdom and New York, NY, USA: Cambridge University Press, 2021, 33−144. DOI: 10.1017/9781009157896.002.

[9] V. et al. van Beek. *Kennis voor Keringen: Syntheserapport pipingonderzoek 2018-2019*. Tech. rep. Rijkswaterstaat Water, Verkeer en Leefomgeving, 2020.

[10] V. M. van Beek. *Backward Erosion Piping Initiation and Progression*. Tech. rep. TU Delft, 2015.

[11] J Bessembinder et al. *KNMI’23 klimaat scenario’s voor Nederland*. 2023.

[12] R. Brolsma. *Tabellen aanleg- en beheerkosten*. 2020. URL: https://publicwiki.deltares.nl/spaces/AST/pages/160236837/Tabellen+aanleg-+en+beheerkosten.

[13] J.G. Canadell et al. “Global Carbon and other Biogeochemical Cycles and Feedbacks”. In: *Climate Change 2021: The Physical Science Basis. Contribution of Working Group I to the Sixth Assessment Report of the Intergovernmental Panel on Climate Change*. Ed. by V. Masson-Delmotte et al. Cambridge, United Kingdom and New York, NY, USA: Cambridge University Press, 2021, pp. 673–816. DOI: 10.1017/9781009157896.007.

[14] CBS. *Civil engineering works; Input price index 2015=100 2012-2024*. 2025. URL: https://www.cbs.nl/nl-nl/cijfers/detail/84538ENG.

[15] CBS. *Civil engineering works; Input price index 2020=100*. 2025. URL: https://www.cbs.nl/en-gb/figures/detail/86049ENG#shortTableDescription.

[16] TU Delft et al. *Factsheet Innovatie - SoSEAL*. 2023.

[17] WENR Deltares TNO. *Bodemdalingsvoorspellingskaarten*. 2025. URL: https://www.klimaateffectatlas.nl/nl/bodemdalingsvoorspellings-kaarten.

[18] john.vanesch@deltares.nl van Esch, J Sellmeijer, and Dieter Stolle. “MODELING TRANSIENT GROUNDWATER FLOW AND PIPING UNDER DIKES AND DAMS”. In: Aug. 2013.

[19] Eurostat. *Producer prices in industry, domestic market - monthly data*. 2025. URL: https://ec.europa.eu/eurostat/databrowser/view/STS_INPPD_M__custom_6851786/default/line?lang=en.

[20] Steunpunt Economische Expertise. *Discontovoet*. 2021. URL: https://www.rwseconomie.nl/discontovoet.

[21] U. Förster and P. Verdoorn. *HWBP-DIV Gebruikersplatform Piping*. 2025. URL: https://publicwiki.deltares.nl/spaces/HWBPPiping/pages/187991101/HWBP-DIV+Gebruikersplatform+Piping.

[22] U. Förster et al. *Zandmeevoerende Wellen*. Tech. rep. Definitief, 10 juli 2013. Ministerie van Infrastructuur en Milieu, Rijkswaterstaat, 2012.

[23] Franki Grondtechnieken. *Cement-bentoniet wand*. 2025. URL: https://www.franki-grondtechnieken.nl/nl/techniques/wanden/andere-kerende-wanden/cement-bentoniet-wand.

[24] M Hegnauer et al. "Generator of Rainfall and Discharge Extremes (GRADE) for the Rhine and Meuse basins. Final report of GRADE 2.0". In: *Deltares, Delft, The Netherlands* (2014).

[25] Moritz Hoffmann. "The Navier-Stokes-Darcy problem". MA thesis. Weierstrass Institute, 2013.

[26] HWBP. *HWBP en HWBP-2: wat is het verschil?* 2025. URL: https://www.hwbp.nl/over-hwbp/wie-we-zijn-en-wat-we-doen/hwbp-en-hwbp2.

[27] HWBP. *Life Cycle Costing (LCC) in dijkversterking*. 2025. URL: https://www.hwbp.nl/kennisbank/life-cycle-costing.

[28] Wojciechowska K. et al. "Application of Fragility Curves in Operational Flood Risk Assessment". In: Jan. 2015. DOI: 10.3233/978-1-61499-580-7-528.

[29] Keller. *Deep Soil Mixing*. 2023. URL: http://keller-funderingstechnieken.nl/expertise/technieken/deep-soil-mixing.

[30] Kennisportaal Klimaatadaptatie. *Oorzaken en gevolgen*. 2021. URL: https://klimaatadaptatienederland.nl/kennisdossiers/bodemdaling/oorzaken-gevolgen/.

[31] et al. Klip-Martin T. *Plan van aanpak dijkversterking grebbedijk verkenningsfase*. Tech. rep. Waterschap Vallei en Veluwe, 2023.

[32] M. van Dijk L. Halbmeijer. *Publicatie Filtertechnieken*. Tech. rep. HWBP, 2023.

[33] J. de Leau et al. "Natuurlijk proces als inspiratie om piping tegen te gaan SoSEAL veelbelovend". In: *Land+Water* (2025).

[34] Informatiepunt Leefomgeving. *Kwelwegverlenging*. 2022. URL: https://tl.iplo.nl/@237475/kwelwegverlenging/.

[35] L Lexin et al. "Potential of low-permeability barriers to mitigate backward erosion piping". In: *Géotechnique* (2025).

[36] J. P. Aguilar Lopez. *Dikes and Backwards Erosion Piping (BEP)*. Online. PowerPoint slide deck. 2023.

[37] T. Maatkamp et al. *Ontwerp-, beoordelings- en onderhoudsrichtlijn van het kunststof filterschem bij deeltraject Salmsteke*. Tech. rep. Hoogheemraadschap de Stichtse Rijnlanden, 2023.

[38] Shirin Malekpour et al. "Bridging Decision Making under Deep Uncertainty (DMDU) and Transition Management (TM) to improve strategic planning for sustainable development". In: *Environmental Science and Policy* 107 (2020), pp. 158–167. ISSN: 1462-9011. DOI: https://doi.org/10.1016/j.envsci.2020.03.002. URL: https://www.sciencedirect.com/science/article/pii/S1462901120302008.

[39] H. van der Most N. Slootjes. *Achtergronden bij de normering van de primaire waterkeringen in Nederland*. Tech. rep. Ministerie van Infrastructuur en Milieu, 2016.

[40] United Nations. *What is climate change?* 2023. URL: https://www.un.org/en/climatechange/what-is-climate-change.

[41] TNO Geologische Dienst Nederland. *Ondergrondgegevens*. 2025. URL: https://www.dinoloket.nl/ondergrondgegevens.

[42] B.T. van Meekeren P.J.N.J. Bart B.H.W.J. van Luit. *Ontwerp- en beoordelingsrichtlijn*. Tech. rep. anteagroup, 2022.

[43] Joost Pol. "Influence of erosion on piping in terms of field conditions By G. Hoffmans, J. Hydraulic Res. 59(3), 512–522. 2020. https://doi.org/10.1080/00221686.2020.1786741". In: *Journal of Hydraulic Research* 61.1 (2023), pp. 162–164. DOI: 10.1080/00221686.2022.2132307. eprint: https://doi.org/10.1080/00221686.2022.2132307. URL: https://doi.org/10.1080/00221686.2022.2132307.

[44] Joost Pol. “Time-dependent development of Backward Erosion Piping”. PhD thesis. TU Delft, Dec. 2022. DOI: 10.4233/uuid:eb5ed3b2-4210-489e-b329-59722a0c50a0.

[45] Prolock. *Prolock Delta filter screen*. 2022. URL: https://prolock-sheetpiling.com/product/prolock-delta-filter-screen/.

[46] Rijkswaterstaat. *Rijkswaterstaat waterinfo*. 2025. URL: https://waterinfo.rws.nl/bulkdownload/kaart.

[47] RIVM Rijkswaterstaat BIJ12. *Kaarten*. 2025. URL: https://www.atlasleefomgeving.nl/kaarten?config=3ef897de-127f-471a-959b-93b7597de188&gm-x=150000&gm-y=455000&gm-z=3&gm-b=1544180834512,true,1;1552982649456,true,0.8;&activateOnStart=info&deactivateOnStart=layercollection.

[48] Water Verkeer en Leefomgeving Rijkswaterstaat. *Schematiseringshandleiding Piping*. Tech. rep. Versie 4.0, Definitief, 28 mei 2021. Ministerie van Infrastructuur en Waterstaat, Rijkswaterstaat, 2021. URL: https://www.helpdeskwater.nl.

[49] Water Verkeer en Leefomgeving Rijkswaterstaat. *Schematiseringshandleiding Piping bij kunstwerk*. Tech. rep. Versie 3.0, Definitief, 28 mei 2021. Ministerie van Infrastructuur en Waterstaat, Rijkswaterstaat, 2021.

[50] Kennisplatform Risicobenadering RWS WVL. *Achtergrondrapport Ontwerpinstrumentarium 2014*. Tech. rep. Ministerie van Infrastructuur en Milieu, 2016.

[51] R. Huting S. Stuij T. de Wit. *Nadere Veiligheidsanalyse Grebbedijk*. Tech. rep. Safety assessment report for Grebbedijk. Royal HaskoningDHV, 2018.

[52] M. A. Schoemaker. *Flood Risk Assessment & Investment Framework*. Tech. rep. TU Delft, 2016. URL: https://resolver.tudelft.nl/uuid:5137a7e4-1397-4b86-80ca-c9d0ae69226d.

[53] Chenxiao Song and Reiichiro Kawai. “Monte Carlo and variance reduction methods for structural reliability analysis: A comprehensive review”. In: *Probabilistic Engineering Mechanics* 73 (2023), p. 103479. ISSN: 0266-8920. DOI: https://doi.org/10.1016/j.probengmech.2023.103479. URL: https://www.sciencedirect.com/science/article/pii/S0266892023000681.

[54] TAUW. *SoSEAL: Een innovatieve dijkversterkingstechniek*. 2023. URL: https://www.tauw.nl/projecten/soseal-%E2%80%93-soil-sealing-by-enhance-aluminium-and-organic-matter-leaching.html.

[55] R Van Dorland et al. “Knmi national climate scenarios 2023 for The Netherlands”. In: *KNMI: De Bilt, The Netherlands* (2023).

[56] Phil Vardon. “Climatic influence on geotechnical infrastructure: a review”. In: *Environmental Geotechnics* 2 (Jan. 2014). DOI: 10.1680/envgeo.13.00055.

[57] Waterschap Vallei en Veluwe. *Bijlage 9.13. Veiligheidsopgave*. 2024. URL: https://www.grebbedijk.com/terinzagelegging.

[58] Waterschap Vallei en Veluwe. *Bijlage 9.17. Factsheets*. 2024. URL: https://www.grebbedijk.com/terinzagelegging.

[59] H.J. de Vriend et al. “Heeft de Rijnafvoer bij Lobith een maximum?” In: *Expertisenetwerk Waterveiligheid* (2016).

[60] J.P. de Waal. “Basisrapport WBI 2017”. In: *Deltares, Delft, The Netherlands* (2017).

[61] R. Wennubst-Pedrini. “SoSeal semi-permeable barrier as a piping erosion risk reduction measure below dikes”. MA thesis. TU Delft, 2022.

[62] Witteveen+Bos. *Planuitwerking gebiedsontwikkeling Grebbedijk*. Tech. rep. Delft: Witteveen+Bos, 2024. URL: https://www.grebbedijk.com/terinzagelegging/revised/2-omgevingsvergunning-beperkingengebiedsactiviteit-rijk/rivierkundige-beoordeling.pdf.

[63] Witteveen+Bos. *Trillingsanalyse Grebbedijk*. Tech. rep. 124281. Witteveen+Bos, 2024.

[64] Wsp. *Waterveiligheid Grebbedijk*. 2020. URL: https://www.wsp.com/nl-nl/projecten/waterveiligheid-grebbedijk.

A

Composite fit for Hydra-NL water levels

The water levels, calculated by Hydra-NL, are fitted using a composite fit of the Weibull and Generalised pareto distribution.

In Figure A.1, the composite fit for scenario G with a capped discharged is shown. The water levels from Hydra-NL are shown in Table A.1.

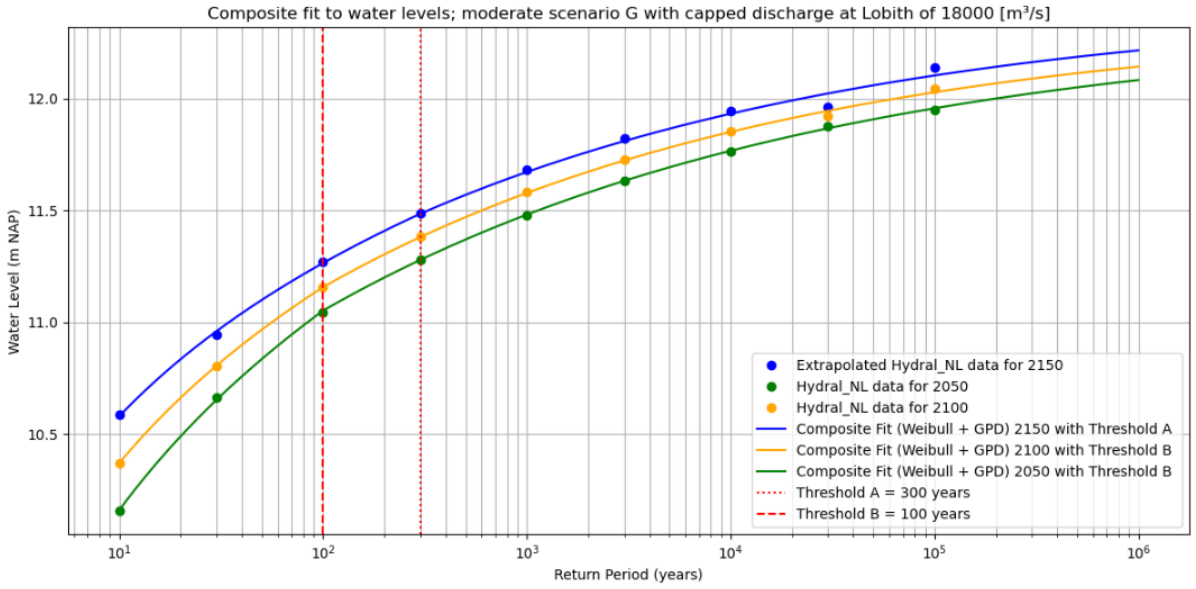

Figure A.1: The composite fit for the water levels of climate scenario G with a capped discharge at Lobith of 18,000 m^3/s.

Return periods	2050	2100
10	10.156	10.372
30	10.664	10.804
100	11.046	11.158
300	11.279	11.383
1000	11.479	11.581
3000	11.630	11.725
10,000	11.764	11.876
30,000	11.854	11.919
100,000	11.921	12.063

Table A.1: The water levels in [m NAP] for a moderate emission scenario [G] with a capped discharged at Lobith of $18\,000\,\mathrm{m}^3/\mathrm{s}$.

In Figure A.2, the composite fit for scenario G with a uncapped discharged is shown. The water levels from Hydra-NL are shown in Table A.2.

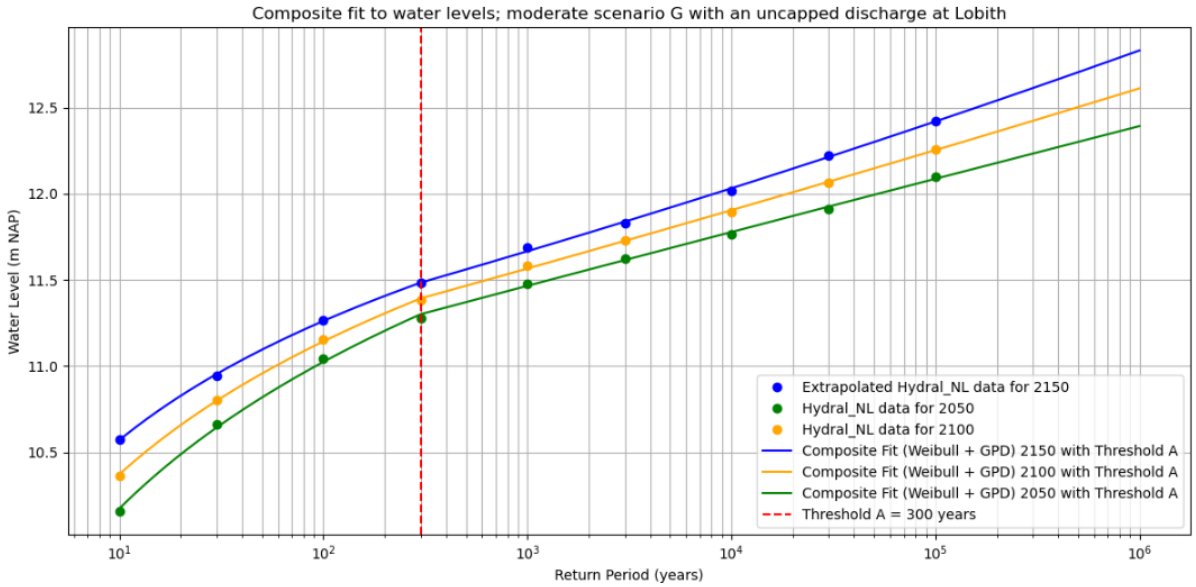

Figure A.2: The composite fit for the water levels of climate scenario G with an uncapped discharge at Lobith.

Return periods	2050	2100
10	10.156	10.366
30	10.665	10.804
100	11.044	11.156
300	11.278	11.381
1000	11.479	11.585
3000	11.626	11.727
10,000	11.767	11.893
30,000	11.911	12.066
100,000	12.097	12.258

Table A.2: The water levels in [m NAP] for a moderate emission scenario [G] with an uncapped discharged at Lobith.

In Figure A.3, the composite fit for scenario W+ with a capped discharged is shown. The water levels from Hydra-NL are shown in Table A.3.

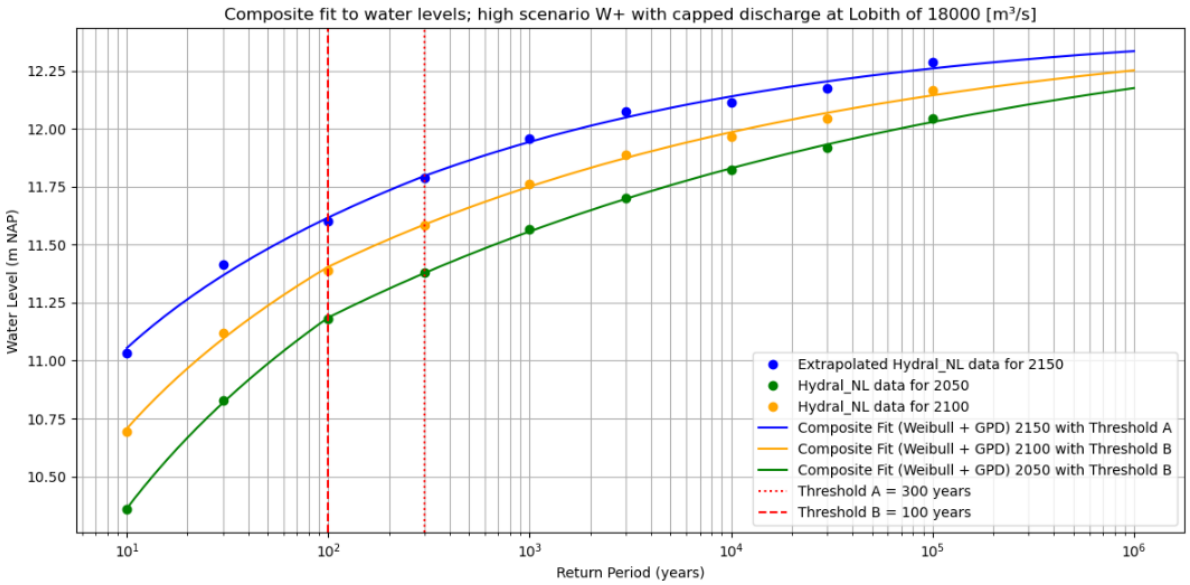

Figure A.3: The composite fit for the water levels of climate scenario W+ with a capped discharge at Lobith of 18,000 m^3/s.

Return periods	2050	2100
10	10.358	10.695
30	10.829	11.121
100	11.180	11.390
300	11.382	11.586
1000	11.565	11.761
3000	11.699	11.887
10,000	11.823	11.968
30,000	11.917	12.045
100,000	12.042	12.165

Table A.3: The water levels in [m NAP] for a high emission scenario [W+] with a capped discharged at Lobith of $18\,000\,\mathrm{m}^3/\mathrm{s}$.

In Figure A.4, the composite fit for scenario W+ with an uncapped discharged is shown. The water levels from Hydra-NL are shown in Table A.4.

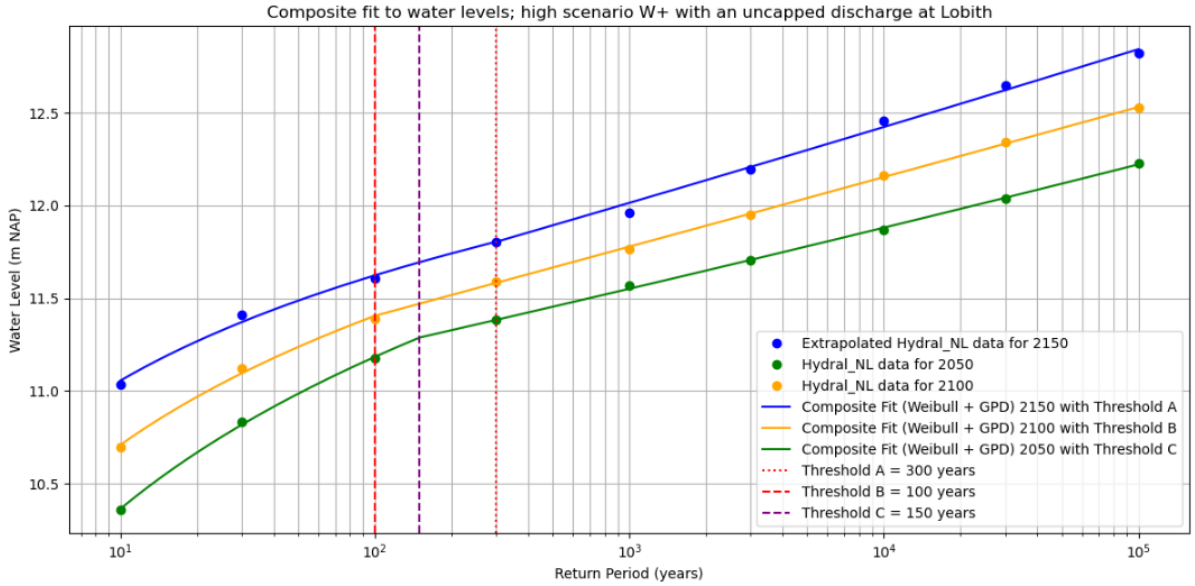

Figure A.4: The composite fit for the water levels of climate scenario W+ with an uncapped discharge at Lobith.

Return periods	2050	2100
10	10.357	10.697
30	10.831	11.120
100	11.176	11.391
300	11.381	11.591
1000	11.571	11.767
3000	11.707	11.951,
10,000	11.866	12.160
30,000	12.036	12.341
100,000	12.229	12.525

Table A.4: The water levels in [m NAP] for a high emission scenario [W+] with an uncapped discharged at Lobith.

B

CPT of dike section 3B at dike post 25

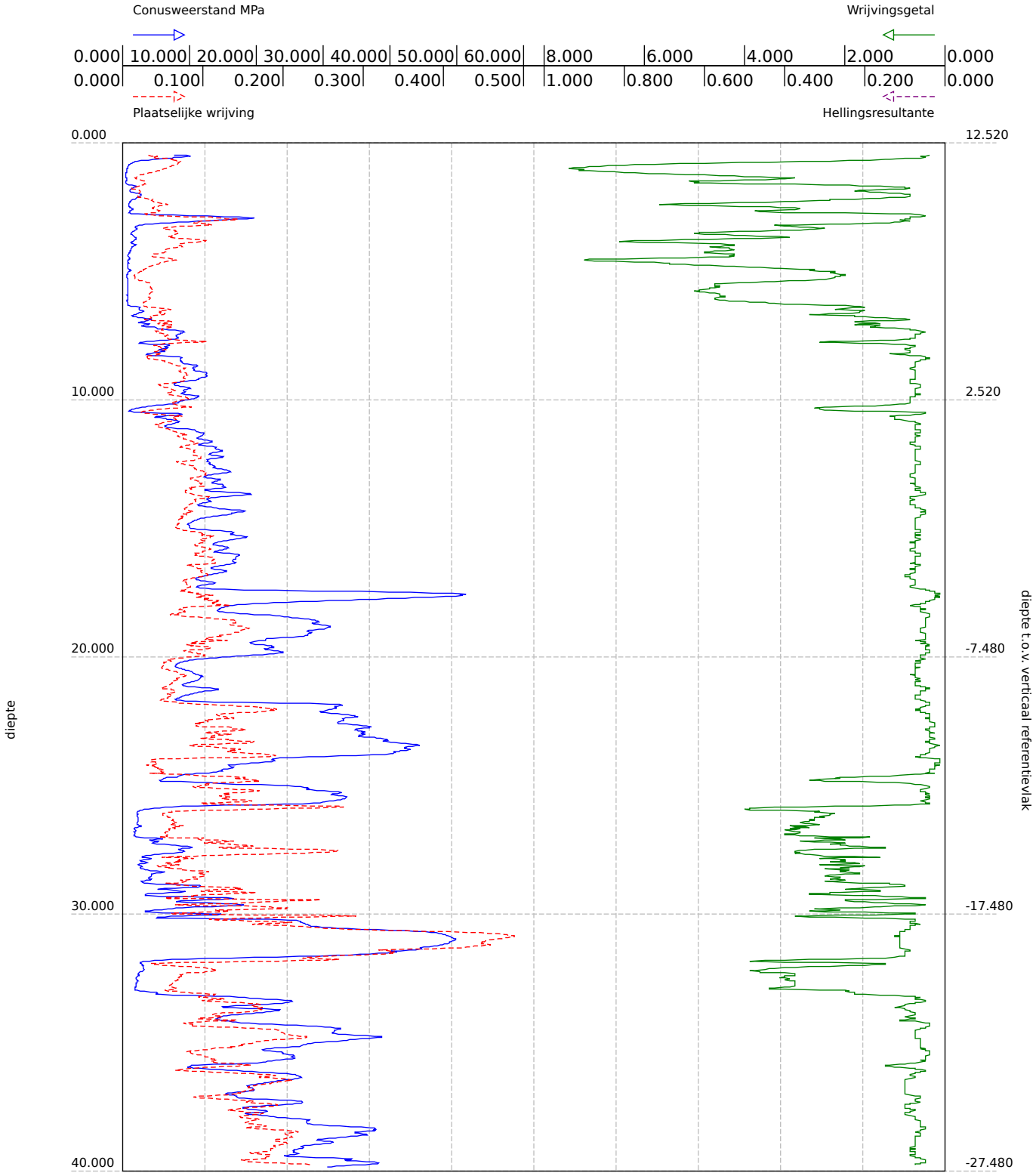

BRO-ID: CPT000000119670
Verticale verschuiving: 12.520 (NAP)
Lokaal verticaal referentiepunt: maaiveld
Aangeleverde coördinaten: 172560.260, 440658.180 (urn:ogc:def:crs:EPSG::28992)

C

Design dimensions

The final dimensions and input of the designs for each solution, are the result of an iterative process. In this process, the behaviour of the solutions is investigated by assessing their respective failure criteria. This is also described in the methodology flow chart, see Figure 5.1.
For water levels of different future sight years, corresponding to the target safety, multiple designs were deterministically evaluated. In Equation C.1, the general inequality criterion for each solution is given.

$$S < R \tag{C.1}$$

So, Equation C.1 is checked for each design with R being the critical gradient and S the acting gradient. Both are represented as deterministic values. The resulting final designs and dimensions serve as input for the probabilistic assessment.

C.1. Dimensions sheet pile

For the sheet pile, the width follows from the AZ24-700 profile and this is fixed for each design. To determine the length of the sheet pile, the following failure criterion is checked, as described in subsection 5.3.3:

$$S < R = i_{avg} < i_c \tag{C.2}$$

Different lengths of the sheet pile were tested for the water level corresponding to the safety target. For this assessment conservative soil parameters were used. The 95% low average was used for the d_{70}, and the 95% high average was used for K.
It was found that an embedded depth of $3.5m$ is the shortest length for the sheet pile to meet the criterion.

C.2. Dimensions plastic filter screen

For the plastic filter screen, the width was derived from the Prolock design and kept constant across the different configurations. Before determining the final length, two alternative filter screen designs were tested:

1. A design with a fixed closed bottom part of 0.5m and a fixed filter section of 1.0m starting 0.5m above the base. The top and bottom sections are closed, meaning that with increasing total length, the closed top section also increases.
2. A design with a fixed closed bottom part of 0.5m, while the remainder of the screen functions as a filter. In this configuration, the filter length increases proportionally with the total screen length.

Both configurations were modelled for varying water levels and soil parameters to compare their behaviour and performance. The second design consistently outperformed the first and was therefore

selected for further modelling. It should be noted, however, that the larger filter section introduces additional uncertainty, as the innovative filter part itself is still associated with performance uncertainties.

To determine the required length of the plastic filter screen, the same failure criterion applied to the sheet pile was used. In the assessment, the conservative values of d_{70} and K were adopted again as well. The analysis showed that an embedded depth of $2.5,$ m is sufficient for the plastic filter screen to meet the criterion without unnecessary over-dimensioning.

C.3. Dimensions SoSEAL barrier

As outlined in section 4.4, current methods and knowledge do not allow for the guarantee of a fully continuous SoSEAL barrier. The most robust and preferred implementation is therefore a barrier that completely seals the aquifer. Consequently, the depth of the SoSEAL barrier is not determined through an iterative process but is instead based directly on the aquifer depth.
Additionally, only a single hydraulic conductivity reduction (HCR) field was designed and applied, as described in subsection 5.5.3.

The contact zone between the barrier and the cover layer, however, was investigated for different configurations. To evaluate these different designs, the failure criterion defined in subsection 5.3.2 was applied:

$$S < R = \frac{dp}{dx_{FEM}} < \frac{dp}{dx_{crit}} \tag{C.3}$$

The initial iteration, conducted without a weakened contact area, produced unrealistically low results. Subsequent evaluations of different contact zone configurations demonstrated that this area strongly affects the performance of the SoSEAL barrier. In particular, the hydraulic conductivity of the contact zone significantly effects whether the criterion was met. Considerable uncertainty remains regarding this parameter due to limitations of current injection techniques. To address this, the contact zone was modelled stochastically, using a log-normal distribution, which provided the most realistic representation of barrier performance. Different reduction factors, applied to the 95% high average aquifer conductivity (see Equation 5.13), were assessed to generate a range of contact zone conductivities. Deterministic evaluation of the criterion for the different factors showed that factors according to a distribution with a 95% high average value of 10 resulted in compliance with the criterion.

D

Parametric sweep for erosion channel height

The mesh of the erosion channel domain depends on the height a. When using different sample values of a for each simulation, means that every time the domain has to be re-meshed. This is very inefficient and time-consuming. Instead, the simulations are run for sampled values of a factor f_a with which a is multiplied. The hydraulic gradient is kept the same and the permeability is changed, through the factor f_a. In the model the flow through the channel needs to stay the same for every run, see Equation D.1.

$$q_1 = q_2 \tag{D.1}$$

The flow q can be expressed as in Equation D.2. As can be seen, the height for the new erosion channel is the previous height a_1 multiplied by the factor f_a.

$$a_1 * k_1 * \frac{dh}{dx}_1 = f_a * a_1 * k_2 * \frac{dh}{dx}_2 \tag{D.2}$$

The gradient needs to stay the same, since the geometry stays the same in the model (there is no re-meshing). Therefore; $\frac{dh}{dx}_1$ is equal to $\frac{dh}{dx}_2$. Equation D.2 can now be rewritten as:

$$k_1 = \frac{f_a * a_1}{a_1} * k_2 = f_a * k_2 \tag{D.3}$$

The formula for the permeability of the pipe is known:

$$k_* = -\frac{2 * D_h^2}{\beta_f} \tag{D.4}$$

Using f_a, Equation D.4 can be written in a generalised form that is applicable to every erosion channel height for each simulation. Since the assumed erosion channel has a square shape D_h is equal to a. The applied formula for the permeability of the pipe then becomes as follows:

$$k_* = f_a * \frac{2 * D_h^2}{\beta_f} = f_a * \frac{2 * (f_a * a)^2}{\beta_f} = f_a^3 * \frac{2 * a^2}{\beta_f} \tag{D.5}$$

E

Sensitivity analysis

E.1. Different discount rate

As stated in subsection 7.2.7, the discount rate can change significantly in the future. An analysis is performed that investigates the use of a discount rate of 2.25% and 4%. The 2.25% discount rate is currently used as the standard discount rate by Steunpunt Economishce Expertise [20]. The 4% discount rate is significantly higher and arbitrarily chosen, but could be a realistic rate in the future.

In Figure E.1, the difference in EAC for a 2.25% discount rate can be seen over the technical lifespan for each solution with constant yearly monitoring & maintenance costs.

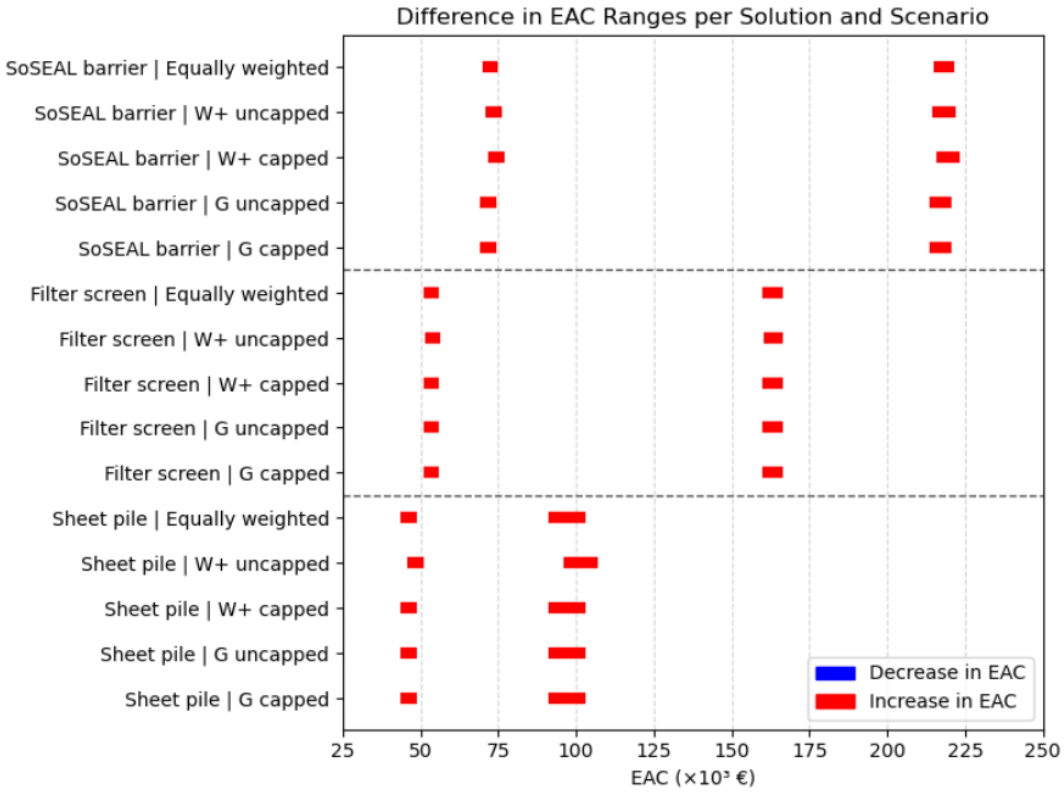

Figure E.1: The difference in EAC when comparing the use of a 2.25% discount rate to a 1.6% discount rate. In this analysis the representative technical lifespans are considered with constant yearly monitoring & maintenance costs.

A higher discount rate results in higher EAC values for all solutions and scenarios. This is primarily due

to its impact on the annuity factor. The total present value (PV) of costs increases approximately log-linearly over time (due to the constant yearly costs), meaning that the additional contribution of each subsequent year to the total PV becomes progressively smaller. When the discount rate increases, these already small increments are further reduced, resulting in only a marginal effect on the total PV. In contrast, the annuity factor is more sensitive to the discount rate and grows at a much slower pace as the discount rate increases. Since the EAC is calculated as $EAC = \frac{PV}{A}$, this relatively stronger effect on the denominator leads to higher EAC values for higher discount rates. This effect becomes stronger with longer lifespans. The increase in EAC is therefore higher for the sheet pile, since its technical lifespan (100 years) is longer than that of the plastic filter screen and SoSEAL barrier (75 years).

The same analysis between the 1.6% and 2.25% is also performed for the scenario with yearly increasing monitoring & maintenance costs, see Figure E.2. Since the monitoring and maintenance costs now increase annually, the total invested costs grow over time. Consequently, the discount rate applies to progressively larger future values, amplifying the discounting effect on the total present value. However, as shown in the graph, the EAC still increases compared to the scenario with a 1.6% discount rate. This indicates that, although the impact of discounting is stronger due to higher future costs, the effect on the annuity factor, as described earlier, remains dominant. This results in higher EAC values overall.

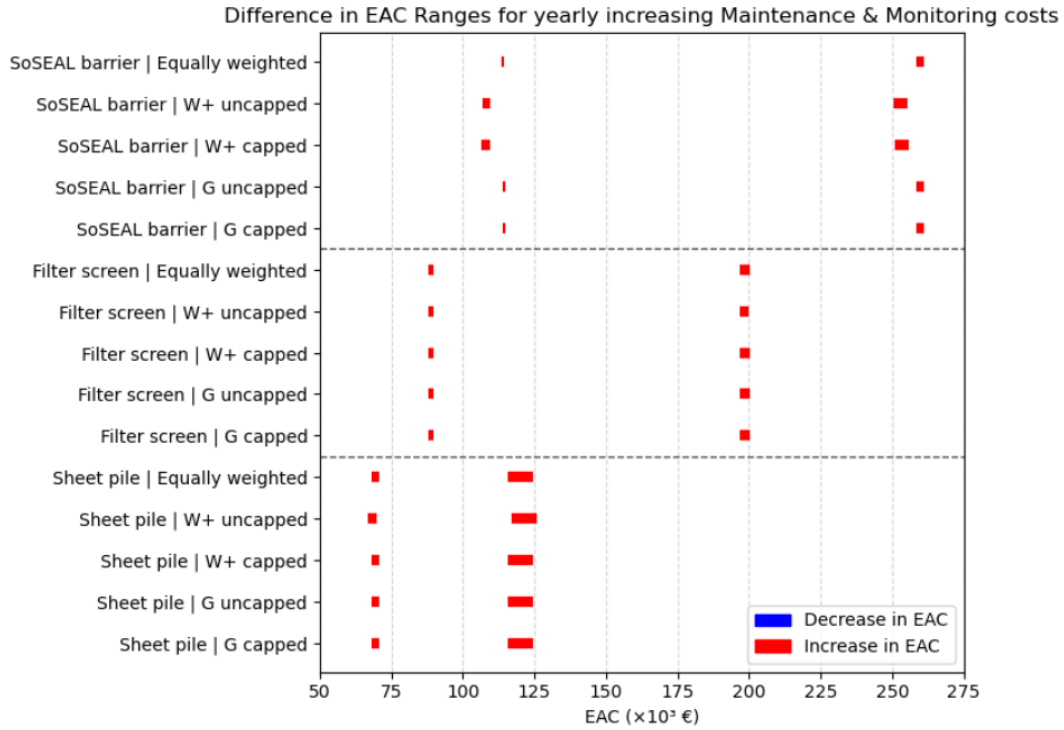

Figure E.2: The difference in EAC when comparing the use of a 2.25% discount rate to a 1.6% discount rate. In this analysis the representative technical lifespans are considered with yearly increasing monitoring & maintenance costs.

The comparison between the difference in a discount rate 4% and 1.6% is presented in Figure E.3.

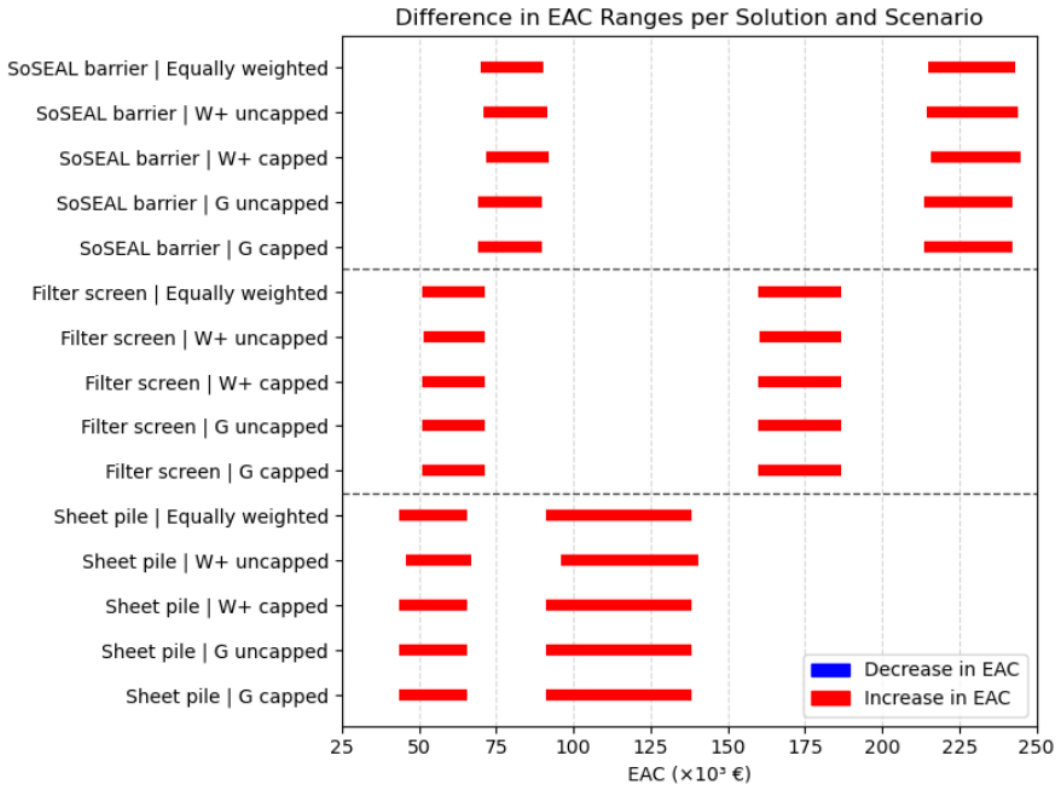

Figure E.3: The difference in EAC when comparing the use of a 4% discount rate to a 1.6% discount rate. In this analysis the representative technical lifespans are considered with constant yearly monitoring & maintenance costs.

The higher discount rate results in increasing EAC for all solutions and scenarios. At a discount rate of 4%, the described effect becomes significantly more pronounced and clearly observable. This is expected, as the influence on the total present value declines further with constant costs, while the impact on the annuity factor continues to increase.

In Figure E.4, it is seen that the effect of the higher discount rate decreases as total invested costs grow over time. As stated before, the discount rate applies to progressively larger future values, amplifying the discounting effect on the total present value. However, the effect on the annuity factor remains dominant.

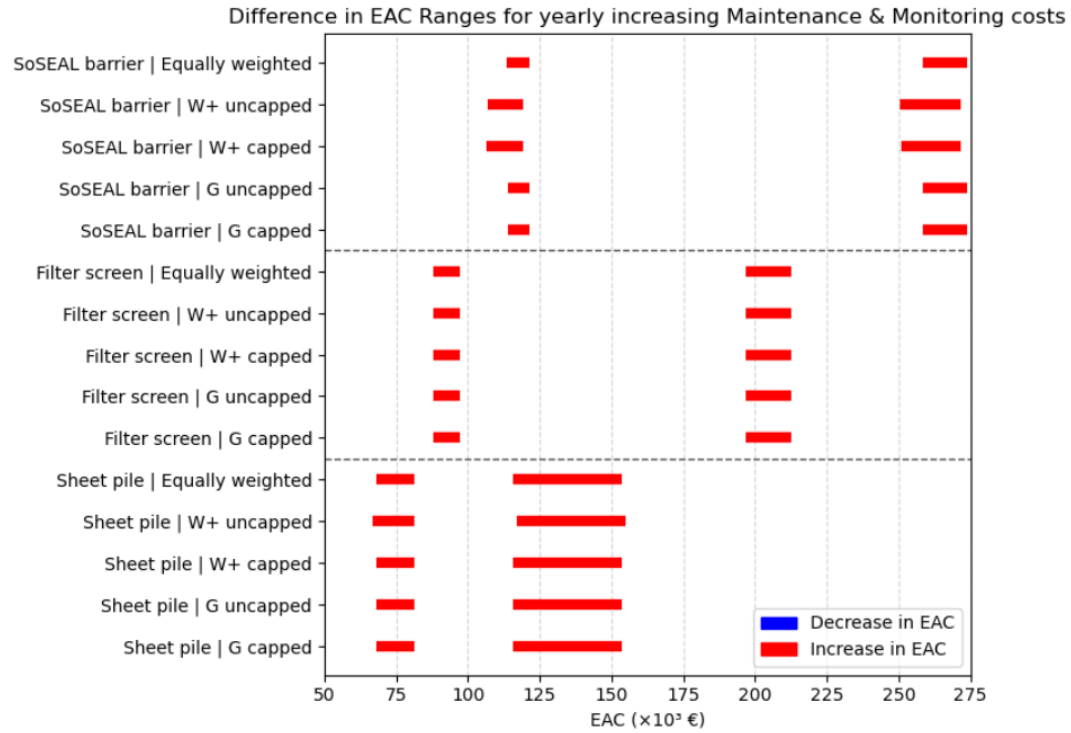

Figure E.4: The difference in EAC when comparing the use of a 4% discount rate to a 1.6% discount rate. In this analysis the representative technical lifespans are considered with increasing yearly monitoring & maintenance costs.

It can be reasoned that if the annual costs were to increase significantly more each year than in the current scenario, the effect of a higher discount rate on the total present value would outweigh its effect on the annuity factor. In that case, the EAC would decrease as the discount rate increases.

E.2. Risk of failure

As stated in section 7.4, risk is a non-constant annually increasing expense. This is because the failure probability increases exponentially with time. To account for risk in the EAC analysis, the risk needs to be added to PV_{tot}. Equation E.1 shows the formula for calculating the total risk.

$$PV_{risk} = \sum_{t=1}^{t^*} P_t * \frac{C_{damage}}{(1+r)^t} \tag{E.1}$$

With:

- PV_{risk}: Total present value of the risk
- P_t: Failure probability in the considered year
- C_{damage}: Estimation of the damage costs of the hinterland after a dike breach

The total damage of a breach of the Grebbedijk is estimated to be €27 billion [31]. By incorporating the risk in the analysis the EAC ranges from Figure E.5 are obtained.

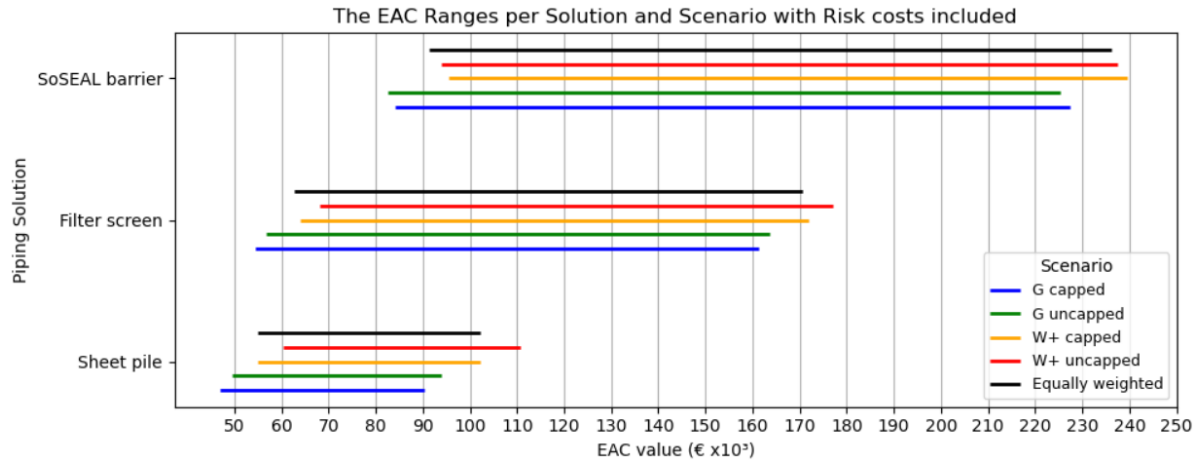

Figure E.5: The EAC ranges per solution and scenario. The risk as presented in Equation E.1, is taken into account for the EAC values.

Since the EAC analysis is conducted over the functional lifespan, all solutions ultimately reach the same failure probability, corresponding to the maximum allowable threshold. However, solutions with a shorter lifespan reach this failure probability earlier. Consequently, while the risk ($P_t * C_{dammage}$) at the end of the respective lifespans is identical, the associated costs are discounted over a shorter time frame. This results in a higher EAC for shorter lifespans. This effect is illustrated in Figure E.5, since the EAC for the W+ climate scenarios is higher than for the moderate scenarios with a longer lifespan.

Figure E.6 shows the difference in EAC between functional and technical lifespans. The largest differences occur in the G scenarios, where the lifespan discrepancies are greatest. The effect is slightly more pronounced for the plastic filter screen and sheet pile compared to the SoSEAL barrier, as the latter has the smallest difference between functional and technical lifespans. Moreover, the failure probability in general increases exponentially, making larger variations in the timespan more influential on the risk-related costs.

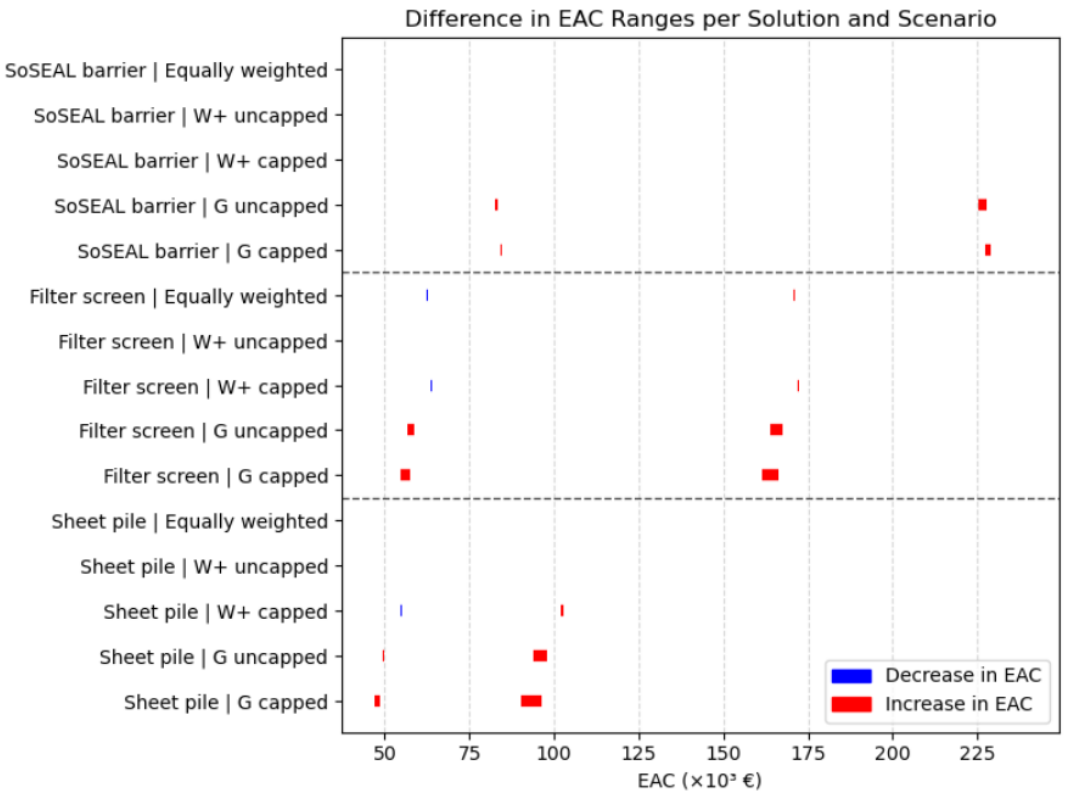

Figure E.6: The difference in EAC for each solution and scenario. The technical lifespan is compared to the functional lifespan. This means the increase or decrease is with respect to the functional lifespan.

The EAC analysis accounting for risk was also performed for the scenario with annually increasing monitoring & maintenance costs. As shown in Figure E.7, longer lifespans for the plastic filter screen and SoSEAL barrier result in higher EAC values, indicating that the impact of increasing monitoring & maintenance costs dominates over risk with increasing time. Although risk grows exponentially, the low failure probabilities keep its contribution relatively small compared to the rising maintenance & monitoring expenses.
For the sheet pile, the two cost components are more balanced. This is because the annual increase in maintenance & monitoring costs is lower than for the plastic filter screen and SoSEAL barrier.

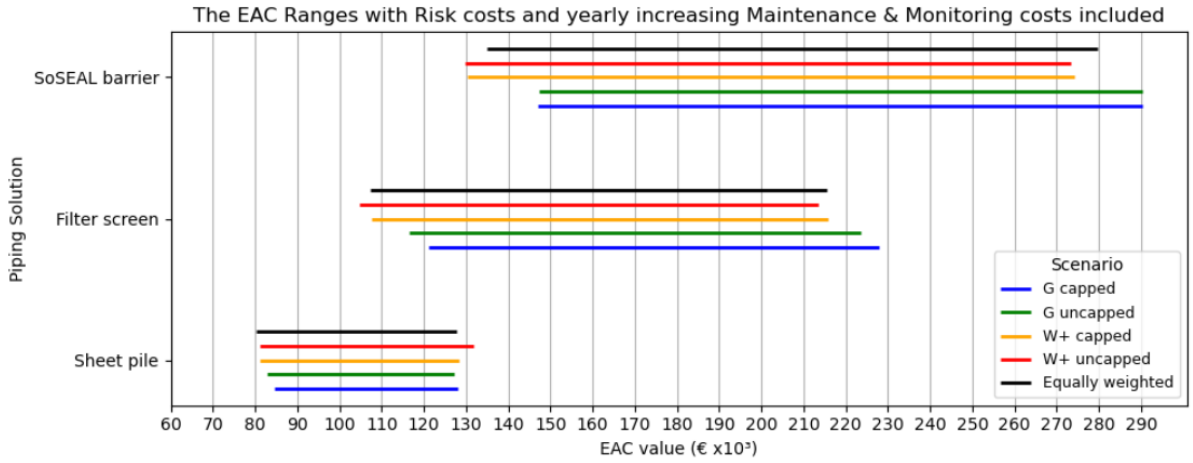

Figure E.7: The EAC ranges for the different solutions and scenarios. The yearly increasing monitoring & maintenance costs and the risk is taken into account.

In Figure E.8 the differences between considering the functional lifespan and technical lifespan are presented. For the SoSEAL barrier and the plastic filter screen, the increase in maintenance costs is the largest. Consequently, a shorter lifespan leads to a significant reduction in EAC, particularly in the G scenarios, where the difference between functional and technical lifespans is greatest.
For the sheet pile, there remains a relatively large EAC difference in the G scenarios. Although the increase in maintenance costs is comparatively small, the substantial difference in timespan still results in a notable impact on EAC.

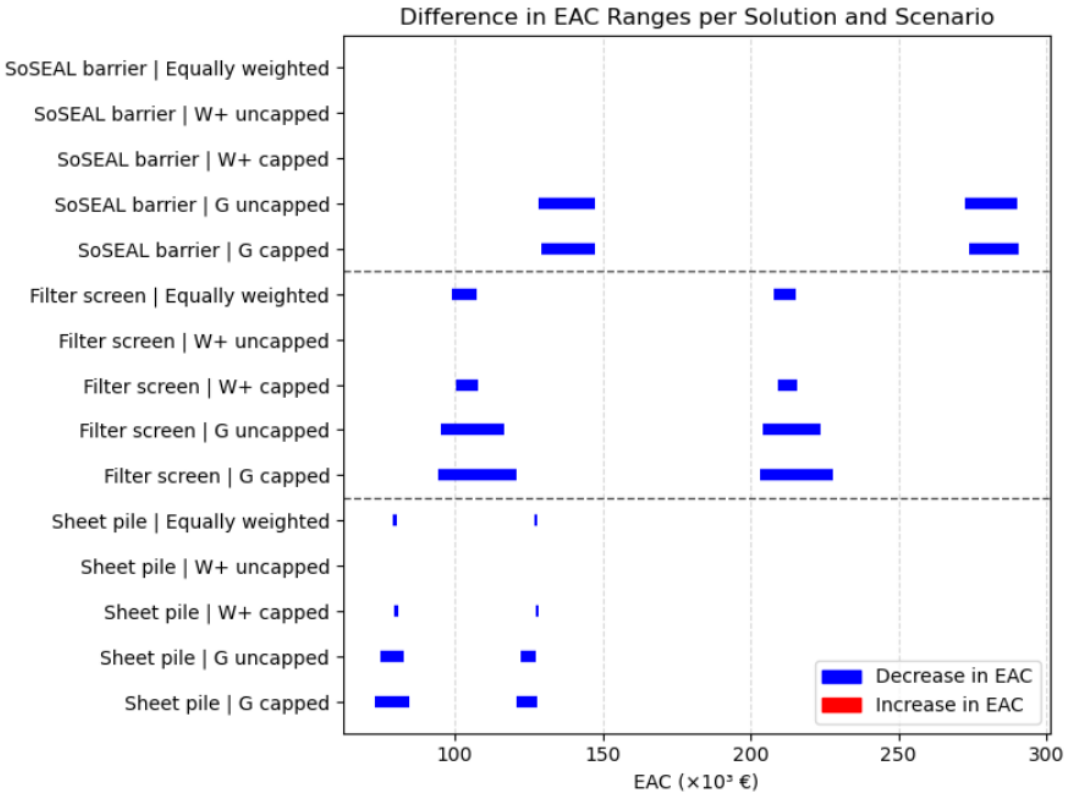

Figure E.8: The difference in EAC for each solution and scenario. The technical lifespan is compared to the functional lifespan. This means the technical lifespan shows a decrease or stays equal with respect to the functional lifespan.